DETERMINING THE ROLE OF HIV-DNA IN RELATION TO ACTIVATED MONOCYTES IN THE DEVELOPMENT OF HIV-ASSOCIATED NEUROCOGNITIVE DISORDERS

A DISSERTATION SUBMITTED TO THE GRADUATE DIVISION OF THE UNIVERSITY OF HAWAI'I AT MÃNOA IN PARTIAL FULFILLMENT OF THE REQUIREMENTS FOR THE DEGREE OF

DOCTOR OF PHILOSOPHY

IN

CELL AND MOLECULAR BIOLOGY

DECEMBER 2010

By

Melissa A. Agsalda

Dissertation Committee:

Bruce Shiramizu, Chairperson
Mariana Gerschenson
Lorey Takahashi
Marla Berry
Andy Stenger

ABSTRACT

There has been an increase in the prevalence of HIV-associated neurocognitive disorders (HAND) in spite of effective antiretroviral therapy (ART). It is believed that activated monocytes, CD14+/16+, are involved in the HAND pathogenesis through trafficking of HIV into the central nervous system (CNS). Once inside, CD14+/16+ cells initiate inflammation resulting in neuronal damage. Monocytes are also able to harbor HIV and serve as viral reservoirs, which are identified by presence of HIV DNA. These concepts are supported by findings in our lab where individuals with HAND have higher HIV DNA copy numbers in circulating CD14+/16+ cells compared to other cell subsets. The goal of this study is to characterize HIV DNA in these cells from other compartments through experiments on cerebrospinal fluid (CSF) and archival CNS tissue. The overall hypothesis is HIV DNA levels in cell subsets correspond to observations in the periphery. We also posit that insertional mutagenesis may be involved in neuropathogenesis through disruption of genes that may drive inflammation and neuronal apoptosis. Thus, HIV integration studies were done to determine genes that within and around the integration sites in the various CSF subsets.

Results of HIV DNA levels in the CSF cell subsets were in contrast to levels reported in the periphery. Non-activated monocytes, CD14+/16-, contained the highest levels of HIV DNA regardless of neurocognitive status. This suggests that CSF viral reservoirs may be present that serve as sanctuaries for HIV evolution and compartmentalization. Conversely, the highest levels of HIV DNA were found in CD14+/16+ in HIV-encephalitis brain sections, which may reflect ongoing inflammation that might be occurring. Furthermore, common CSF integration sites were found within

genes that were involved in apoptosis, macrophage behavior, and transcriptional regulation; all of which could promote HAND. The studies included the use of a unique flow cytometry technique that was shown to be comparable to our current quantitative real-time PCR assay to detect HIV DNA. The information obtained through these studies sets the stage for the focus of future studies and provide additional molecular tools to monitor the involvement of monocytes throughout the progression of HAND.

TABLE OF CONTENTS

LIST OF TABLES

LIST OF FIGURES

CHAPTER 1

Introduction

Overview of HIV and HIV-Associated Diseases

In December 2008, the World Health Organization (WHO) and UNAIDS estimated that 33.4 million people in the world are living with HIV, a 20% increase from 2000. Despite the increase in prevalence, they estimated a global incidence of 2.7 million, which a 30% decrease from the peak in 1996, Figure 1.1. This increase in prevalence and decrease in incidence is most likely contributed to the availability of antiretroviral therapy (ART) though it must be noted that incidence is hard to predict due to many unreported cases. Additionally, it is found that individuals infected with HIV are also living longer. UNAIDS and WHO estimated that 2 million people worldwide died of AIDS-related deaths during 2008, which is a 10% decrease from 2004, Figure 1.1. Generally, the highest rates are found in Sub-Saharan Africa, Figure 1.2, where an estimated 22.4 million are living with HIV. In the United States, approximately 1.4 million people are infected with HIV with the majority being black/African American males. It is also estimated that there were 55,000 new cases in 2008, Figure 1.3.

HIV is a single stranded RNA lentivirus belonging to the retroviridae family that causes acquired immunodeficiency (AIDS), a disease where life-threatening opportunistic infections occur due to a faulty immune system. Two species of HIV exist and are depicted as HIV-1 and HIV-2. It is belived that HIV-1 is transmitted from chimpanzees and HIV-2 from sooty mangabey [1]. Since HIV-2 is primarily confined to

West Africa due to its lower virulence and infectivity, this dissertation will focus on HIV-1 infections. There are three classes of HIV-1: group M, group O and group N. Group M comprises 90% of worldwide HIV/AIDS cases and consists of nine major subtypes (A-D, F-H, J, and K) [1]. Intersubtype recombinants also exist and result from recombination. Subtype B accounts for approximately 10% of worldwide infections and predominates in Europe, Australia, and America but is also seen in Africa, the Middle East, and Asia [1]. The other main group M subtypes are subtype A, which accounts for 17% of infections and subtype C accounting for 49% of infections. Interestingly, areas with predominate subtype C infections appear to have lower frequencies of HIV-related neurotoxicity than areas with predominate subtype B infections [2]. Although the reasons for this finding is unknown, current studies attribute it to the Tat protein and reduced MCP-1 astrocyte production [3]. HIV-1 can be transmitted through blood, semen, vaginal and pre-ejaculation fluid, and breast milk.

There are two main structures of HIV: the viral membrane and inner core. The viral membrane contains viral proteins that bind to receptors of host cells and the inner core contains viral RNA and enzymes. Viral RNA consists of several HIV-1 genes that code for both structural (*gag, pol,* and *env)* and accessory proteins (*tat, rev, nef, vif, vpr* and *vpu)*, Figure 1.4. *Gag* codes for viral capsid proteins, *pol* codes for reverse transcriptase, integrase and protease enzymes, and *env* codes for envelope proteins.

The typical life cycle of HIV-1, Figure 1.5, begins with binding and fusion of the virus to the host cell (cell being infected). During binding, the HIV-1 glycoprotein gp120 binds to the CD4 receptor on the host cell along with a co-receptor CCR5 or CXCR4. Once the viral membrane fuses with the host membrane, the virus releases its RNA into

the host cell. The HIV-1 enzyme reverse transcriptase then converts the single stranded viral RNA (vRNA) into double stranded viral DNA (vDNA), which then gets transported into the nucleus. Another HIV-1 enzyme integrase is used to integrate vDNA into the host genome leading to the formation of a provirus. This provirus may remain inactive for many years or may be activated for transcription. During transcription, mRNA results from the vDNA by the host cell's RNA polymerase. mRNA is then transported outside of the nucleus for use as a template for protein production through translation. New viral particles are formed from these newly made proteins by the HIV enzyme protease. The last stage of the HIV-1 life cycle is budding, where the new viral particles are released from the host cell and are able to infect other immune cells increasing the abundance of HIV-1.

An individual progresses to AIDS when their CD4+ T-cells fall below 200 cells/mm^3. Opportunistic infections from pathogens such as protozoa, other viruses, mycotic agents, and intacellular bacteria [4] are often associated with AIDS, occurring when the immune system begins to fail. However, AIDS and opportunistic infections occur less frequently due to the widespread use of ARTs, resulting in longer lifespans for those with HIV. Due to longer life expectancies, HIV-1 infected individuals are more prone to other HIV-associated disorders, such as cardiovascular events, metabolic complications, HIV-associated malignancies (HAMs) and HIV-associated neurocognitive disorders (HAND).

Neuropathology of HAND

Approximately 20-30% of HIV-infected individuals are inflicted with HAND, which is characterized by abnormalities in cognitive, motor and behavioral functions that include slowing of thought processes, memory loss, impaired manipulation of acquired knowledge, and personality changes such as apathy, inertia and irritability [5, 6]. The introduction of ART in 1996 led to variations in the disease course, resulting in a decrease in its incidence. Regardless, the prevalence remained unaffected and shown to be either unchanged or increased. These data suggest that ART does not provide complete protection against the development of HAD and could account for the increase in milder forms including minor cognitive motor disorder (MCMD) and asymptomatic neurocognitive impairment (ANI). Collectively, HAD, MCMD and ANI are categorized as HIV-associated neurocognitive disorders (HAND). The mildest form of HAND is ANI and does not impact an individual's life but is measurable through neurocognitive testing. MCMD causes mild impairment in work and daily lifestyle. It is characterized by impairment in cognitive or behavioral function in at least two of the following areas: impaired attention-concentration, mental slowing, abnormal memory or other cognitive functions, slowed movements, incoordination, personality change, irritability, or lability. HAD is the most severe form of HAND and causes a dramatic impact on the quality of life and survival. ART has made a tremendous impact on HAD, lowering its prevalence to 2-8% [7].

The pathological correlate of HAD is HIV encephalitis (HIVE), which is characterized by astrocytosis, myelin pallor, infiltration of monocytoid cells such as macrophages, microglia and multinucleated giant cells, and neuronal dysfunction and loss

[4, 8]. Once the monocytes enter the CNS, they are able to become productively infected with HIV-1 [4]. Infected macrophages are able to remain latent and upon activation are able to maintain HIV-1 levels within the CNS.

CD14+/CD16+ Monocytes

It was found that HIV-inflicted individuals had higher percentages of activated CD14+/CD16+ and CD14+/CD69+ monocytes/macrophages; with individuals diagnosed with HAD having higher percentages than those with normal cognition (NC) [9-13]. In non-HIV-infected individuals, CD14+/16+ phenotype comprises approximately 10% of all monocytes and 1% of the total peripheral blood mononuclear cells. CD14 is the receptor for lipopolysaccharide (LPS) and CD16 is a FCγ receptor type III. An increase in CD14+/CD16+ expression has also been reported in Alzheimer's disease, Parkinson's disease, septicemia, atherosclerosis, rheumatoid arthritis, multiple sclerosis, Kawasaki disease and some cancers [14-19].

Ziegler-Heitbrock et al used flow cytometry to first describe CD14+/16+ monocytes in 1988 [20]. The cell surface molecules represent classical monocytes with increased HLA-DR, epidermal growth factor module-containing mucin-like receptor 2 (EMR2), Ig-like transcript 4 (ILT-4), CD43, CD45RA expression, and MDC8 expression [21]. Functionally, CD14+/16+ cells have been identified as a proinflammatory monocytes due increased amount TNF (inflammatory) and decreased amounts of IL-10 (anti-inflammatory) with a role as an antigen presenting cell (APC) [21]. CD14+/16+ monocytes are associated with their name of activated monocytes due to their role in increased inflammation. It has been demonstrated that CD14+/CD16+ monocytes are

more permissive to infection than CD14+/CD16- monocytes and more readily cross the BBB [17, 22, 23]. It is believed that CD14+/16+ cells transmigrate through the BBB and differentiate into perivascular macrophages. This transmigration concept is supported by the fact that CD14+/16+ cells exhibit the features of tissue macrophages [19]. Viral susceptibility within CNS expands to microglia and astrocytes, although productive infection has only been portrayed by macrophage and microglial cells. In addition, the presence of viral proteins results in the activation of microglia and astrocytes, causing alterations in cytokine and chemokine expression and instability of the BBB, all of which contribute to neuronal injury and death.

Mechanism of HAND

HIV-1 tropism involves binding to the CD4 primary receptor and a co-receptor. Monocytes, macrophages and microglia are primarily infected through the CCR5 co-receptor but there have been some speculation that CXCR4 may also be involved [24]. CXCR4 is the primary co-receptor for T-lymphocytes but is also expressed on neurons, microglia, astrocytes and brain endothelia. It naturally binds to stromal-derived factor (SDF-1) produced by astrocytes, macrophages, neurons, and Schwann cells [8]. Nonetheless, infections in monocytes/macrophages occur primarily through the CCR5 co-receptor that is expressed on neurons, microglia and astrocytes and binds to RANTES or MIP-1 [8]. It is believed that binding of these co-receptors by their natural ligands interfere with HIV/gp120 binding. When these receptors are activated by ligand engagement, the transcription factor MEF2C becomes activated leading to the production of inflammatory cytokines that activate adjacent macrophages, microglia, and astrocytes.

The p38 mitogen-activated protein kinase (MAPK) is identified as the involved signaling pathway. HIV-1 infection occurs in CD4+ immune cells but can also infect CD4- cells such as astrocytes, oligodendrocytes and brain endothelial cells; however, non-productive infections result [5].

HIV-1 infection of the central nervous system (CNS) occurs early during initial infection within a few days to weeks after infection but development of HAND does not occur until later [10, 23, 25]. Neuropathologic studies found HIV to be primarily contained within CD14+ (monocyte) cells in perivascular regions. Clay et al observed flourescein-labeled monocytes trafficking into choroid plexus stromata and perivascualar spaces of rhesus macaques at 12-14 days post-infection with simian immunodeficiency virus (SIV) [26]. These fluorescein-positive cells were also CD16-positive [26]. Currently, HIV is believed to traffic to the CNS through a "Trojan Horse" mechanism where monocytes, particulary the activated subset (CD14+/16+), transport the virus through the blood brain barrier (BBB), Figure 1.6. Monocytes that orginate from the bone marrow circulate through the blood and migrate through the BBB to replenish perivascular macrophages. Therefore, it is thought that HIV first infects peripheral monocytes, which then crosses the BBB and initiates CNS infection [10]. Analysis of HIV sequences from the gp160 V3 loop (hypervariable region 3) revealed that sequences from the marrow and deep white matter were more closely related than those from the choroid plexus, meninges, lymph node, lung or head of caudate [27]; thus supporting the Trojan Horse theory. Further analysis of gp160 showed that HIV brain isolates were macrophage-tropic because they code for the CCR5 co-receptor [10, 27]. The brain is compartmentalized and different CNS regions, including the CSF, appear to be impacted

uniquely [27, 28]. Thus, compartments within the brain structure may play different roles in neuropathogenesis.

Neuronal Injury/Death

Neuronal injury and death are thought to occur through both direct and indirect mechanisms. Direct mechanisms include the production of viral proteins such as gp120, Tat, Vpr and Nef, which have been shown to directly cause neuronal death through binding with the CXCR4 and CCR5 neuronal receptors, thus inducing neuronal signaling and apoptosis [29-31]. This is supported by studies showing inhibition of the viral protein and receptor interaction blocking neuronal apoptosis [32]. Viral proteins are also able to bind to NMDA receptors, causing increased calcium influx that leads to increased cytochrome c release from the mitochondria, formation of an apoptosome and activation of the caspase cascade. The role of NMDA receptors in neuronal damages led to the development of a NMDA receptor antagonist called memantine [33]. Indirect mechanisms occur when neurons are damaged as a consequence of inflammatory processes through the release of neurotoxins from macrophages, and microglial cells. These neurotoxins are primarily chemokines and proinflammatory cytokines such as TNF-α, IL-1β, IL-1α, IL-6 and TGFβ [9, 29, 34-36]. The overproduction of these cytokines results in neuronal injury and ultimately leads to death. In addition to cytokines, excitatory molecules such as glutamate, quinolate, platelet-activating factor and cysteine are also secreted and result in excitotoxicity [37, 38]. An overstimulation of glutamate receptors occurs upon the release of these excitants, causing excess calcium influx with subsequent caspase activation and p53 expression. Although perivascular

macrophages and parenchymal microglia are the only cells that productively produce virus, the other CNS cells such as astrocytes also contribute to neurodegeneration [5]. The normal roles of astrocytes are to maintain homeostasis in the CNS through regulation of neurotransmitters (primarily glutamate) and to keep the integrity of the BBB through their interactions with the brain microvascular endothelial cells (BMVEC). However, upon exposure to HIV, astrocytes become activated and begin producing cytokines such as TNF, resulting in increased glutamate secretion and decreased glutamate uptake [5, 36, 39]. Excessive glutamate in the CNS results in uncontrolled neuronal calcium influx and perturbance in homeostasis [36]. The dysfunction of astrocytes also affects their interaction with BMVEC and disrupts BBB integrity. Upregulation of adhesion molecules such as intracellular adhesion molecule 1 and vascular cell adhesion molecule 1 on BMVEC also leads to cytokine production [5, 39]. The increased adhesion molecules further disrupt the BBB and allow for greater monocyte binding and migration across the BBB. In summary, all of the above contribute to neuronal injury and death through increases in intracellular calcium uptake and in oxidative stress [37, 38].

Antiretroviral Therapy and its Influence on HAND

Classes of antiretroviral therapy (ART) include nucleoside and non-nucleoside reverse transcriptase inhibitors, protease inhibitors, chemokine receptor antagonists, maturation inhibitors, entry inhibitors, and integrase inhibitors, Figure 1.5. The US Department of Health and Human Services recommend that a combination of ART drugs should begin when CD4 count is $< 350/mm^3$ or plasma HIV RNA is > 100,000 copies per mL [7].

ART has proven to be successful through its effects in the reduction of HIV RNA levels and opportunistic infections by controlling viral replication. It has also decreased the incidence of HAD and improved cognitive function [40, 41]. Regardless, its effect on HAND prevalence has been rather unimpressive. It is known that not all drugs in ART regimens effectively cross the BBB and that it attenuates rather than fully suppresses viral replication [38, 42]. Treatment regimens containing protease inhibitors (PIs) were capable of reversing neurocognitive deficits; however, CSF concentrations of PIs are lower than plasma concentrations and active efflux pumps have the ability to eliminate PIs from the CNS [7]. The BBB presents an obstacle in which ART CNS delivery is limited [43, 44]. Letendre et al proposed a CNS penetration effectiveness (CPE) scoring system to approximate the CNS penetrance of ART drugs. Through this scoring system, they found that a higher CPE score resulted in lower CSF viral loads [45]. Despite the increased viral suppression with better CNS penetrating drugs, individuals are still capable of developing neurocognitive impairment suggesting that complications may contribute to chronic low-level infection [2]. It is speculated that neuronal damage prior to treatment occurs through direct HIV damage and neuronal damage after treatment occurs indirectly through chronic cellular activation [46]. There are also claims that ART drugs can cause direct neuronal toxcities due to their effects on mitochondrial polymerase [44]. The incomplete nature of ART-induced reversal of neurocognitive dysfunction may explain the increase in minor neurocognitive deficits such as asymptomatic neurocognitive impairment (ANI) and minor cognitive motor disorder (MCMD), all of which are classified into HAND. Since monocytes and macrophages are the primary targets for HIV in the CNS and are less vulnerable to ART therapy in comparison to

lymphocytes, it is proposed that these cells serve as a sanctuary or reservoir for the virus [42].

Viral Reservoirs

Though CNS human studies have provided valuable information in the realm of HAND, these are restricted to disease endpoints because samples are obtained when the individual has deceased. These limitations validate the importance of animal models such as simian immunodeficiency virus (SIV) in macaque. SIV studies have demonstrated macrophage involvement in encephalitis by showing that virus incapable of replicating in macrophages are incapable of causing SIV encephalitis (SIVE) [4]. In untreated animals, SIV RNA is measured in the brain parenchyma within days of infection and is decreased in the following days; however, SIV RNA levels are measurable several months later in animals with SIVE [7, 47]. Further studies have shown that SIV DNA persists regardless of controlled viral replication and reactivation of preexisting CNS strains leads to continued replication [48]. Regardless of ART treatment, SIV DNA was still detected at significant levels [49]. Unlike its effects on HIV RNA replication and levels, ART has proven to have little impact on HIV DNA, which may provide clues on mechanisms why eradication of the virus remains elusive. Subjects with HAND have higher circulating HIV DNA compared to those with NC [50, 51]. The persistence of HIV DNA suggests a role in HIV disease progression [52-56] and could be indicative of the presence of viral reservoirs; many of which are believed to lie in memory T-cells [42, 57-59], but the involvement of monocytes is highly undervalued. The fact that monocytes are less susceptible to cytopathic effects in comparison to CD4+ lymphoblasts [60, 61] and their

long-lived nature make them particularly interesting. Detection of low levels of HIV genes that are expressed late (multiply spliced RNA) suggests that infection may be active with low levels of replication occurring to replenish these reservoirs [42].

CNS Compartments

Imaging techniques have allowed researchers to study regions of the CNS that are most affected in individuals with HAND. Through these studies it has been proposed that the frontal cortex, basal ganglia, caudate nucleus, putamen, globus pallidus and substantia nigra are involved in neurodegeneration. Despite these claims, actual associations are difficult to make because many conflicting results exist. Nevertheless, the basal ganglia has repeatedly been reported to be a major target of HIV infection [62, 63], particularly the caudate nucleus as an area that has consistent reports of atrophy, decreased blood flow and viral load, which correlate to the degree of neurocognitive deficit in HIV-positive individuals [28, 64, 65]. These findings are of interest because the caudate has been shown to be an important component of the brain's learning and memory system [66].

Viral Integration

Previously, HIV was thought to integrate randomly within the host's genome; however, studies have reported preferential integration sites such as transcriptionally active genomic regions [67, 68], repetitive elements [69, 70], and those proximal to genes that are associated with the regulation of cellular processes such as transcription and translation [67]. In a study conducted by Mack et al, 15 chromosomal insertion sites were

identified in the CNS of an AIDS-dementia individual [67]. Furthermore, the tissue contained high amounts of HIV DNA and p24, which was predominantly localized to macrophages that were interspersed in a background of p24-negative neurons [67]. These data imply that pathogenesis of HAD may be induced through the mechanism of insertional mutagenesis, which occurs when HIV inserts itself into an essential coding region, causing gene disruption and dysregulation [71, 72].

Significance

The significance of this study continues to build upon our hypothesis that the pathogenesis of HAND involves peripheral events of monocyte trafficking, particularly activated monocytes (CD14+/16+), which harbor virus and migrate into the CNS. This hypothesis is supported by work showing that circulating CD14+/16+ subsets have increased HIV DNA; and others demonstrating that these activated cells are found in perivascular regions in the brain of individuals with neurocognitive problems. The goal is to further study and cauterize these cells involved in the development and progression to HAND by monitoring HIV DNA in CNS compartments and cellular subsets. To accomplish the set goal, several feasibility studies will be done to study CD14+/16+ cells in areas that have not been studied before. We believe that HIV DNA is indicative of persistent viral reservoirs, which prevent the eradication of the virus and contributes to HAND neuropathogenesis.

Based on current paradigms, HIV DNA may be a potential biomarker for neurocognitive diseases as it has been shown to correlate to disease severity independent of HIV RNA levels and CD4+ T-cell counts [56]. Although our previous studies

provided some insight into the pathogenic role of HIV DNA, further advances in understanding how viral DNA is involved in the mechanisms could benefit from improvements in molecular tools to measure HIV DNA. The results from our specific aims will continue to broaden our knowledge in HAND pathogenesis and additionally provide us with more powerful tools to assess HIV DNA. We hope to further understand viral transition from the periphery into the CNS and its contribution to HAND manifestation. The information gained through these studies can also be clinically translated and possibly indentify therapeutic targets to benefit patients in the future. Future research possibilities include HIV DNA as a potential screening and monitoring too for HIV-1 related neurocognitive decline and the initiation of alternate therapy protocols, which may be more effective in targeting the cells of interest. It is also possible to develop new drugs that inhibit the mechanistic action of CD14+/16+ monocytes. Furthermore, such information may also be pertinent to other neurocognitive disorders. Listed below are the specific aims of this study:

Specific Aim 1: To assess if HIV DNA levels in the cerebrospinal fluid (CSF) match levels in peripheral mononuclear cells (PBMCs) from subjects along the spectrum of HAND (HIV-associated dementia, HAD; minor cognitive motor disorder, MCMD; and normal cognition, NC).

a. To determine which monocyte subsets contribute to high HIV DNA copy numbers in CSF cells of individuals with HAND (CD14+/16+ monocytes, CD14+/16- monocytes, and CD14- lymphocytes).

Hypothesis: HIV DNA in CD14+/16+ monocytes will be highest in subjects with HAND

and will be mirrored by levels measured in CSF.

Specific Aim 2: To assess HIV DNA in CNS compartments, which correspond to neurocognitive deficits, characterized by HAND.

Hypothesis: HIV DNA will be highest in CD14+/16+ monocytes isolated from the basal ganglia with lower copy numbers in the frontal cortex.

Specific Aim 3: To identify HIV-1 integration sites in activated monocytes and if preferential sites are found in subjects with HAND.

Hypothesis: HIV-1 will preferentially integrate near regulatory or cytokine genes, which will result in an altercation of their expression resulting in a selective advantage for the cell with that integration.

Specific Aim 4: To assess the feasibility of an HIV DNA assay using a peptide nucleic acid (PNA) probe in combination with flow cytometry to analyze PBMC and CSF cells.

Hypothesis: The PNA-probe based flow assay will be as sensitive as the real-time PCR assay currently used.

Figure 1.1 – Global estimates for 1990-2008 of prevalence, incidence, and AIDS deaths. Obtained from the 2009 AIDS epidemic update, UNAIDS/WHO.

Figure 1.1

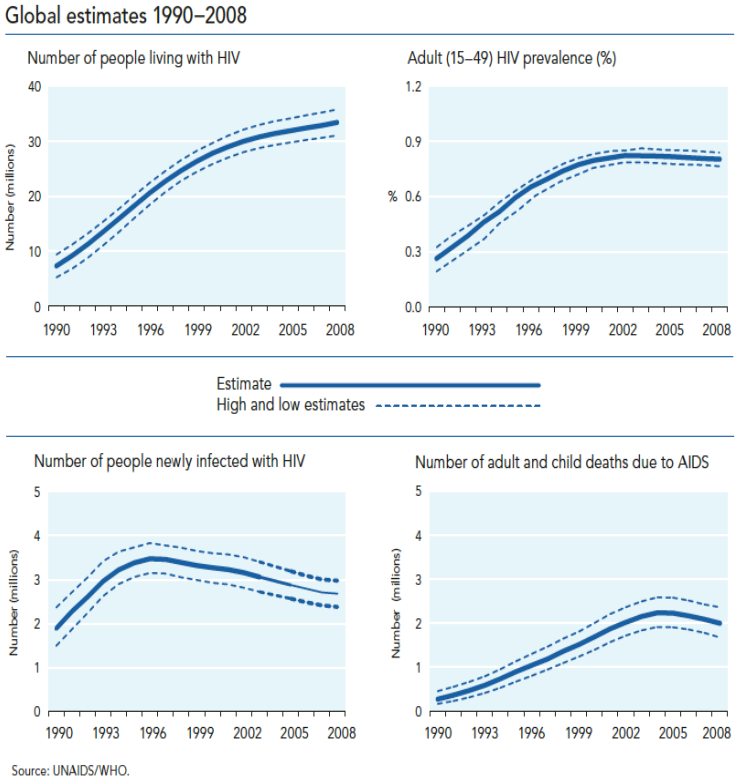
Global estimates 1990–2008
Number of people living with HIV
Number (millions)
40
30
20
10
0
1990 1993 1996 1999 2002 2005 2008
Adult (15–49) HIV prevalence (%)
%
1.2
0.9
0.6
0.3
0.0
1990 1993 1996 1999 2002 2005 2008
Estimate
High and low estimates
Number of people newly infected with HIV
Number (millions)
5
4
3
2
1
0
1990 1993 1996 1999 2002 2005 2008
Number of adult and child deaths due to AIDS
Number (millions)
5
4
3
2
1
0
1990 1993 1996 1999 2002 2005 2008
Source: UNAIDS/WHO.

Figure 1.2 – Worldwide estimates of adults and children living with HIV. Obtained from the 2009 AIDS epidemic update, UNAIDS/WHO.

Figure 1.2

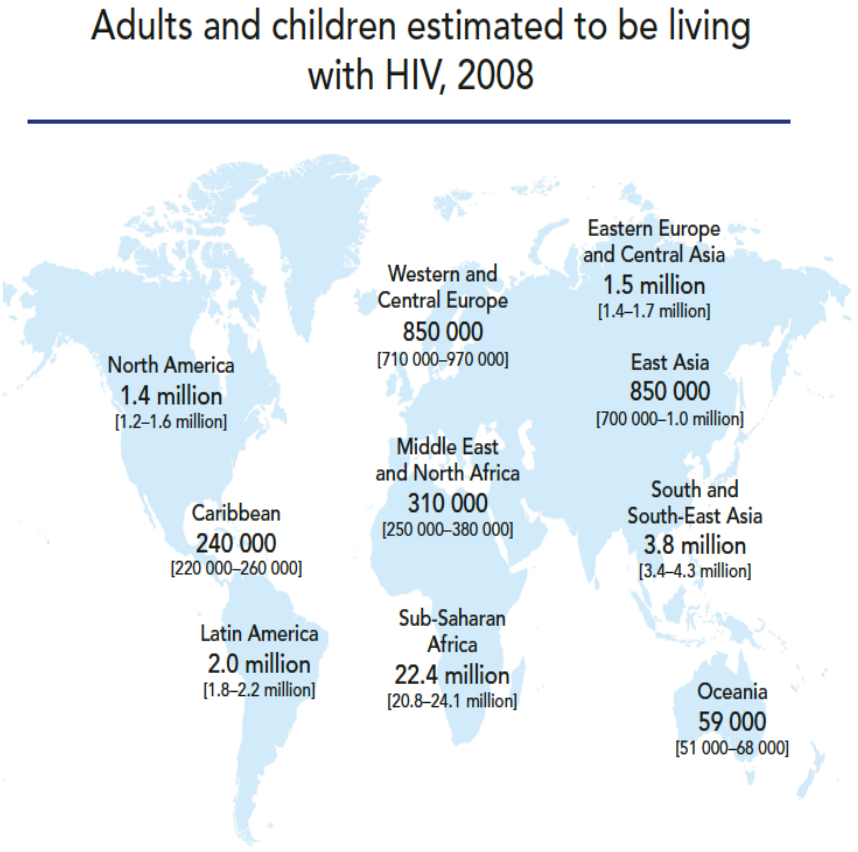
Adults and children estimated to be living with HIV, 2008
North America
1.4 million
[1.2–1.6 million]
Caribbean
240 000
[220 000–260 000]
Latin America
2.0 million
[1.8–2.2 million]
Western and Central Europe
850 000
[710 000–970 000]
Middle East and North Africa
310 000
[250 000–380 000]
Sub-Saharan Africa
22.4 million
[20.8–24.1 million]
Eastern Europe and Central Asia
1.5 million
[1.4–1.7 million]
East Asia
850 000
[700 000–1.0 million]
South and South-East Asia
3.8 million
[3.4–4.3 million]
Oceania
59 000
[51 000–68 000]

Figure 1.3 – Worldwide estimates of adults and children newly infected with HIV. Obtained from the 2009 AIDS epidemic update, UNAIDS/WHO.

Figure 1.3

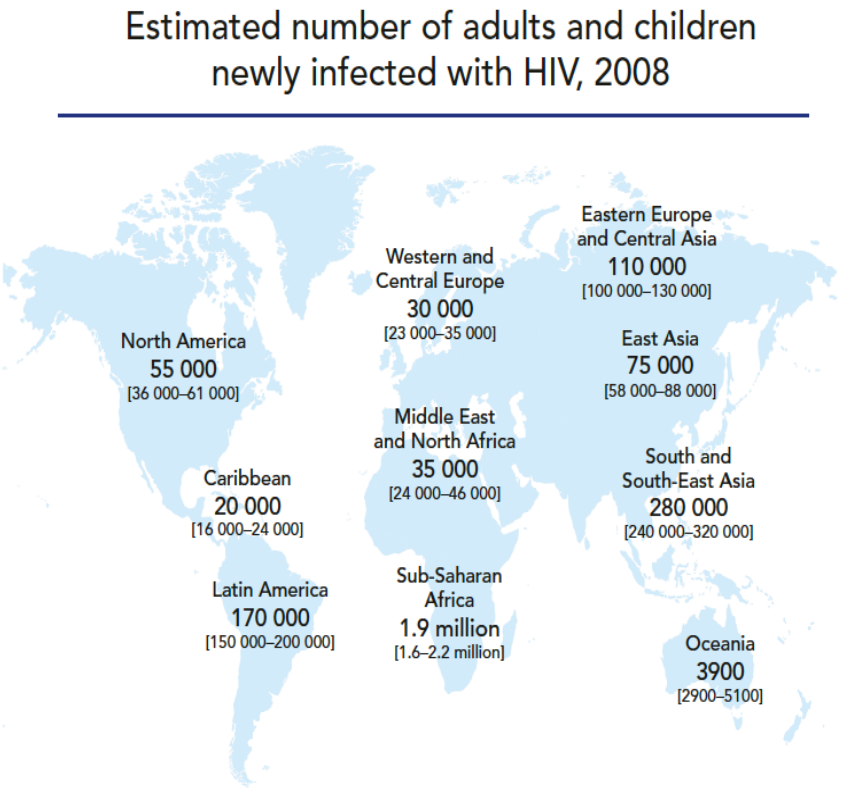
Estimated number of adults and children newly infected with HIV, 2008
North America
55 000
[36 000–61 000]
Western and Central Europe
30 000
[23 000–35 000]
Eastern Europe and Central Asia
110 000
[100 000–130 000]
East Asia
75 000
[58 000–88 000]
Middle East and North Africa
35 000
[24 000–46 000]
South and South-East Asia
280 000
[240 000–320 000]
Caribbean
20 000
[16 000–24 000]
Latin America
170 000
[150 000–200 000]
Sub-Saharan Africa
1.9 million
[1.6–2.2 million]
Oceania
3900
[2900–5100]

Figure 1.4 – Genome structure of human immunodeficiency virus type 1 (HIV-1) with its flanking long terminal repeats (LTR). Obtained from Wikipedia (http://en.wikipedia.org/wiki/File:HIV_genome.png).

Figure 1.4

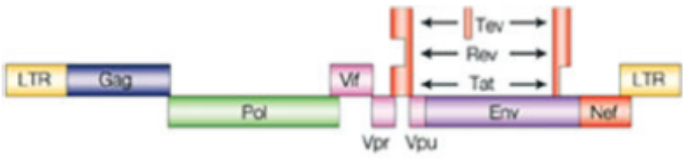

Figure 1.5 – Flow chart of the life cycle of human immunodeficiency virus (HIV) showing target sites for therapeutic intervention. Obtained from De Clercq, E., *The design of drugs for HIV and HCV*. Nat Rev Drug Discov, 2007. **6**(12): p. 1001-18.

Figure 1.5

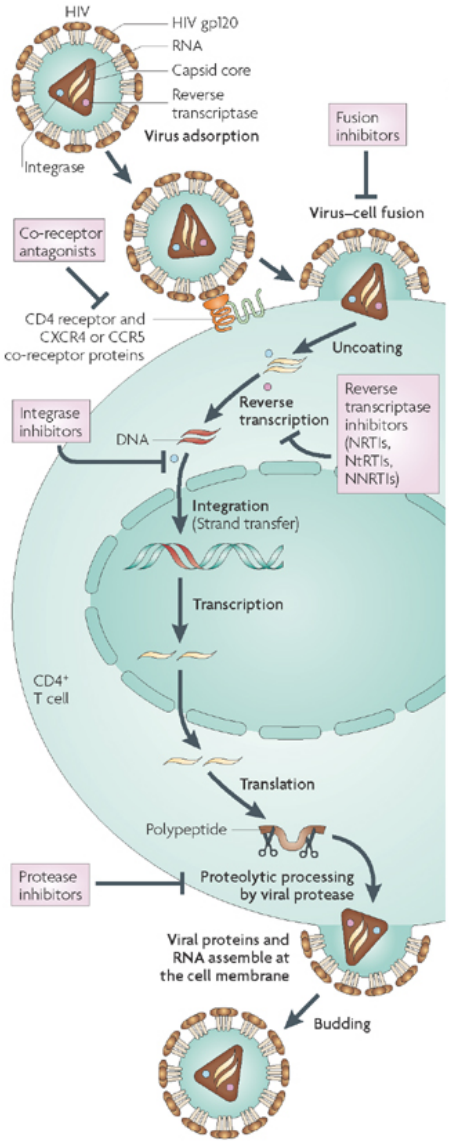

De Clercq, E., *Nat Rev Drug Discov, 2007.*

Figure 1.6 – An illustration depicting the believed Trojan Horse mechanism theory for neurodegeneration in HIV-infected individuals showing a) HIV-infected activated monocytes migrating into the central nervous system (CNS) where they differentiate inot perivascular macrophages or microglial cells and releases viral proteins, cytokines, chemokines, and excitatory amino acids and molecules, which b) activates other microglial cells and astrocytes resulting in c) astrocyte dysregulation or astrocytosis and causes d) increased calcium, glutamate and neurotoxin release, ultimately leading to neuronal apoptosis. It should be noted that e) several neuroprotective pathways exist.

Figure 1.6

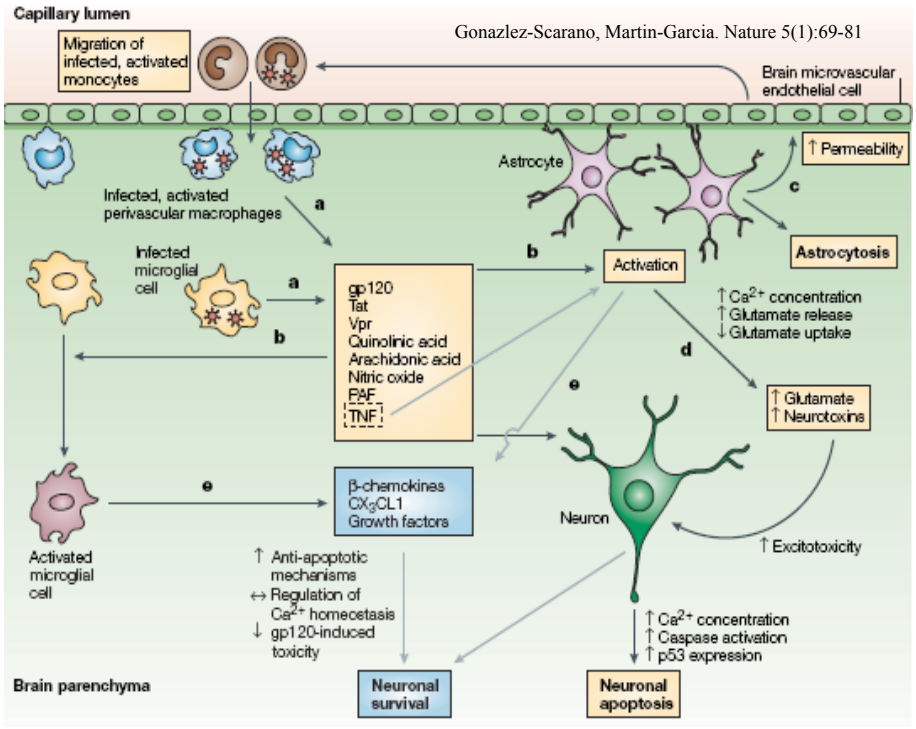
Capillary lumen
Gonazlez-Scarano, Martin-Garcia. Nature 5(1):69-81
Migration of infected, activated monocytes
Brain microvascular endothelial cell
Astrocyte
↑ Permeability
Infected, activated perivascular macrophages
a
c
Astrocytosis
Infected microglial cell
b
Activation
gp120
Tat
Vpr
Quinolinic acid
Arachidonic acid
Nitric oxide
PAF
TNF
↑ Ca2+ concentration
↑ Glutamate release
↓ Glutamate uptake
d
e
↑ Glutamate
↑ Neurotoxins
β-chemokines
CX3CL1
Growth factors
Neuron
Activated microglial cell
↑ Excitotoxicity
↑ Anti-apoptotic mechanisms
↔ Regulation of Ca2+ homeostasis
↓ gp120-induced toxicity
↑ Ca2+ concentration
↑ Caspase activation
↑ p53 expression
Brain parenchyma
Neuronal survival
Neuronal apoptosis

CHAPTER 2

Peripheral Blood Mononuclear Cells and Cerebrospinal Fluid Cellular HIV DNA in Neurocognitive Disorders

Abstract

Background: It has previously been shown that HIV DNA within peripheral monocytes, particularly those of the activated subset, corresponded to an individual's neurocognitive status. In this study, we demonstrate this through the use of peripheral blood mononuclear cells (PBMC) and report for the first time the feasibility of separating cerebrospinal fluid (CSF) cellular subsets (activated monocytes, CD14+/16+; non-activated monocytes, CD14+/16-; and non-monocytes, CD14-) and measuring HIV DNA in each cellular compartment. **Materials and Methods:** 53 PBMC and 12 CSF samples were analyzed. PBMC samples were obtained from HIV-positive individuals with HAND (n=29) and with normal cognition, NC (n=24). CSF samples were also obtained from individuals with HAND (n=6) and with NC (n=6) that were enrolled in established cohorts from the University of Puerto Rico (n=6) or the University of Hawaii (n=6). Samples were sorted and HIV DNA levels were measured using a multiplex real-time PCR assay. **Results and Conclusions:** In the PBMC HAND samples, differences in the average HIV DNA levels between the cell fractions were significant ($p<0.0001$) with highest levels in CD14+/16+ cells. The average HIV DNA levels in NC samples were also significant ($p=0.02$) with highest levels in CD14+/16- cells. On the other hand, CSF samples contained highest average HIV DNA levels in CD14+/16- cells regardless of

diagnosis. High CD14+/16+ HIV DNA levels may reflect the amount of inflammation, while high CD14+/16- levels may reflect reservoir formation.

Overview

Clinical improvements associated with active anti-retroviral therapy (ART) are reflected in the reduced incidence of HIV-associated neurocognitive disorders (HAND). Despite these advancements, there is an increased prevalence of HAND. The increased prevalence occurs in the less severe forms of HAND, such as asymptomatic neurocognitive impairment (ANI) and minor cognitive motor disorder (MCMD) [73]. The continued presence of HAND suggests that even with effective ART, other factors may be impacting the neuropathogenesis of HAND. One such influence may be presence of chronic neuro-inflammation due to low-level but active HIV-1 replication.

Early in the evaluation of ART-era cognitive impairment, the percentages of a unique population of peripheral activated monocytes with the $CD14^{+}/16^{+}$ phenotype were noted to be elevated in subjects with HIV-associated dementia (HAD) [11]. Monocytes are known to be a site of latent HIV-infection and activated monocytes are particularly permissive to HIV-infection [5, 74, 75]. Our lab has also done extensive work verifying the involvement of CD14+/16+ cells in HAD [51, 76-78]. These studies support the Trojan Horse theory that purposes CD14+/16+ cell involvement in trafficking HIV-1 into the CNS [5].

Neuenburg et al also reported the increased percentages and numbers of activated monocytes in cerebrospinal fluid (CSF) from HIV-infected patients receiving ART [12]. In other studies, monocytes were shown to traffic to the choroid plexus stroma and perivascular spaces, where many of the infiltrating monocytes in the choroid plexus were activated [26, 79]. Adhesion molecules (E-selectin and P-selectin) and increased cytokine production (MCP-1) are thought to be involved in leukocyte recruitment into the

choroid plexus [26, 80, 81]. Once through the blood-brain barrier via monocytes, HIV-1 is then transported into the choroid plexus and into the CSF. Studies on viral evolution suggest that cellular compartmentalization within the CSF evolves and that the CSF serves as a unique reservoir for cells with latent virus possibly contributing to viral persistence within the CNS [82-86].

These CNS-infiltrating monocytes with HIV DNA may contribute to viral reservoirs in spite of effective ART. In simian immunodeficiency virus (SIV) studies, monocytes with SIV DNA represented viral reservoirs when low-level viral replication was demonstrated from the cells [49, 74]. These findings suggest that ongoing viral replication contributes to chronic inflammation with viral protein production, which could contribute to neuronal damage.

Because CSF monocytes are known to have slower CSF-compartmentalized variant viral decay from individuals with HAND, we hypothesize that CSF $CD14^{+}/16^{+}$ cells may be important in neuropathogenesis [82]. Thus, designing a strategy to identify CSF $CD14^{+}/16^{+}$ cells and assessing HIV DNA levels in cellular subsets was the focus of this exploratory study. In this chapter, a method is described to measure HIV DNA in CSF cells; the results will then be compared against results obtained from PBMC HIV DNA to determine if the same observations are made. A diagram illustrating the procedure is shown in Figure 2.1. This technique could potentially be a tool to investigate the role of HIV DNA in the pathogenesis of HAND. The small amounts of cells make CSF studies extremely limited, especially studies that separate the cells into various monocytic cell fractions. It is essential then to prove feasibility of measuring HIV DNA within various CSF cell fraction as its future application can shed light on HIV-1

evolution and on the behavior on monocytes in the periphery and CSF, which will assist with our current knowledge reservoir formation within the CNS.

Materials and Methods

PBMC Samples. Frozen PBMC cells stored in PBS and DMSO were obtained from subjects enrolled in the Hawaii Aging with HIV Cohort, University of Hawaii (UH). All the patients signed informed consent forms under the guidelines of the University of Hawaii Institutional Review Board. Samples included PBMC from individuals diagnosed with HIV-associated neurocognitive disorders or HAND (n=22) and normal cognition or NC (n=39).

CSF Samples. Frozen CSF cells stored in PBS and DMSO (10 mL CSF) were obtained at entry from 12 subjects enrolled in longitudinal HIV-1-infected cohorts from two sites, Hispanic-Latino Longitudinal Cohort of HIV-seropositive women (HLLC, n=6), University of Puerto Rico Medical Sciences Campus (UPRMSC) and the Hawaii Aging with HIV Cohort (HAHC, n=6), University of Hawaii. After signing informed consents, each subject underwent a macroneurological exam, which included a lumbar puncture. They also completed a battery of neuropsychological tests as per guidelines established by the Institutional Review Boards at each respective institution [87, 88]. The two cohorts were previously described [89, 90]. Briefly, subjects from HAHC were living in Hawaii, ≥ 50 years or between 20-30 years, and were excluded for the following: history of head injury, learning disability, major neurologic/psychiatric disease, or opportunistic brain disease. In addition to the exams noted above, baseline evaluations also included medical history, risk behavior inventory, viral load, CD4 count, nadir CD4 count, medication history, and co-morbid illnesses. While demographically different, HLLC subjects also underwent similar evaluations as the subjects enrolled in the HAHC. The

current study was a cross-sectional study to determine the feasibility of measuring HIV DNA in CSF cellular subsets.

HIV-Associated Neurocognitive Disorder Assessment. Cognitive function was determined using the American Academy of Neurology HIV dementia criteria (1991) as described previously [91] into normal cognition (NC), minor cognitive motor disorder (MCMD), and HIV-associated dementia (HAD) following review of all of the clinical data at a consensus conference as previously reported [87, 89].

Magnetic Cell Sorting. A modified protocol from EasySep human monocyte enrichment kit without CD16 depletion (StemCell Technologies, Vancouver, BC, Canada) was used for magnetic separation. Patient frozen PBMC cells were first thawed in 20% fetal bovine serum (FBS), resuspended and treated for 10 minutes with Accumax (Innovative Cell Technologies, Inc., San Diego, CA) at 37°C (10 minutes) and filtered through a 30 um CellTrics filter (Partec, Germany). The cells were resuspended in 2 mL 2% FBS, PBS, and 1 mM EDTA and placed in a 5 mL polystyrene tube. Prior to surface receptor labeling, anti-CD32 blocking was added and incubated at room temperature (5 minutes). Then 100 uL of EasySep human monocyte enrichment cocktail without CD16 depletion and 1.2 uL of biotinylated CD16 antibody (Biolegend, San Diego, CA) were added and cells were incubated at room temperature (10 minutes). Cells were washed with 2% FBS, 1mM EDTA, and PBS; fixed with 2% PFA, PBS and incubated at room temperature (5 minutes). After two washes the first separation that sorts the monocytes (CD14+) from the non-moncytes (CD14-) occurred through the addition of EasySep D

magnetic particles and incubation of the tubes in the EasySep magnet for 2.5 minutes at room temperature. The tube still remaining in the magnet is then decanted into another tube, which serves as the CD14+ cells. The CD14- tube is kept for further analysis, while the CD14+ tube undergoes a second separation that sorts the CD14+ cells into activated (CD14+/16+) and non-activated (CD14+/16-) cell fractions. This occurs through the addition of a siMAG streptavidin magnetic bead (Chemicell, Berlin, Germany) that binds to the CD16-biotin antibody. The tube is placed in EasySep magnet for 2.5 minutes and is decanted into another tube serving as the CD14+/16-. The tube in the magnet contains the CD14+/16+ cells. After the two separations, all the tubes (CD14-, CD14+/16+, and CD14+/16-) are spun down in preparation for DNA extraction.

Fluorescent Activated Cell Sorting (FACS). Frozen CSF cells were thawed in 100% FBS, treated for 10 minutes with Accumax (Innovative Cell Technologies, Inc., San Diego, CA) and filtered through a 30 um CellTrics filter (Partec, Germany). Cell staining followed with anti-CD3-PerCp/Cy5.5, anti-CD14-FITC and anti-CD16-PE (BioLegend, San Diego, CA) for 20 minutes at room temperature, washed with 2% FBS, PBS and fixed with a 2% paraformaldehyde (PFA) solution. After fixation, the cells were diluted with PBS and underwent cell sorting using the FACSAria (BD Biosciences, San Jose, CA) to get the desired cell populations: non-monocytes (CD14-), activated monocytes (CD14+/16+), and non-activated (CD14+/16-) monocytes. Acquisition started with gating on CD14+ and CD14-. The CD14+ cells underwent a second sort into CD14+/16+ cells and CD14+/16- cells. The CD14- cells were ensured to be CD14- through a second

CD14- sort, Figure 2.2. The cells were sorted directly into lysis buffer in preparation for DNA extraction.

HIV DNA Extraction and Quantification. DNA was extracted from the PBMC and CSF cell fractions using the QIAamp DNA Micro Kit (Qiagen, Valencia, CA) as per guidelines by the manufacturer and eluted 30 uL TE buffer for the PBMC cells and in 20 uL TE buffer for the CSF cells.

To quantify HIV DNA, we designed a multiplex real-time PCR assay modified from our previous singleplex assay [92, 93]. While both assays yield identical amplification curves for the *b-globin* housekeeping gene and *gag* HIV gene (Appendix A); the multiplex PCR greatly reduces time and labor, making HIV-DNA quantification more efficient and possibly more clinically useful.

Briefly, two standard curves were generated using a cocktail of two different plasmids each containing a single copy of gag gene (HXB2, GenBank accession #K03455) or a single copy of b-globin gene (GenBank accession #2253431); with 1:10 dilutions from 1 X 10^6 copies to 1 X 10^1 copies. Standards and unknowns were set up in triplicate containing 2x TaqMan® Gene Expression Master Mix, 1.25 pmol of Gag primers, 0.625 pmol B-globin primers, 1.25 pmol of each probe (b-globin and Gag), 3 uL of DNA and water for a final volume of 10 uL. The primers amplified a 111 bp gag segment (5'-GACATCAAGCAGCCATGCAA-3' and 3'CTCA TCT GGC CTG GTG CAA T-5') and a 109 bp b-globin segment (5'-TCA CTA GCA ACC TCA AAC AGA CAC C-3' and 3'-AGG GCC TCA CCA CCA ACT TC-5'). Reactions were run in a StepOne™ Real-Time PCR System (Applied Biosystems, Foster City, CA) with PCR cycling parameters of:

95°C for 15 min; 40 cycles of 95°C for 1 min, and 60°C for 1 min. Analyses were done using the StepOne™ Real-Time PCR System software. The copy numbers of each gene of the unknowns were determined from the standard curves. HIV DNA copy numbers were calculated from each run suing appropriate positive and control DNA: 8E5, T-lymphoblastoid cell line containing approximately one copy of HIV per cell; and HIV-negative DNA from control peripheral blood mononuclear cells, respectively.

Statistical Analyses. PBMC HIV DNA data was analyzed through the use of non-parametric Kruskal-Wallis test and the Wilcoxon (rank sums) pairwise comparison test. The HIV DNA data obtained from CSF cells were assessed from subjects with HAND and NC and analyzed using the Generalized Estimating Equations (GEE) model and WALD test.

Results

PBMC HIV DNA. For HIV-positive normal cognition (NC) individuals, there was a significant difference in HIV DNA levels between all the cell fractions ($p=0.02$) with the average HIV DNA levels being highest in the non-activated monocytes (CD14+/16-) in comparison to the non-monocytes (CD14-) and activated monocytes (CD14+/16+), Figure 2.3. A significance difference ($p<0.5$) was observed between the CD14+/16- and CD14+/16+ monocytic cell fractions. For HAND individuals, there was a significant difference in HIV DNA levels between all cell fractions ($p<0.0001$) with the highest HIV DNA levels found in activated monocytes (CD14+/16+) with significant differences across all cell fractions ($p<0.01$), Figure 2.4.

CSF Subject Demographics. Gender, age, CNS penetration-Effectiveness (CPE) score of ART, and clinical characteristics are summarized in Table 2.1. CPE score was calculated based on guidelines set by Letendre et al [45]. All of the HLLC subjects and 1 of the 6 HAHC subjects were females. Six subjects were from UPRMSC HLLC and diagnosed with MCMD (n=1), HAD (n=2), or NC (n=3); six subjects were from UH HAHC and diagnosed with HAD (n=3) or NC (n=3). With the exception of patients PR6 and H5, all patients were on ART at the time of the LP. The majority of the CSF specimens had relatively low CSF WBC with only 3 (PR4, PR6, H6) subjects having mild CSF pleocytosis. Overall, most subjects had concordant undetectable plasma and CSF viral levels. There were 3 subjects with discordant plasma and CSF HIV RNA levels (PR3, PR6, H6).

HLLC CSF Specimens. In the subjects with HAND (PR4-6) and one subject with NC (PR2), the highest HIV DNA copies per cell were found in the $CD14^{+}/16^{-}$ subsets with the lowest copies of HIV DNA found in non-monocytic cellular subsets ($CD14^{-}$), Table 2.2 and Figure 2.5. All of the subjects diagnosed with HAND had higher percentages of activated monocytes ($CD14^{+}/16^{+}$) compared to subjects with NC (PR1-3), Figure 2.6. In contrast, the subjects with NC had higher $CD14^{-}$ and non-monocytic cells ($CD14^{+}/16^{-}$) percentages, Figure 2.6.

HAHC CSF Specimens. From subjects with HAD (H4-6), HIV DNA was detected only in the $CD14^{+}/16^{-}$ fraction in patient H4 and the $CD14^{-}$ fraction in H6, however this may reflect the minimal number of cells recovered from sorting, Table 2.3. Similar to the HIV DNA data from the UPRMSC specimens, a slight increase in HIV DNA copy numbers were found in $CD14^{+}/16^{+}$ cells compared to $CD14^{-}$ cells from the NC subjects, Figure 2.7. Subjects with NC (H1-3; n=3) had higher amounts of $CD14^{+}/16^{+}$ and $CD14^{+}/16^{-}$ cells compared to those diagnosed with HAD (H4-6; n=3) who had higher amounts of $CD14^{-}$ cells, Table 2.3, Figure 2.6. Overall, regardless of cohort and diagnosis, levels of HIV DNA copies were significantly higher in $CD14^{+}/16^{-}$ cells compared to $CD14^{-}$ subsets, $p=0.03$, Figure 2.8.

Discussion

This proof-of-concept study demonstrated the ability to measure HIV DNA from sorted CSF cellular subsets. Our data suggest that levels of HIV DNA in different CSF cellular subsets may vary across the spectrum of HAND. It was hypothesized that the CSF data would complement PBMC cellular subset data previously reported showing high HIV DNA copy numbers in circulating activated monocytes in subjects with HAND [76, 94]. We acknowledge that the current study was not designed or powered to compare CSF with PBMC cellular subset HIV DNA, thus future studies are planned to assess concordance or discordance between circulating monocytes and CSF monocytes. The methods could be used as a tool to study longitudinal cohorts with access to more specimens to determine the significance of these cellular subsets in viral persistence.

The data obtained from the various PBMC cell fractions of HAND and HIV-positive normal cognition (NC) individuals were as expected, with the highest HIV DNA levels in the activated monocytes (CD14+/16+) in HAND individuals. While NC individuals had highest HIV DNA levels in non-activated monocytes (CD14+/16-). It is suggested from these results that peripheral monocytes generally contain the highest levels of HIV DNA in comparison to the other cell fractions, which are primarily comprised of T-lymphocytes. A finding that may be contributed to the longer-lived nature of monocytic cells, their higher resistance of antiretroviral therapy (ART) drugs, and higher permissiveness to HIV-1 infection. However, the divergence in HIV DNA between HAND and NC individuals occurs at the level monocytic activation where the HAND individuals contain the highest HIV DNA levels in CD14+/16+ cells. Interestingly, the majority of HIV DNA in HAND CD14+/16- cells was undetectable;

therefore, the majority of their monocytes are activated and infected with HIV. This results in a greater inflammatory reaction and may provide an explanation for their neurocognitive states. This data stresses the importance of monocytes in the development of HAND and supports immune overstimulation that leads to inflammation, which indirectly causes neuronal apoptosis [5].

Since monocytes are able to enter the CSF through the choroid plexus, they are able to establish viral reservoirs within the CSF where HIV-1 is able to evolve [82, 83, 95]. It would be of interest then to analyze HIV DNA within various CSF monocytic cell fractions to find any relation to PBMC monocytic cell fractions in the context of HAND. Currently, this is the first report of HIV DNA levels measured from CSF cellular fractions. The high levels of HIV DNA copies from $CD14^{+}/16^{-}$ cells compared to $CD14^{-}$ subsets were found in both cohorts, HLLC and HAHC, however this difference was primarily observed in subjects with HAND from HLLC and in the NC group from HAHC. The limited number of specimens precludes any conclusions being drawn, but we speculate that multiple factors might contribute to differences in HIV DNA copies in different cellular subsets including gender, ethnicity, and/or ART. In the subjects with high HIV DNA copies in the $CD14^{+}/16^{-}$ monocytes, we hypothesize that these subsets may represent an accumulating viral reservoir in the CSF suggestive of viral persistence leading to viral evolution and while in the CSF, lose their activation phenotype. The efficacy and mechanisms of controlling HIV infection in the brain remains unknown, but likely the combination of ART and immune function are involved in restricting viral replication as is observed with undetectable CSF viral loads and decreased numbers of activated CSF monocytes.

We also speculate that the differences seen between the percentages of $CD14^+/16^+$ cells from the HLLC and HAHC subjects might reflect current or ongoing HAND. In the HLLC cohort, the individuals diagnosed with HAND contained higher percentages of $CD14^+/16^+$ cells, while the HAHC cohort demonstrated higher $CD14^+/16^+$ percentages in individuals diagnosed with NC. Again, the numbers were small but influence of ART, level of chronic activation, and all of the HAHC NC individuals progressed to HAND within the next year might suggest the transient change of monocyte activation phenotype in the CSF.

CSF viral reservoirs may play a role in HAND pathogenesis because these latent cells upon activation, are able to maintain low levels of viral replication. Because these reservoirs persist in the CSF and harbor HIV variants, others have suggested that CSF compartmentalization develops [82]. The evolution of CSF variants may contribute to resistant viral strains. Therefore, we hypothesize that infiltrating monocytes, particularly activated monocytes ($CD14^+/16^+$) from the choroid plexus could contribute to the inflammatory milieu and HIV DNA levels in the non-activated monocytes ($CD14^+/16^-$) may be represent latent viral reservoirs that allows the virus to evolve. The methods developed in the current study could be implemented in longitudinal studies or retrospective studies of HAND cohorts designed to determine the significance of HIV DNA in CSF cellular subsets in neuropathogenesis.

Table 2.1 Clinical Parameters of Subjects

Patient	ART	CPE Score[1]	Diagnosis	Gender	Age	CD4 Nadir (cells/mm)	CD4 (cells/mm)	CSF WBC[2]	Viral Load (copies/mL)	
									CSF	Plasma
PR1	EFV,TDF+FTC	1	NC	F	44	28	194	2	UND	UND
PR2	ABC+3TC,ATV	2	NC	F	40	69	134	3	11,871	100,000
PR3	AZT+3TC,NFV	1.5	NC	F	25	379	379	1	UND	76,563
PR4	SQV,LPV/r,TDF +FTC	1.5	MCMD	F	34	111	197	6	UND	UND
PR5	ATV,ABC+3TC	2	HAD	F	42	111	314	4	UND	UND
PR6	None	N/A	HAD	F	51	300	337	10	UND	413
H1	LPV/r,EFV	1.5	NC	M	53	137	742	0	UND	UND
H2	ABC,IDV,EFV,RTV	2.5	NC	M	61	151	331	2	UND	UND
H3	AZT+3TC,EFV	2	NC	M	37	302	628	1	UND	UND
H4	TDF,EFV,ddI	0.5	HAD	M	35	72	98	0	299	85,386
H5	3TC,d4T,NFV	1	HAD	M	38	197	262	1	UND	137
H6	TDF,d4T,LPV/r	1.5	HAD	F	37	34	40	9	2,561	125,872

[1]Based on classification by Letendre et al (Letendre, Marquie-Beck et al. 2008); [2]White blood cell (WBC) values are counts per mL; [3]Viral Load (VL) were considered undetectable (UND) if they contained copies ≤ 50 copies/mL; EFV: Efavirenz, TDF: Tenofovir, FTC: Emtricitabine, ABC: Abacavir, 3TC: Lamivudine, ATV: Atazanavir, AZT: Zidovudine, NFV: Nelfinavir, SQV: Saquinavir, LPV/r: Lopinavir/Ritonavir, IDV: Indinavir, RTV: Ritonavir, ddI: Didanosine, d4T: Stavudine

Table 2.2. HLLC CSF HIV DNA Results

Patient	CSF Cell Fraction	CSF Cell Count	HIV DNA per Cell	Diagnosis
PR1	CD14-	33	0.4	[2]NC
	CD14+/16+	0	[1]UND	
	CD14+/16-	18	[1]UND	
PR2	CD14-	595	0.2	[2]NC
	CD14+/16+	4	1.8	
	CD14+/16-	1	16.9	
PR3	CD14-	825	0.9	[2]NC
	CD14+/16+	0	[1]UND	
	CD14+/16-	7	0.7	
PR4	CD14-	1648	0.2	[3]MCMD
	CD14+/16+	93	1.1	
	CD14+/16-	68	5.0	
PR5	CD14-	488	0.3	[4]HAD
	CD14+/16+	212	0.6	
	CD14+/16-	55	2.5	
PR6	CD14-	1050	6.6	[4]HAD
	CD14+/16+	65	9.7	
	CD14+/16-	236	11.9	

PR: Puerto Rico; [1]Undetermined; [2]Normal Cognition; [3]Minor Cognitive Motor Disorder; [4]HIV-Associated Dementia;

Table 2.3. HAHC CSF HIV DNA Results

Patient	CSF Cell Fraction	CSF Cell Count	HIV DNA per Cell	Diagnosis
H1	CD14-	40	8.6	Entry - [2]NC Yr 3 - MCMD
	CD14+/16+	5	11.0	
	CD14+/16-	10	12.1	
H2	CD14-	612	1.5	Entry - [2]NC Yr 2, 3 – [3]MCMD Yr 4 - [4]NPA
	CD14+/16+	74	1.8	
	CD14+/16-	36	1.9	
H3	CD14-	2134	1.1	Entry - [2]NC Yr 3 – [4]NPA Yr 4 - [3]MCMD
	CD14+/16+	44	1.1	
	CD14+/16-	105	1.8	
H4	CD14-	222	[1]UND	Entry - [5]HAD
	CD14+/16+	5	[1]UND	
	CD14+/16-	8	2.3	
H5	CD14-	720	[1]UND	Entry - [5]HAD Yr 3 – [4]NPA Yr 4 - [3]MCMD
	CD14+/16+	3	[1]UND	
	CD14+/16-	19	[1]UND	
H6	CD14-	13	0.8	Entry - [5]HAD
	CD14+/16+	0	[1]UND	
	CD14+/16-	0	[1]UND	

H: Hawaii; [1]Undetermined; [2]Normal Cognition; [3]Minor Cognitive Motor Disorder; [4]Neuropsychologically abnormal; [5]HIV-Associated Dementia;

Figure 2.1 – Flow chart illustrating the cell sorting process to separate the cells into three different cell fractions that include non-monocytes (CD14-), activated monocytes (CD14+/16+), and non-activated monocytes (CD14+/16-); followed with DNA extraction and determination of HIV DNA copy number.

Figure 2.1

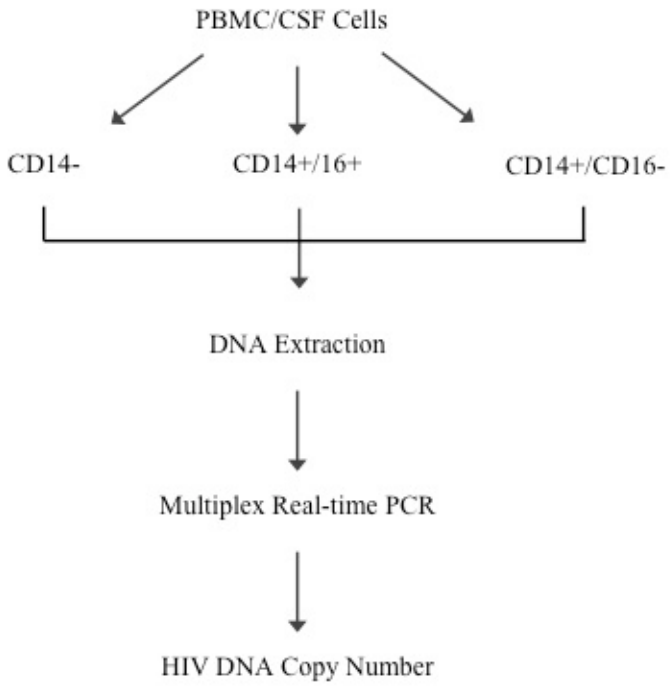
PBMC/CSF Cells
CD14-
CD14+/16+
CD14+/CD16-
DNA Extraction
Multiplex Real-time PCR
HIV DNA Copy Number

Figure 2.2 – Fluorescence activated cell sorting (FACS) strategy to obtain various CSF cell populations. a) Cells were first separated between CD14-/CD3+ (P7) and CD14+/CD3- (P4) cells. These cells underwent a second separation where b) the CD14- population was ensure to be CD14- (P8) and the CD14+ cells were sorted into CD14+/16- (P5) and CD14+/16+ (P8) cells.

Figure 2.2

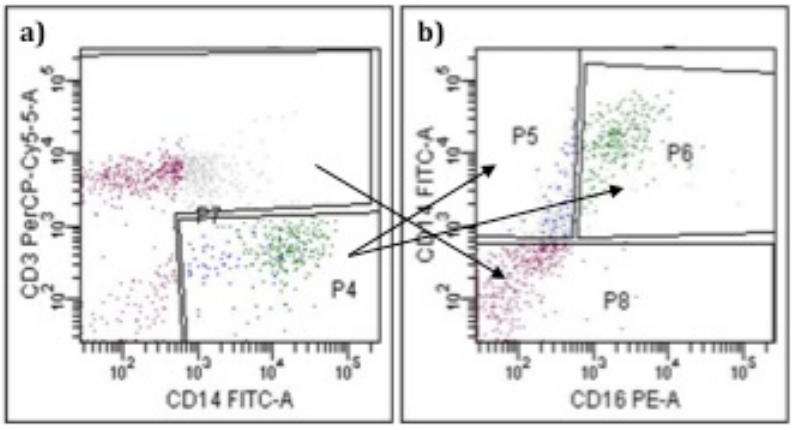

Figure 2.3 – PBMC HIV DNA copy numbers from the CD14-, CD14+/16+, CD14+/16- cell populations of HIV-positive normal cognition individuals. Significance ($p < 0.5$) was found between the CD14+/16- and CD14+/16+ fractions.

Figure 2.3

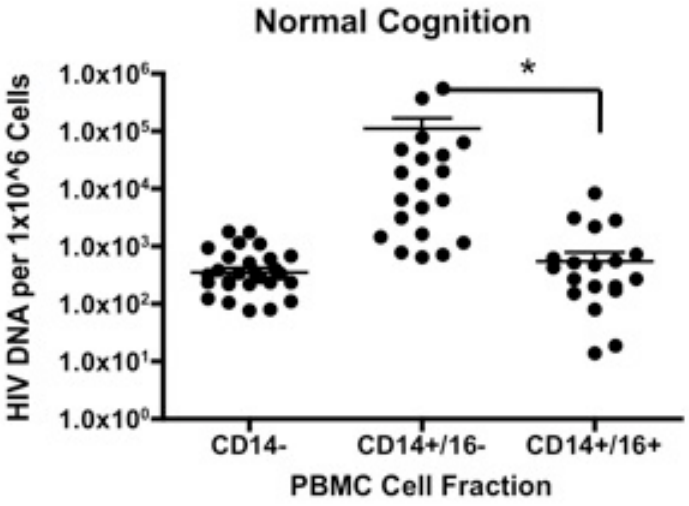
Normal Cognition
HIV DNA per 1x10^6 Cells
1.0x10^6
1.0x10^5
1.0x10^4
1.0x10^3
1.0x10^2
1.0x10^1
1.0x10^0
*
CD14-
CD14+/16-
CD14+/16+
PBMC Cell Fraction

Figure 2.4 – PBMC HIV DNA copy numbers from the CD14-, CD14+/16-, and CD14+/16+ cell populations of HIV-associated neurocognitive disorder (HAND) individuals. Significance was found between all fractions with ** $p<0.1$ and *** $p<0.001$.

Figure 2.4

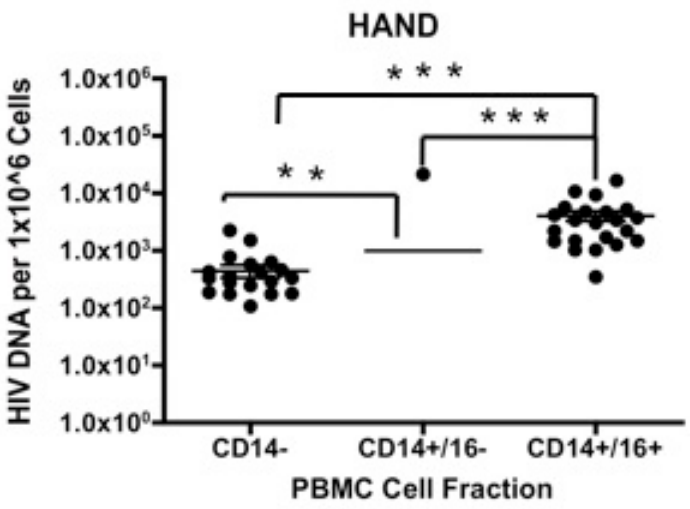
HAND
HIV DNA per 1x10^6 Cells
1.0x10^6
1.0x10^5
1.0x10^4
1.0x10^3
1.0x10^2
1.0x10^1
1.0x10^0
* * *
* * *
* *
CD14-
CD14+/16-
CD14+/16+
PBMC Cell Fraction

Figure 2.5 – Plot of HIV DNA Levels within CSF Cellular Subsets of HHLC subjects (PR1-6), HIV DNA copies from CSF fractions for $CD14^-$ (PR-); $CD14^+/CD16^+$ (PR++); and $CD14^+/CD16^-$ (PR+-) cells.

Figure 2.5

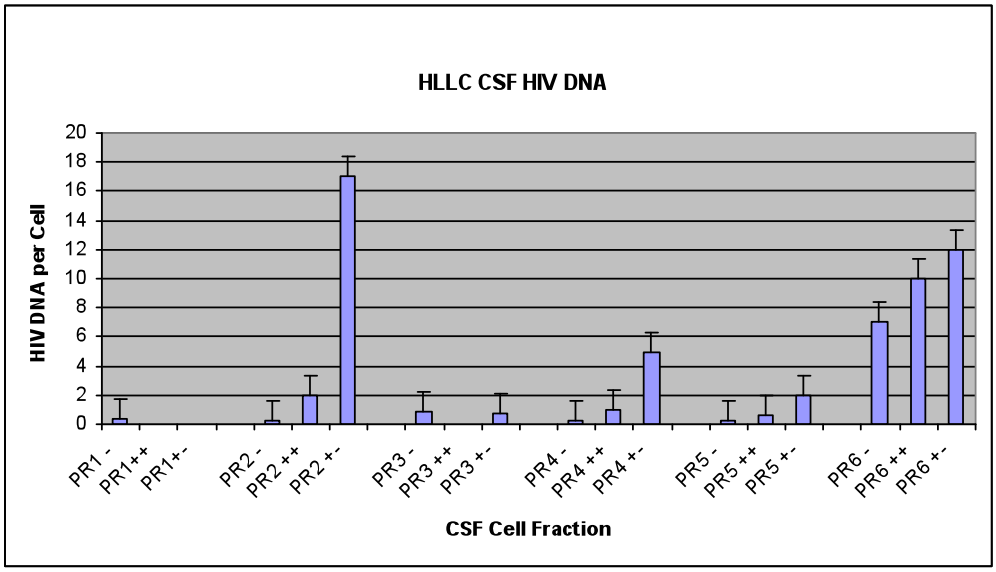
HLLC CSF HIV DNA
HIV DNA per Cell
20
18
16
14
12
10
8
6
4
2
0
PR1 -
PR1++
PR1+-
PR2 -
PR2 ++
PR2 +-
PR3 -
PR3 ++
PR3 +-
PR4 -
PR4 ++
PR4 +-
PR5 -
PR5 ++
PR5 +-
PR6 -
PR6 ++
PR6 +-
CSF Cell Fraction

Figure 2.6 – Percentages of CSF Sorted cells. The average percentage of total number of CSF cells sorted from HHLC and HAHC subjects with HAND and NC.

Figure 2.6

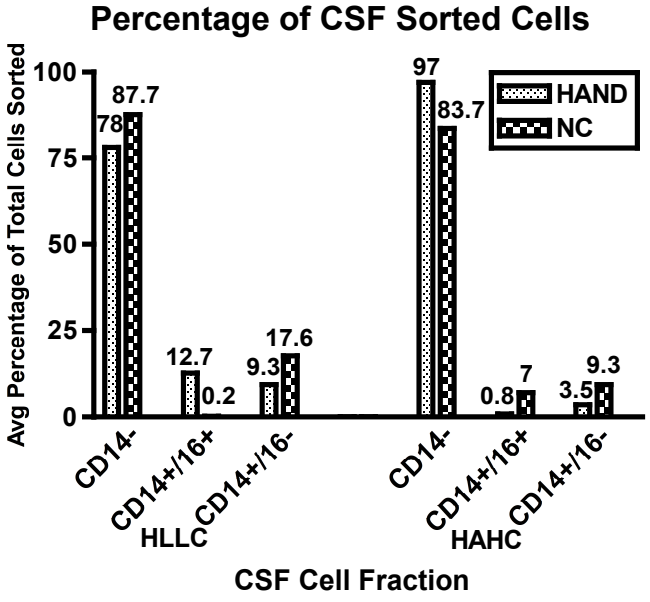
Percentage of CSF Sorted Cells
Avg Percentage of Total Cells Sorted
100
75
50
25
0
78
87.7
12.7
0.2
9.3
17.6
97
83.7
0.8
7
3.5
9.3
HAND
NC
CD14-
CD14+/16+
CD14+/16-
CD14-
CD14+/16+
CD14+/16-
HLLC
HAHC
CSF Cell Fraction

Figure 2.7 – Plot of HIV DNA Levels within CSF Cellular Subsets of HAHC subjects (H1-3), HIV DNA copies from CSF fractions for $CD14^-$ (H-); $CD14^+/CD16^+$ (H++); and $CD14^+/CD16^-$ (H+-) cells.

Figure 2.7

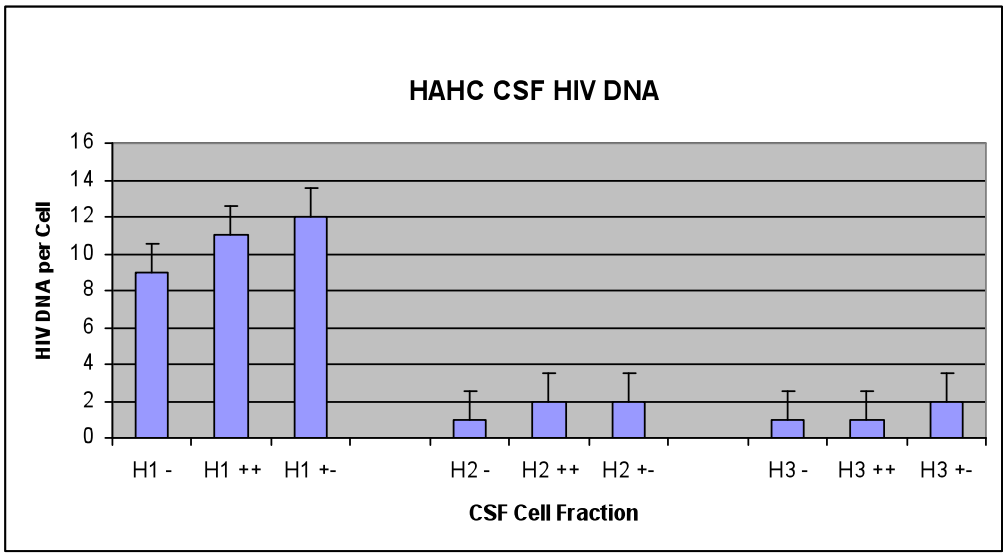
HAHC CSF HIV DNA
HIV DNA per Cell
16
14
12
10
8
6
4
2
0
H1 -
H1 ++
H1 +-
H2 -
H2 ++
H2 +-
H3 -
H3 ++
H3 +-
CSF Cell Fraction

Figure 2.8 – HIV DNA Copies in CSF Cellular Subsets. Total average HIV DNA copies per cell in the CSF cellular subsets from both HLLC and HAHC cohorts.

Figure 2.8

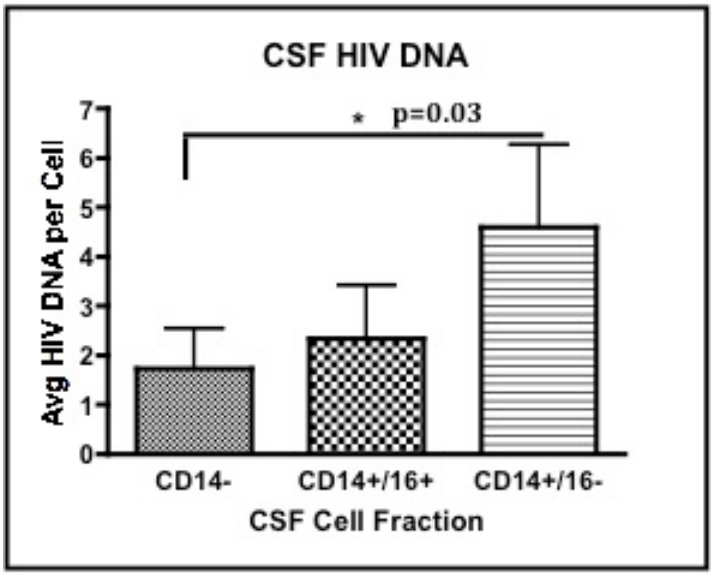
CSF HIV DNA
* p=0.03
Avg HIV DNA per Cell
0
1
2
3
4
5
6
7
CD14-
CD14+/16+
CD14+/16-
CSF Cell Fraction

CHAPTER 3

HIV DNA in CNS Compartments that Correspond to Neurocognitive Deficits Characterized by HAND

Abstract

Background: The importance of activated monocytes in HIV-associated neurocognitive disorders have been demonstrated through studies done with peripheral blood mononuclear cells (PBMC) and cerebrospinal fluid (CSF) cells; however, few studies have been done in the central nervous system (CNS). CNS areas with known involvement in HAND include the basal ganglia (BG) and frontal cortex (FC). Therefore in this study, laser capture microdissection (LCM) is utilized to identify and extract activated macrophages from basal ganglia and frontal cortex brain tissue. **Materials and Methods:** Brain sections were obtained from HIV-positive individuals diagnosed with HIV-encephalitis, HIVE (n=10) and without HIVE (n=10) that were from the BG (n=5) and FC (n=5). Of the total samples, 4 HIVE and 3 non-HIVE were matched samples from the same patient. CD14+/16+ cells were fluorescently labeled and extracted using LCM. CD14- regions were also excised. HIV DNA levels were determined from the extracted regions. **Results and Conclusions:** With the exception of HIVE FC, HIV DNA levels were higher in CD14- cells in both regions of both HIVE and non-HIVE. Limiting analyses to matched samples, resulted in HIVE samples containing higher HIV DNA levels in CD14+/16+ cells, while non-HIVE had higher HIV DNA levels in CD14- cells in both regions. These results demonstrate the importance of CD14+/16+ cells in brain inflammation.

Overview

It has become increasingly evident that viral reservoirs persist in patients despite effective treatment with combination antiretroviral therapy (cART). These reservoirs are believed to be memory T-cells and monocytes; and are characterized with integrated HIV DNA [96-98]. Monocytes are known to play an important role in HIV-associated neurocognitive disorders (HAND) and the fact that patients with HAND also have dysfunctional immune system, further challenges our understanding of the mechanisms involved.

Analogous to the hidden Trojan Horse, the activated states of CD16-positive monocyte provide the vehicles to be infected with HIV in the periphery to transport virus into the central nervous system (CNS) [8]. These monocytes that transverse the blood brain barrier (BBB) transition into perivascular macrophages or microglia cells, which become resting macrophages in the CNS. Upon activation, these cells potentially produce HIV in the CNS resulting in chemokine and cytokine production that cause neuronal damage and ultimately lead to HAND [5, 25, 38]

Because the frontal cortex and basal ganglia are areas previously shown to be involved in the development of HAND [5, 99-101], we hypothesize that activated macrophages and microglial cells, characterized by CD14+/16+, will contain high levels of HIV DNA in these particular CNS regions. The significance of this finding lies in understanding the pathogenic role that the virus plays specifically in macrophages and microglial cells both of which are characterized through the detection of CD14.

Laser capture microdissection (LCM), a method that isolates purified cell populations from heterogenous tissues, was used to isolate CD14+/16+ and CD14- cells from brain tissue. This technique utilizes both microscopy and laser dissection to obtain the cells of interest [102] where cells are stained either with fluorescent or non-fluorescent dyes and visualized under the microscope, Figure 3.1. When the cells are identified, they are labeled by the user to be laser cut and are captured onto the cap of an isolation tube. DNA from the cells can be extracted directly from the tube and used for downstream molecular analyses. In this study, the CD14 and CD16 are fluorescently labeled and the DNA extracted from the CD14- and CD14+/16+ cells from the basal ganglia and frontal cortex brain regions will be used to determine HIV DNA levels using quantitative real-time PCR.

This exploratory study is the first report of CD14+/16+ cell isolation from brain tissue and measurement of HIV DNA from the extracted cells. Thus, the main purpose of this chapter is to demonstrate the feasibility of this method in the assessment of HIV DNA in CNS compartments. Having the ability to analyze the CD14+/16+ cell population in the CNS will allow for its comparison to other CD14+/16+ populations that are located in other compartments such as the periphery and cerebrospinal fluid (CSF). Information obtained from these analyses will provide insight on the monocytic reservoirs in various compartments. This knowledge will assist with our understanding of the role that monocytes play in viral persistence through their formation of monocytic reservoirs in these particular locations.

Materials and Methods

Antibody verification through microscopy. Anti-CD14 and anti-CD16 antibodies were verified prior to use to identify CD14 and CD16 surface receptors. This verification process was done using laboratory activated and non-activated monocytes. Monocytes were isolated from frozen normal peripheral blood mononuclear cells (PBMC); catalog number PB002, which were processed by AllCells, LLC (Emeryville, CA).

Frozen PBMC were thawed and resuspended in 20% fetal bovine serum (FBS), 5% L-glutamine, 5% penicillin/streptomycin (P/S), and Dulbecco's modified eagle medium (DMEM) and cultured for 24 hours at 37°C in 5% $C0_2$. From this culture, cells were resuspended at approximately $2x10^8$ cells per mL with 2% FBS, PBS. Monocytes were isolated using the StemSep human CD14 positive selection kit (Stemcell Technologies, Vancouver, BC, Canada). 1 mL of PBMC ($2x10^8$ cells/mL) were placed in a 5 mL polystyrene tube and EasySep positive selection cocktail was added followed by vortexing and incubation at room temperature (5 minutes). The EasySep magnetic nanoparticles were then added followed with another room temperature incubation (5 minutes). The total volume was brought up to 2.5 mL with 2% FBS, PBS and mixed through pipetting. This tube was then placed into the magnet and incubated at room temperature (5 minutes). After incubation, the magnet is picked up and the supernatant from the tube that contains the unwanted non-monocytic cells is poured off. The cells of interest, monocytes, will remain in the tube. The tube is removed from the magnet and 2.5 mL of 2% FBS, PBS is added and the tube is replaced into the magnet. A second decanting step follows to ensure that only the monocytes will remain. The monocytes that remain are then resuspended in 4 mL of culture media: 10% fetal bovine serum (FBS),

5% L-glutamine, 5% penicillin/streptomycin (P/S), and Dulbecco's modified eagle medium (DMEM). The monocytes will be split into 2 mL cultures (approximately $2x10^7$ cells) to obtain activated and non-activated fractions. These two fractions will be placed in two separate hydro-cell plates that prevent the monocytes from adhering to the bottom of the plate.

The non-activated fraction was maintained in 10% FBS, 5% L-gluatmine, 5% P/S, and DMEM and cultured for an additional 24 hours. The media in the activated fraction was changed to include the activating component comprising of 20 ng/mL macrophage colony stimulating factor (M-CSF) in 10% FBS, 5% L-glutamine, 5% P/S, and DMEM. The cells were cultured for 24 hours and then washed and resuspend in the same media as the non-activated cells containing no M-CSF.

After establishing activated and non-activated monocytes, the cells were fixed with 2% paraformaldehyde for 5 minutes at room temperature, washed and resuspended in PBS at $1x10^6$ cell per mL. The resuspended cells were then pipetted (50 uL) onto a glass slides (50,000 cells) and remained in the hood for 1 hour to allow the cells to dehydrate onto the slide for preparation of cell staining. The cells were heat-fixed onto the slides through incubation in the oven at 56°C (1 hour).

Prior to cell staining, the cells were treated in 100% ethanol (30 sec); 95% ethanol (30 sec); 75% ethanol (30 sec) and dH_20 (30 sec). The staining was based on a modified protocol from the Vector Mouse on Mouse (M.O.M) Immunodetection kit (Vector Laboratories, Burlingame, CA). Before staining, the sections underwent a 5 minute protein blocking incubation step using the MOM diluent included in the kit. The staining

procedure was identical for both cell fractions and began with CD14 labeling with 50 ug/mL CD14 biotinylated antibody (Biolegend, San Diego, CA) and incubated for 20-30 mincutes followed by two (2 minute) PBS washes. An avidin conjugate (Fluorescein-Avidin DCS) diluted in PBS was then allowed to bind the bioltinylated antibody in a 5 minute incubation. Two 5 minute PBS washes immediately followed incubation to remove non-specific binding. Prior staining for CD16, avidin and biotin sites were blocked using the Biotin-Avidin Blocking Kit (Vector Laboratories, Burlingame, CA) as per directions included in the kit. Protein blocking then ensued using the MOM diluent included in the MOM Immunodetection kit through a 5 minute incubation. After blocking steps were completed, 50 ug/mL biotinylated CD16 anitbody (Biolegend, San Diego, CA) was added and incubation occurred for 20-30 minutes. Two washes with PBS followed (2 min each). An avidin conjugate (Texas-Red Avidin DCS) diluted in 0.1 M sodium bicarbonate to 20ug/mL was added and incubated for 5-10 minutes. Two PBS washes followed (5 min per wash). 20 uL of PBS was added onto cells to permit addition of coverslip. Cells were visualized using the Olympus BX-51 microscope with an attached digital camera.

Archival Tissue Specimens. Ten paraffin-embedded CNS tissue specimens from the basal ganglia and 10 from the frontal cortex were obtained from the AIDS and Cancer Specimen Resource (ACSR) repository. The 10 specimens from each region were from HIV-associated encephalitis (HIVE) cases (n=5) and HIV-associated non-HIVE cases (n=5), Table 1. Tissue sections were prepared on mmi Membrane Slides (Molecular Machines and Industries, Haslett, MI)

Tissue Sectioning. The FFPE CNS tissue specimens were sectioned according to guidelines set by Molecular Machines and Industries. The tissues were cut into 5-10 μm sections and mounted onto mmi Membrane Slides (Molecular Machines and Industries, Haslett, MI) prior to staining.

Section staining. The specimen sections were first soaked in acetone to remove the paraffin (10 min). They were then treated in 100% ethanol (30 sec); 95% ethanol (30 sec); 75% ethanol (30 sec) and dH_20 (30 sec). The sections were stained using the Vector Mouse on Mouse (M.O.M) Immunodetection kit (Vector Laboratories, Burlingame, CA) using a modified protocol tailored to human samples. Before staining, the sections underwent a protein blocking incubation step using MOM diluent included in the kit (5 min). CD14 was then labeled with 50 ug/mL CD14 biotinylated antibody (Biolegend, San Diego, CA) and incubated for 20-30 mincutes. Incublation proceeded with two PBS washes (2 min each). An avidin conjugate (Fluorescein-Avidin DCS) diluted in PBS was then allowed to bind the bioltinylated antibody in a 5 minute incubation. To remove non-specific binding, sections were washed twice with PBS (5 min each). Prior staining for CD16, avidin and biotin sites were blocked using the Biotin-Avidin Blocking Kit (Vector Laboratories, Burlingame, CA) as per directions included in the kit. Protein blocking then ensued using the MOM diluent included in the MOM Immunodetection kit through a 5 minute incubation. After blocking steps were completed, 50 ug/mL biotinylated CD16 anitbody (Biolegend, San Diego, CA) was added and incubation occurred for 20-30 minutes. Two washes with PBS followed (2 min each). An avidin conjugate (Texas-Red Avidin DCS) diluted in 0.1 M sodium bicarbonate to 20ug/mL was added and incubated for 5-10 minutes. Two PBS washes followed (5 min per wash). After washes were

completed, sections were left uncovered and allowed to dry before pursing with laser-capture microdissection. CD14+/16+ cells were identified through double fluorescence of fluorescein and Texas-Red, Figure 3.2.

Laser-Capture Microdissection (LCM). LCM was completed using the mmi Cellcut Plus machine (Molecular Machines and Industries, Haslett, MI). Fluorescently labeled cells were identified for laser dissection, Figure 3.3, and captured onto mmi Isolation Caps (Molecular Machines and Industries, Haslett, MI). DNA was then isolated from the captured cells using the QIAamp DNA micro kit (Qiagen, Valencia, CA) as per directions listed in the Laser-Microdissected Tissue section in the QIAamp DNA micro handbook and eluted in 20 uL Tris-EDTA buffer.

HIV DNA Multiplex-Realtime PCR Assay. Extracted DNA was used to assay for HIV DNA using a quantitative multiplex-realtime PCR assay. Two standard curves were generated using a mixture of two plasmids containing a single copy of gag gene (HXB2, GenBank accession #K03455) and a single copy of β-globin gene (GenBank accession #2253431); in 1:10 dilutions starting at 1 X 106 and ending at 1 X 101 copies. All standards and samples were set up in triplicate with each containing 2x TaqMan® Gene Expression Master Mix, 1.25 pmol of Gag primers, 0.625 pmol B-globin primers, 1.25 pmol of each probe (β-globin and Gag), 3 μL of eluted DNA and water for a final volume of 10 μL. The primers amplified a 111 bp gag segment (5'GACATCAAGCAGCCATGCAA and 3'CTCA TCT GGC CTG GTG CAA T) and a 109 bp b-globin segment (5'TCA CTA GCA ACC TCA AAC AGA CAC C and 3'AGG GCC TCA CCA CCA ACT TC). Samples were run in a StepOne™ Real-Time PCR System (Applied Biosystems, Foster City, CA) with cycling parameters of: 95°C for 15

min; 40 cycles of 95°C for 1 min, and 60°C for 1 min followed by analyses using the StepOne™ Real-Time PCR System software. The copy numbers of each gene within the unknowns were determined against the standard curves generated by the plasmids. The copy numbers were used to calculate HIV DNA copy number per cell. 8E5, a T-lymphoblastoid cell line was used as positive control containing approximately one copy of HIV per cell; HIV-negative DNA and water were used as negative controls.

Statistical Analysis. Analyses were performed using a Generalized Estimating Equation (GEE) model. HIV DNA copies per cell estimates were calculated in the basal ganglia and frontal cortex, along with the CD14- and CD14+/16+ cells within the HIVE and non-HIVE diagnoses using the following equation: HIV DNA per cell = 11.9040-0.3513*Age-2.2796*Brain Region-1.7785*Cell Fraction-1.4039+3.2906*(Cell Fraction*Diagnosis), where the asterisk in the parentheses depicts the interaction term between the cell fraction and diagnosis.

Results

Antibody verification. Detection of both CD14-fluorescein and CD16-Texas Red in the activated cells and only CD14-fluorescein in the non-activated cells demonstrates the specificity of the anti-CD14 and anti-CD16 antibodies because the non-activated cells should not express the CD16 activation marker, Figure 3.4-5. Based on these results, we can assume that fluorescence detection in the brain sections is accurate and reliable.

Section staining. Fluorescent detection in the fluorescein, Figure 3.2A, and Texas Red channels, Figure 3.2B, revealed the areas containing the CD14+/16+ cell populations. The cells that fluoresced in both channels were labeled for excision, Figure 3.3. The majority of the staining occurred in the brain parenchyma, Figure 3.6A-B, or perivascular, Figure 3.6C-D.

Unmatched samples. All samples were run in triplicate. In the frontal cortex, slightly higher HIV DNA levels are found in CD14+/16+ cells in comparison to CD14- cells in the individuals with HIVE (7 and 6 HIV DNA copies per 10 cells respectively). The CD14- DNA levels were higher than the CD14+/16+ cells in the basal ganglia of both HIVE (12 versus 3 HIV copies per 10 cells) and non-HIVE individuals (16 versus 10 HIV copies per 10 cells). The CD14-HIV DNA levels were also higher than CD14+/16+ cells (5 versus 0 HIV copies per 10 cells), Figure 3.7.

Matched samples. All samples were run in triplicate. However, when taking into account only the matched sections (4 HIVE and 3 non-HIVE), Table 3.2, where the frontal cortex and basal ganglia sections were taken from the same patient; the higher HIV DNA levels in the CD14+/16+ cells in comparison to CD14- cells were apparent in

both the basal ganglia and frontal cortex in HIVE individuals (9 versus 3; and 7 versus 0 HIV copies per 10 cells respectively). Conversely, HIV DNA levels were higher in the CD14- cells than the CD14+/16+ cells in both the basal ganglia and frontal cortex in the non-HIVE individuals (20 versus 13; and 7 versus 0 HIV copies per 10 cells respectively), Figure 3.8. Based on these matched section results, analysis using the Generalized Estimating Equation (GEE) Model that estimates the average response over the population, estimates that the HIV DNA per cell in HIVE individuals is 4.54 folds higher in the CD14+/16+ cells in comparison to the CD14- cells and is independent of brain region. Conversely, CD14+/16+ HIV DNA per cell in the non-HIVE individuals is estimated to be 16.9% less than CD14- cells. Further analyses shows that HIV DNA per cell is statistically different between the various brain regions where the mean HIV DNA per cell in the frontal cortex is less than in the basal ganglia ($p<0.0001$), which is regardless of diagnosis. Additionally, the model estimates that the mean HIV DNA per cell in the basal ganglia to be 10% higher than that of the frontal cortex.

Discussion

Prior to analyzing the CNS tissue sections with laser capture microdissection (LCM), non-activated monocytes (CD14+/16-) and lab-activated monocytes (CD14+/16+) were labeled with the anti-CD14 and CD16 antibodies to verify their accuracy. As expected, all the cells were labeled with anti-CD14 but only the CD14+/16+ cells were labeled with anti-CD16, Figure 3.4-5. Upon closer inspection of the monocytes, it realized that they are brown, Figure 3.4A-5A. The monocytes were magnetically separated from PBMC by positive selection, Figure 3.9, so the monocytes contain the magnetic beads on their surface. Therefore, it is presumed that the brownish color of the monocytes is caused from the magnetic beads. It seems also seems that less staining occurs when more beads are contained by the cell, Figure 3.4-5. Nonetheless, the specificity of the antibodies in the detection of the target was still verified. The majority of the fluorescent detection was observed in the brain parenchyma and around blood vessels, which are indicative of the activated microglia and macrophages, Figure 3.6.

Analysis using unmatched samples, revealed that the average HIV DNA levels were higher in basal ganglia CD14- cells in comparison to CD14+/16+ cells in both HIVE and non-HIVE individuals. However, when analysis is limited to only matched basal ganglia samples, higher HIV DNA levels in CD14+/16+ cells are revealed in HIVE individuals, whereas the CD14- HIV DNA levels were still higher than CD14+/16+ cells in non-HIVE individuals. The same HIVE and non-HIVE frontal cortex results were obtained for both unmatched and matched samples but the higher HIV DNA levels in CD14+/16+ cells were emphasized in the matched HIVE samples.

Due to the complex nature of HIV inflammation, analysis using only matched samples is probably more reliable; thus, highlighting the role of CD14+/16+ cells in inflammation in both the basal ganglia and frontal cortex. Nonetheless, HIV DNA levels were higher in non-HIVE individuals in comparison to HIVE individuals for both CD14- and CD14+/16+ cell fractions in the basal ganglia. Though the exact reason for this result is unknown, it may be explained by the fact that the basal ganglia is an important target region for HIV. Furthermore, it is currently unknown whether these individuals contained any other HIV-associated diseases such as cardiovascular diseases (CVD), which also has been correlated to high CNS HIV DNA levels. Additionally, the exact areas of the basal ganglia and frontal cortex sections are unknown and particular regions may have more of a contributing effect on HIV DNA.

Based on these data, statistical analysis using with the GEE model states that regardless of diagnosis and cell fraction, the mean HIV DNA per cell is statistically different between the various brain regions where higher levels are found in the basal ganglia, Figure 3.10. Furthermore, when taking into account the total average HIV DNA levels per cell in both regions, Figure 3.11; the model estimates that HIV DNA per cell in the HIVE individuals to be 4.54 more in CD14+/16+ cells than CD14- cells and is independent of brain region. For non-HIVE individuals, the reverse is found where HIV DNA per cell is estimated to be 0.17 more in CD14- cells than CD14+/16+ cells independent of brain region. These estimates emphasize the importance that CD14+/16+ cells have on inflammation and presumably HAND in both the basal ganglia and frontal cortex. The significantly higher difference in HIV DNA levels in the basal ganglia is unknown but may again be due to higher viral targeting to this particular brain region.

The findings of the study are the first to demonstrate higher HIV DNA copies in CD14+/16+ cells compared to CD14- cells in HIVE specimens from the basal ganglia. This is in sharp contrast to brain specimens from non-HIVE specimens in which higher HIV DNA copies were located CD14- cells compared to CD14+/16+ cells. Infection with HIV results in a complex and multifactorial inflammatory environment and the current study using paired specimens provides an intra-subject comparison of HIV DNA copies in CD14+/16+ and CD14- cells from both basal ganglia and frontal cortex regions of the brain. The high HIV DNA copies in CD14+/16+ cells in the basal ganglia from HIVE specimens highlight the potential importance of these cells in HAND pathogenesis.

Targeting and capturing CD14+/16+ cells by LCM in this report from archival necropsy specimens from HIVE and non-HIVE CNS tissue and demonstrating differences in HIV DNA copies in CD14- cells substantiates and expands upon studies by others the possible neuropathogenic importance of CD14+/16+ cells in the brain. This is the first report that demonstrates the feasibility of measuring HIV DNA in CD14+/16+ CNS cells through the use of LCM. Although the sample size was limited and more samples would need to be analyzed to confirm findings, the results highlight the importance of frontal cortex and basal ganglia CD14+/16+ cells in inflammation.

Table 3.1. Total ACSR Specimens

Patient	Diagnosis	CNS Region
3000540	HIVE	Basal Ganglia
3000540	HIVE	Frontal Cortex
3000510	HIVE	Basal Ganglia
3000510	HIVE	Frontal Cortex
3007098	HIVE	Basal Ganglia
3007098	HIVE	Frontal Cortex
3007894	HIVE	Basal Ganglia
3007894	HIVE	Frontal Cortex
3000590	HIVE	Basal Ganglia
3008203	HIVE	Frontal Cortex
3008196	NC	Basal Ganglia
3008196	NC	Frontal Cortex
3008195	NC	Basal Ganglia
3008195	NC	Frontal Cortex
3008194	NC	Basal Ganglia
3008194	NC	Frontal Cortex
3005120	NC	Basal Ganglia
3008259	NC	Frontal Cortex
3002100	NC	Basal Ganglia
3005870	NC	Frontal Cortex

Table 3.2. Matched ACSR Specimens

Patient	Diagnosis	CNS Region
3000540	HIVE	Basal Ganglia
3000540	HIVE	Frontal Cortex
3000510	HIVE	Basal Ganglia
3000510	HIVE	Frontal Cortex
3007098	HIVE	Basal Ganglia
3007098	HIVE	Frontal Cortex
3007894	HIVE	Basal Ganglia
3007894	HIVE	Frontal Cortex
3008196	NC	Basal Ganglia
3008196	NC	Frontal Cortex
3008195	NC	Basal Ganglia
3008195	NC	Frontal Cortex
3008194	NC	Basal Ganglia
3008194	NC	Frontal Cortex

Figure 3.1 – Illustration of the Laser capture microdissection (LCM) process obtained from Arcturus Engineering, Inc. The process starts with the 1) placement of the tube cap onto the tissue prior to 2) laser cutting the targeted cells that are 3) adhered onto the tube cap. 4) The DNA from the captured cells can be extracted directly from the tube.

Figure 3.1

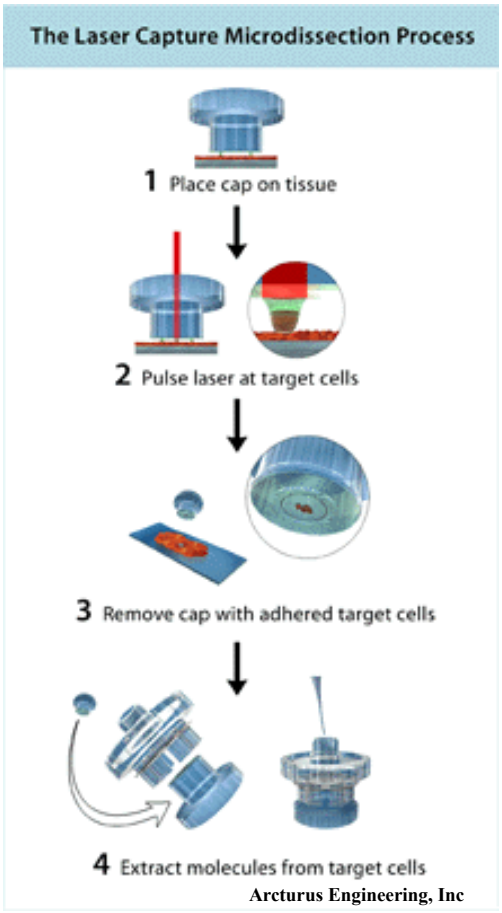
The Laser Capture Microdissection Process
1 Place cap on tissue
2 Pulse laser at target cells
3 Remove cap with adhered target cells
4 Extract molecules from target cells
Arcturus Engineering, Inc

Figure 3.2 – Laser capture microdissection microscopy images of brain tissue showing the cells that are positive for both A) CD14-fluorescein (green) and B) CD16-Texas red (Red).

Figure 3.2

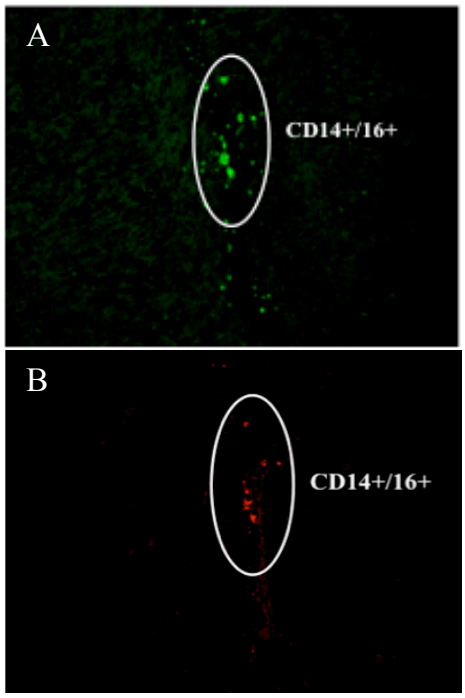

Figure 3.3 – Laser capture microdissection microscopy images that shows the process of identifying the A) CD14 and B) CD16 positive cells for laser capture. C) Image of brain tissue after the cells are extracted.

Figure 3.3

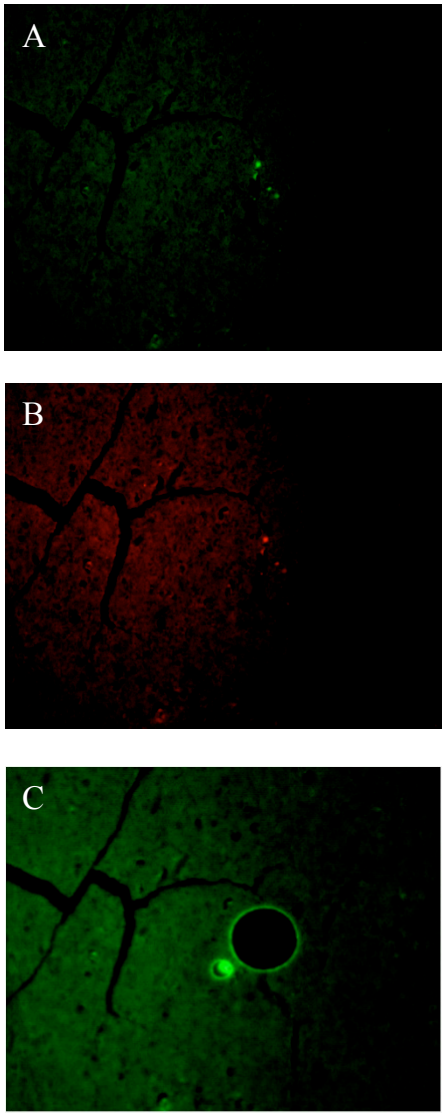

Figure 3.4 – Fluorescent microscopy images of laboratory activated monocytes that were labeled with CD14 and CD16 antibodies. A) Brightfield image, B) Image showing detection of CD14 and C) Image showing detection of CD16.

Figure 3.4

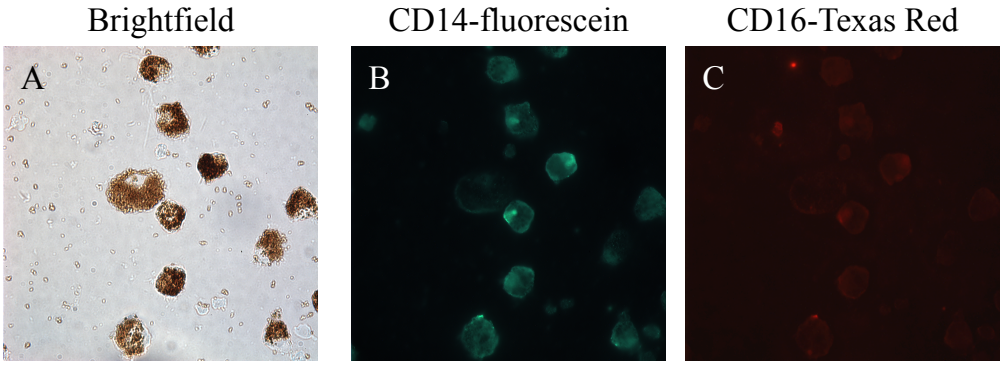

Figure 3.5 – Fluorescent microscopy images of non-activated monocytes that were labeled with CD14 and CD16 antibodies. A) Brightfield image, B) Image showing detection of CD14 and C) Image showing negative CD16 detection.

Figure 3.5

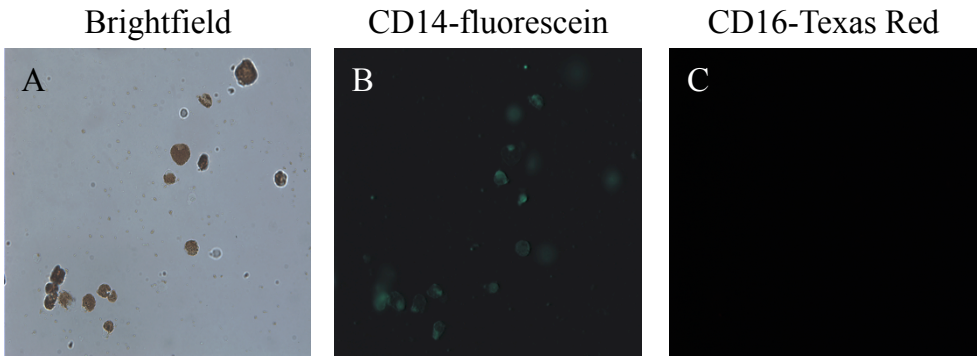

Figure 3.6 – Laser capture microdissection images that reveal CD14 fluorescence detection. Cells were visualized in the brain parenchyma depicting microglial cells (A-B) and found perivascularly depicting macrophages (C-D).

Figure 3.6

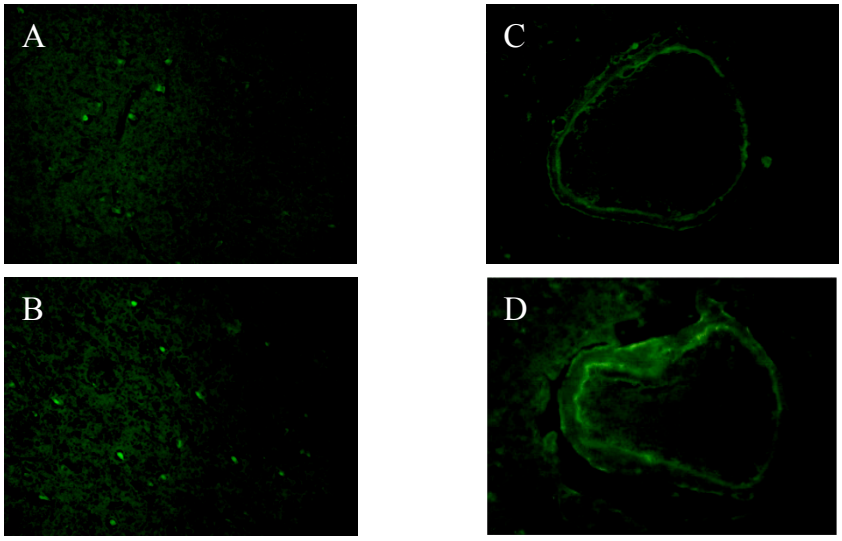

Figure 3.7 – CNS HIV DNA copy numbers in the basal ganglia (BG) and frontal cortex (FC) regions in HIV-encephalitis (HIVE) and non-HIVE (non-HIVE) brain sections.

Figure 3.7

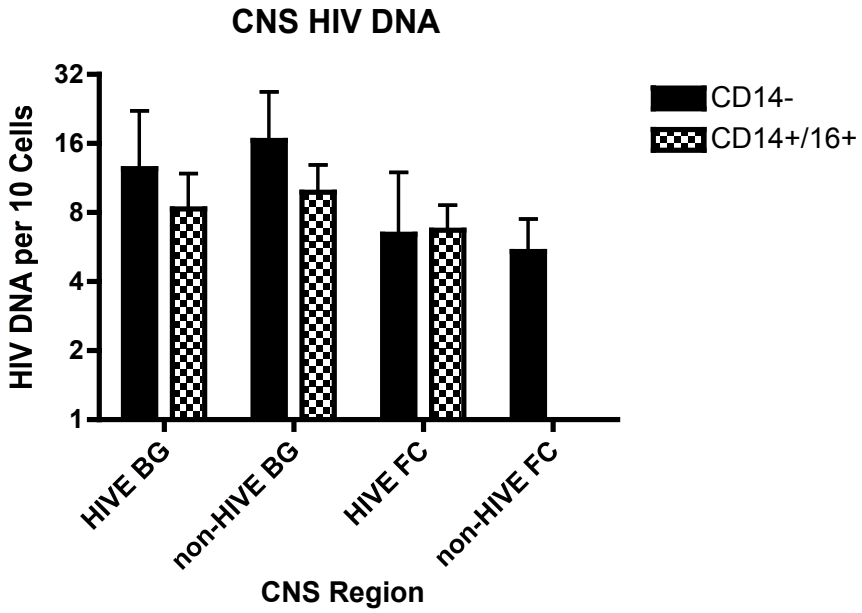
CNS HIV DNA
HIV DNA per 10 Cells
32
16
8
4
2
1
CD14-
CD14+/16+
HIVE BG
non-HIVE BG
HIVE FC
non-HIVE FC
CNS Region

Figure 3.8 – CNS HIV DNA copy numbers for matched samples in the basal ganglia (BG) and frontal cortex (FC) regions in HIV-encephalitis (HIVE) and non-HIVE (non-HIVE) brain sections.

Figure 3.8

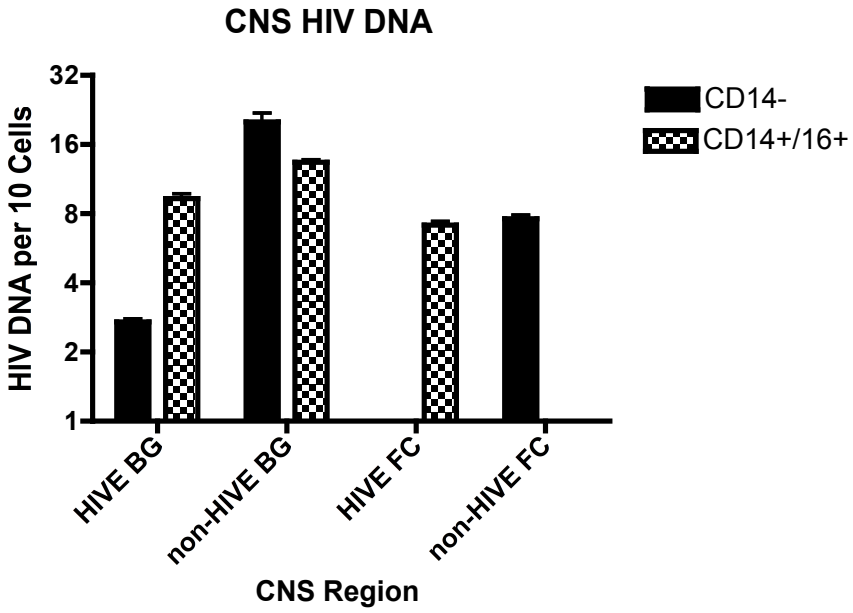
CNS HIV DNA
HIV DNA per 10 Cells
32
16
8
4
2
1
CD14-
CD14+/16+
HIVE BG
non-HIVE BG
HIVE FC
non-HIVE FC
CNS Region

Figure 3.9 – Illustration of magnetic cell separation that was used for separting monocytes from peripheral blood mononuclear cells (PBMC) using the EasySep human CD14 selection kit (StemCell Technologies, Vancouver, BC, Canada). Taken from the EasySep product information sheet, version 3.2.1 (catalog #18058).

Figure 3.9

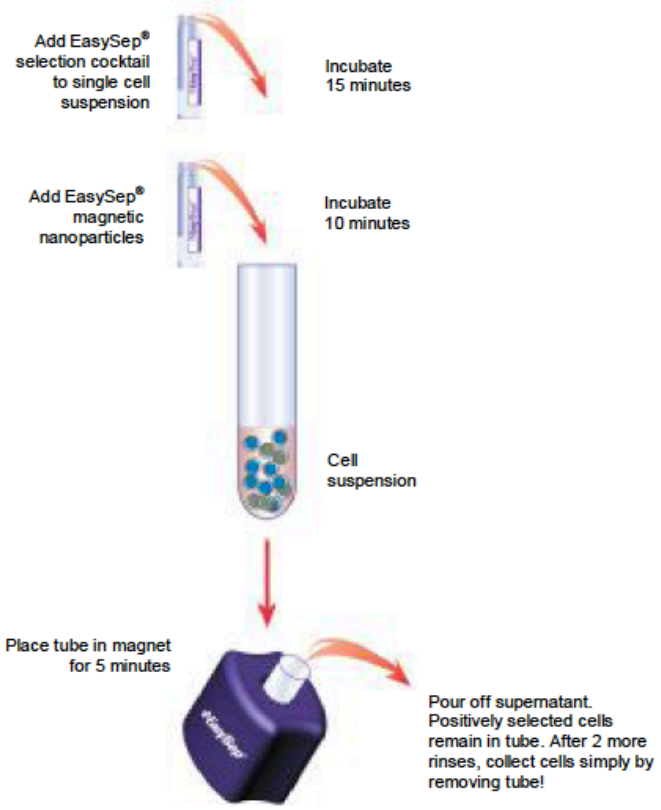
Add EasySep® selection cocktail to single cell suspension
Incubate 15 minutes
Add EasySep® magnetic nanoparticles
Incubate 10 minutes
Cell suspension
Place tube in magnet for 5 minutes
Pour off supernatant. Positively selected cells remain in tube. After 2 more rinses, collect cells simply by removing tube!

Figure 3.10 – Average HIV DNA per 10 cells of both HIV-encephalitis (HIVE) and non-HIVE brain sections in the basal ganglia and frontal cortex. A statistical difference *$p < 0.5$ was found between the two regions.

Figure 3.10

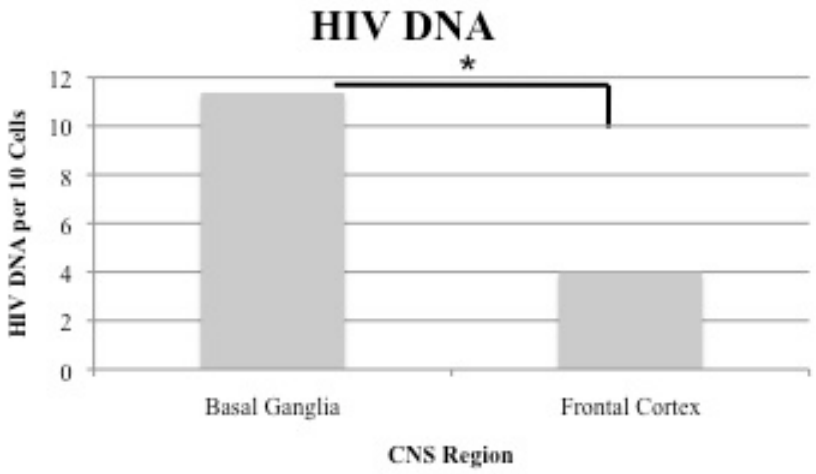
HIV DNA
*
HIV DNA per 10 Cells
12
10
8
6
4
2
0
Basal Ganglia
Frontal Cortex
CNS Region

Figure 3.11 – Average HIV DNA per 10 cells in CD14- and CD14+/16+ cells of HIV-encephalitis (HIVE) and non-HIVE brain sections.

Figure 3.11

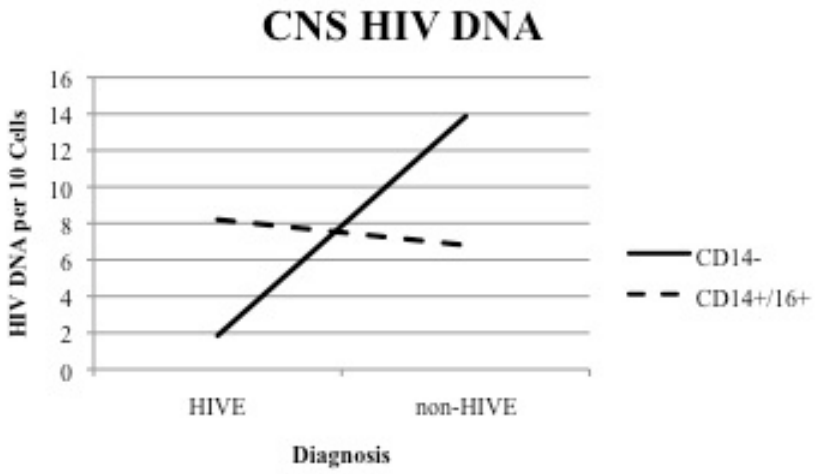
CNS HIV DNA
HIV DNA per 10 Cells
16
14
12
10
8
6
4
2
0
HIVE
non-HIVE
Diagnosis
CD14-
CD14+/16+

CHAPTER 4

A Novel Technique to Detect HIV DNA Using a Peptide Nucleic Acid

Abstract

Background: Since monocytes are an important viral reservoir and are associated with HAND, it is of high interest to measure HIV DNA within these cells, particularly those of the activated subset. In this study, we introduce a novel technique called fish-FLOW that incorporates the use of a peptide nucleic acid (PNA) probe to identify HIV DNA while simultaneously characterizing cells that contain the PNA through flow cytometry. When used in conjunction to current methods, fish-FLOW could provide additional information that may help to strengthen our understanding of the neuropathogenesis of HAND. **Materials and Methods:** A PNA probe designed to target the *pol* region of HIV-1 was validated in various HIV-positive and HIV-negative cell lines. It was also used in conjunction with anti-CD14 and anti-CD16 antibodies to characterize cells containing HIV DNA in HIV-positive PBMC samples (n=2). Laboratory HIV infected PBMC was used to compare the results from the fish-FLOW technique to the current method of cell sorting and multiplex PCR to determine HIV DNA levels. These tests were done as a proof-of-concept and were only tested once. **Results and Conclusion:** This proof-of-concept aim validated the PNA probe through HIV cell line studies that demonstrate the HIV DNA detection. The feasibility of the fish-FLOW technique was also proven through the characterization of cells containing HIV DNA. Comparable results were obtained from the flow-FISH assay and current method with some variability that may be contributed to the difference of the HIV region that is detected.

Overview

Peptide nucleic acids (PNAs) are synthetic oligonucleotides that mimic DNA. These molecules were created in 1991 by Peter Nielsen and his colleagues and contain N-2-aminoethylglycine linkages, which replace the deoxyribose phosphate backbone [103-105], Figure 4.1A. This substitution causes the molecule to be neutrally-charged removing electrostatic repulsion and giving it its characteristics of increased affinity, specificity and binding. As an analogue of DNA, PNA hybridizes to complementary oligonucleotides in a typical Watson-Crick fashion, forming a D-loop [104, 105]. The D-loop refers to the PNA/DNA duplex with a displaced DNA strand [103], Figure 4.1B. When it is conjugated to fluorescent dyes, these probes can be utilized in fluorescent in situ hybridization [106] and flow cytometry [107]. More recently, a technique that combines FISH using the PNA probe and fluorescent measurements of cell identity using flow cytometry has been developed and coined flow-FISH. While the use of flow-FISH deems advantageous in the area of single-cell analysis, one disadvantage is the harsh conditions that are associated with the use of a PNA probe. The high temperature exposure makes simultaneous immunolabeling difficult due to the limited amount of thermal stable organic fluorescent dyes. Therefore, in this study the incorporation of quantum dot (Qdot) nanocrystals, developed by Invitrogen (Carlsbad, CA) was used to circumvent this limitation. Qdots are beneficial due to their optimal photostability, intrinsic brightness, and narrow emission properties, Figure 4.2. Others labs have also utilized Qdots in their flow-FISH studies and showed its effectiveness in retaining fluorescence [108]. The feasibility of the use of PNA probes in these various techniques

was demonstrated by the extensive work related to telomere detection [107, 109-112]; however, limited work has been done in the area of HIV-1 [113].

In 2001, Murakami et al published the first report of the use of a PNA probe in the detection of HIV-1 [113]. The study designed a PNA probe to target HIV-1 DNA, which has potential translational application in clinical research. With the use of fluorescent microscopy, the authors showed the specificity of the PNA probe to HIV-1 infected lymphocytes, Figure 4.3A-B. Since the main interest of our lab was to utilize HIV DNA to monitor various HIV-associated disorders, such as HIV-associated neurocognitive disorders (HAND), the purpose of this chapter is to apply the PNA probe to a novel flow-FISH technique that identifies the cell containing HIV DNA in specimens from subjects with HAND. With the increasing recognition that activated monocytes (CD14+/16+) might be involved in the development HAND through its role in trafficking HIV-1 into the CNS and causing an increased release of inflammatory cytokines, the potential to monitor these cells using flow-FISH might contribute to the understanding of AIDS neuropathogenesis. Additionally, it is thought that these cells also serve as viral reservoirs, which are identifiable through HIV DNA, and maintain viral infection in the CNS. Through the use of this assay, HIV DNA within these particular cells along with other immune cells can be analyzed in patients. To identify activated monocytes, a CD14 Alexa 488 conjugated antibody and a biotinylated CD16 antibody will be added to label surface the receptors. Then a streptavidin conjugated Qdot will be used to fluorescently label the CD16 antibody prior to the addition of the PNA probe that will label HIV DNA, Figure 4.4. The main goal of this chapter is to demonstrate the feasibility and reliability of this assay in conjunction with other technologies and applying it to future studies.

Materials and Methods

Peptide Nucleic Acid. The peptide nucleic acid (PNA) probe used in this study targets the *pol* region of HIV-1 (NC_001802.1) and binds to region 2124-2138. It is conjugated to cyanine 5 (Cy5) at its N-terminus with the following sequence: Cy5-HN-OO-CTG GCT TTA TTA-CONH2 (Biosynthesis, Lewisville, TX). This probe was adapted from previous work by Murakami et al. The lyophilized PNA probes were resuspended in water to 100 uM. A working solution of 500 nM diluted in water was used for all PNA assays.

Control Cell Lines. Several HIV-infected and HIV-negative cell lines were used as controls for verifying PNA specificity. The HIV-positive control cell lines included: ACH-2 (T-lymphocytic cells derived from A3.01), OM10.1 (promyelocytic cells derived from HL-60), U1 (infected monocytic cells derived from U937), and 8E5 (infected T-lymphocytic cells derived from A3.01). The HIV-negative control cell lines included: U397 (monocytic cells), THP-1 (monocytic cells), and Ramos (B-lymphocytic cells).

PNA Verification with Cell Lines. Approximately $5x10^6$ cells were used for testing the PNA probe. The cells were thawed in 13 mL of PBS supplemented with FBS (10% FBS, PBS) and centrifuged at 2000 rpm (5 minutes). The cells were resuspended in 1.5 mL of Accumax (Innovative Cell Technologies, San Diego, CA) and incubated at 37°C (10 minutes). After incubation the cells were filtered through a 30 um CellTrics filter (Partec, Germany) and transferred into a 1.5 mL microcentrifuge tube. 500 uL of the filtered cells were aliquoted into a separate tube to be used as the unstained fraction. Both tubes were

centrifuged at 2300 rpm (5 minutes). The cells were resuspended in 500 uL of fixation solution consisting of 2% paraformaldehyde, PBS and stored at room temperature for 5 minutes. To minimize toxicity induced by fixation, the cells were washed away with PBS. The unstained cells were resuspended in 1.25x In Situ Hybridization Buffer (Enzo Life Sciences, Plymouth Meeting, PA) diluted with water in a total volume of 200 uL. 500 nM of the PNA probe was added to the stained cell fraction in the following solution: 1.25x In Situ Hybridization Buffer (Enzo Life Sciences, Plymouth Meeting, PA), 500 nM PNA-Cy5 diluted with water in a total volume of 200 uL. Both the unstained and stained tubes were underwent an incubation at 80°C (10 minutes) followed by an overnight incubation at room temperature protected from light. The cells were washed the following day through the addition of 1 mL of 40°C pre-warmed PBS and incubation at 40°C (10 minutes). All tubes were centrifuged at 2300 rpm (5 minutes) and cells were resuspended in 200 uL PBS. PNA probe binding to the cells were analyzed through flow cytometry using the FACSAria (BD Biosciences, San Jose, CA). Multiple tests in singlet were done on ACH-2, OM10.1, and 8E5 with a 5-10% variation between runs. Due to time constraints and machine availability limitations, U1 was only tested once.

PNA Sensitivity. The PNA probe's sensitivity in detecting HIV-1 was tested by diluting the HIV-infected cell line (OM10.1) with an HIV-negative cell line (H9). The dilutions were as follows: 100% OM10.1 (0% H9), 75% OM10.1 (25% H9), 50% OM10.1 (50% H9), 25% OM10.1 (75% H9), and 0% OM10.1 (100% H9); calculated based on a total of $4x10^6$ cells. The diluted controls were subjected to the same procedure as noted above to verify the PNA specificity. Dilutions were tested once.

Antibody Stability. The stability of the antibody was tested by comparing flow cytometry results of the CD14-Alexa 488 antibody after undergoing the PNA protocol with the results of standard flow cytometry staining.

For the standard staining procedure, two vials of frozen $5x10^6$ peripheral blood mononuclear cells (PBMC) were thawed in 10% FBS, DMEM and centrifuged at 2000 rpm (5 minutes). The cells were resuspended in Accumax (Innovative Cell Technologies, San Diego, CA), incubated at 37°C (10 minutes) and filtered through a 30 um CellTrics filter (Partec, Germany) to minimize clumping. Cells were resuspended in 2% PBS, transferred to 1.5 mL microcentrifuge tubes, and centrifuged at 2300 rpm (5 minutes). Anti-CD14-Alexa488 (BioLegend, San Diego, CA) was added to the dry cell pellets and incubated at room temperature (10 minutes) to label the CD14 surface receptor. Cells were washed twice with PBS to remove unbound antibodies. Fixation followed with resuspension in 2% PFA, PBS and incubation at room temperature (5 minutes). Two more PBS washes followed prior to resuspension in PBS and analysis on the FACSAria (BD Biosciences, San Jose, CA).

For the flow-FISH technique, the same procedure using an aliquot of the same cells was followed as above with some modifications. Following the washes and fixation, the cells were resuspended in 1.25x In Situ Hybridization Buffer diluted in water, incubated at 80°C (10 minutes) and stored overnight at room temperature. The cells were washed the next day with pre-warmed 40°C PBS and incubated at 40°C (10 minutes) before analysis on the FACSAria.

CD14 and HIV DNA Labeling. Frozen PBMC ($5x10^6$) were thawed in 10% FBS, DMEM and centrifuged at 2000 rpm (5 minutes). The cells were resuspended in Accumax (Innovative Cell Technologies, San Diego, CA), incubated at 37°C (10 minutes), and filtered though a 30 um CellTrics filter (Partec, Germany). Anti-CD14-Alexa488 was added to the dry pellet and incubated at room temperature (10 minutes). Cells were washed twice in PBS then fixed with 2% PFA, PBS at room temperature (5 minutes). Two PBS washes followed prior to the addition of PNA, which was contained in the following solution 1.25x In Situ Hybridization Buffer (Enzo Life Sciences, Plymouth Meeting, PA), 500 nM PNA diluted in water for a total volume of 200 uL. The cells were then incubated at 80°C (10 minutes) and overnight at room temperature. PNA was washed from the cells during the following day with the addition of pre-warmed 40°C PBS, incubation at 40°C (10 minutes), and centrifugation at 2300 rpm (5 minutes). The stained cells were then analyzed with flow cytometry using the FACSAria (BD Biosciences, San Jose, CA). Additional analysis was done through fluorescent microscopy using the Olympus BX-51 microscope to visualize the stained cells.

Quantum dot Fluorescence. The quantum dot (Qdot) 605 streptavidin conjugated nanocrystal (Invitrogen, Carlsbad, CA) was combined with biotinylated beads and visualized through flow cytometry to ensure that its emission profile does not bleed into the FITC and APC channels, which are the channels used for the detection of CD14-Alexa488 and PNA-Cy5 respectively.

CD14, CD16 and HIV DNA Labeling with Qdots. HIV-positive PBMC ($5x10^6$ cells) were thawed in 10% FBS, DMEM and resuspended in Accumax (Innovative Cell Technologies, San Diego, CA). Incubation at 37°C followed (10 minutes) followed with filtering through a 30 um CellTrics filter (Partec, Germany). The filtered cells were transferred to 1.5 mL microcentrifuge tubes and centrifuged at 2300 rpm (5 minutes). Surface antibodies, anti-CD14-Alexa488 and anti-CD16-biotin (BioLegend, San Diego, CA) were added to dry pellets and tubes were incubated at room temperature (10 minutes). Cells were washed with PBS prior to the addition of Qdot605-Streptavidin, which binds to the CD-biotin antibody. Another room temperature incubation followed (10 minutes) along with another PBS wash. The surface labeled cells were fixed with 2% PFA, PBS and incubated at room temperature (5 minutes). Two PBS washes were completed before the addition of the PNA mix that consisted of 1.25x In Situ Hybridization Buffer (Enzo Life Sciences, Plymouth Meeting, PA) and 500 nM PNA-Cy5 diluted in water for a final volume of 200 uL. The tubes were then incubated at 80°C (10 minutes) followed with an overnight incubation at room temperature. Unbound probe was removed from the cells the following day during a wash with pre-warmed 40°C PBS and incubation at 40°C (10 minutes). All the tubes were centrifuged at 2300 rpm (5 minutes) and resuspended in PBS prior to analysis with flow cytometry using the FACSAria (BD Biosciences, San Jose, CA). To set fluorescence thresholds, unstained cells that did not contain PNA-Cy5 was used.

Flow-FISH versus HIV DNA Real-Time PCR. Comparison of the PNA assay to our traditional HIV DNA real-time PCR assay was done using HIV-infected cell lines along with HIV-infected PBMC that were established in the laboratory.

The same HIV-infected cell lines that were used to validate the specificity of the PNA probe (U1, ACH-2, 8E5 and OM10.1) were used to compare the traditional multiplex real-time PCR assay that our lab currently uses to analyze HIV DNA to the flow-FISH assay. The DNA from these cell lines were extracted using the QIAamp DNA micro kit (Qiagen, Valencia, CA) and was used in the multiplex PCR assay (see appendix) completed in triplicate.

Approximately $20x10^6$ frozen PBMC (AllCells, Emeryville, California) were thawed in 20% FBS, DMEM and resuspended in culture media consisting of 20% FBS, 1% penicillin/streptomycin (p/s), 1% L-glutamine, and DMEM supplemented with 10% human serum albumin. The cells were transferred to a plate and cultured overnight to help stabilize them. Infection occurred the following day where the cells were spun down and resuspended in viral media consisting of 337.45 ng/mL HIV-1 BaL virus (R5 strain) in 2% FBS, DMEM. The cells were exposed to the virus for 6 hours at 37°C, after which the cells were washed and remained in normal culture media containing 10% FBS, 1% p/s, % L-glutamine, and DMEM for 10 days. Two aliquots ($1x10^6$ cells each) were taken on Days 1, 5, and 10 post-infection along with their corresponding supernatants that were used for the detection of p24. All aliquots were frozen down until they were ready to be used.

An aliquot of cells from each respective day underwent fluorescence-activated cell sorting (FACS) followed by our multiplex real time PCR assay. Briefly, the cells

were stained anti-CD3-PerCp/Cy5.5, anti-CD14-FITC and anti-CD16-PE (BioLegend, San Diego, CA) for 20 minutes at room temperature, washed with 2% FBS, PBS and fixed with a 2% paraformaldehyde (PFA) solution. After fixation, the cells were diluted with PBS and underwent cell sorting using the FACSAria (BD Biosciences, San Jose, CA) to get the desired cell populations: non-monocytes (CD14-), activated monocytes (CD14+/16+), and non-activated (CD14+/16-) monocytes. Acquisition started with gating on CD14+ and CD14-. The CD14+ cells underwent a second sort into CD14+/16+ cells and CD14+/16- cells. The CD14- cells were ensured to be CD14- through a second CD14- sort. The cells were sorted directly into lysis buffer in preparation for DNA extraction. The DNA was extracted using the QIAamp DNA micro kit (Qiagen, Valencia, CA) and was used in the multiplex PCR assay.

The DNA from one of the two aliquots was assayed by multiplex real-time PCR using a previously–established protocol in our lab while the other aliquot was assessed by the novel PNA assay described above. The exact same protocol listed under "Modified CD14, CD16 and HIV DNA Labeling with Qdots" was used. An overview of this procedure is illustrated in Figure 4.5. Samples were tested in triplicate.

This experiment was designed as a proof-of-concept test that was completed to compare the current method to measure HIV DNA with the novel flow-FISH assay and was completed only once. Future tests must be completed for further validation.

Results

PNA Probe Specificity. Each of the following specificity experiments were performed once to demonstrate feasibility and specificity. Positive and negative controls were analyzed with PNA to determine the specificity of the probe for HIV DNA. The positive controls consisted of the following HIV-infected cell lines: U1, ACH-2, 8E5, and OM10.1. Addition of the PNA probe to these cell lines and analysis by flow cytometry revealed that 50% of the U1 cells contained HIV DNA, followed by 43% positivity for ACH-2, 74% for 8E5, and 74% for OM10.1, Figure 4.6A-D.

The negative controls consisted of the following non-HIV infected cell lines: U937, Ramos, and THP-1. Analyzing these cell lines with flow cytometry to detect any non-specific PNA probe binding revealed 6.2% positivity for U937, 7.0% for Ramos, and 2.4% for THP-1, Figure 4.7A-C.

PNA Probe Sensitivity. This titration assay to demonstrate probe sensitivity was completed once to show proof-of-concept. The sensitivity of the PNA probe for HIV detection was assessed by titrating the HIV-infected cell line, OM1O.1, with a non-HIV infected cell line, H9. DNA from the OM10.1 cell line was titrated with DNA from the H9 cell line as follows: 100% OM10.1 (0% H9), 75% OM10.1 (25% H9), 50% OM10.1 (50% H9), 25% OM10.1 (75% H9), and 0% OM10.1 (100% H9). Analysis with the PNA probe resulted in following: 68% positivity for the 100% OM10.1 sample; 28% for the 75% OM10.1 sample; 19% for the 50% OM10.1 sample; 10% for the 25% OM10.1 sample; and 5% for the 0% OM10.1 sample, Figure 4.8A-F.

Surface Receptor Labeling Accuracy. To validate the integrity of the antibody under the harsh conditions required for the PNA probe, fluorescence detection from a standard staining procedure was compared to that of the flow-FISH technique. Based on the forward scatter of the cells, the high temperature exposure to the flow-FISH cells causes them to be larger than the normal stained cells, Figure 4.9A-B. Despite the change in cell size, the CD14 positivity was approximately the same for the standard staining and flow-FISH cells, 13.10% and 13.05% respectively, Figure 4.10A-B.

Single Receptor and PNA probe labeling. Identification of CD14 cells and the amount of HIV DNA harbored by the cells using flow cytometry is depicted in Figure 4.11. The dot plots demonstrated that 45.9% of the cells are labeled with the PNA probe (yellow), and 15.9% are labeled with anti-CD14-Alexa488 antibody (purple), i.e. approximately half of the CD14 cells contain HIV DNA and that 15.9% of the total cells analyzed were monocytes. The plots also revealed that of the total monocytes, only 1.1% contain HIV DNA, which represent the double-positive cells.

Fluorescent microscopy enabled visualization of the PBMC that were monocytes and the cells containing HIV DNA, Figure 4.12. The cells with HIV DNA were labeled with the PNA probe and identified by Cy5 emission (red), Figure 4.12B. The CD14-stained monocytes were identified by Alexa 488 emission (green), Figure 4.12C. By overlaying the two images, the monocytes containing HIV DNA were identified, Figure 4.12D.

Modified Protocol with Qdots. Detection of Qdot 605 fluorescence in only the PE and PE-Texas Red channels validated its use in the flow-FISH assay because it does not interfere with the FITC and APC channels, which were used for Alexa 488 and Cy5 fluorescence, and only emitted in the PE and PE-Texas Red channels, Figure 4.13.

Analysis of CD14 and CD16 in another HIV-positive PBMC sample revealed that 13.7% of the total cell population were activated non-monocytes (CD14-/16+); 3.4% were activated monocytes (CD14+/16+); 70.1% were non-activated non-monocytes (CD14-/16); and 12.8% were non-activated monocytes (CD14+/16-), Figure 4.14A, 4.14B, 4.14C, and Table 4.1. In these various PBMC populations, 48.6% of the activated non-monocytes contained HIV DNA; 73.4% of the activated monocytes contained HIV DNA; 40.6% of the non-activated non-monocytes contained HIV DNA; and 59.9% of the non-activated monocytes contained HIV DNA, Figure 4.14D and Table 4.1.

Multiplex Real-Time PCR versus flow-FISH. Comparison of the PNA probe positivity to the HIV DNA multiplex real-time PCR assay is depicted in Table 4.2. This experiment was done once to demonstrate proof-of-concept. The U1 cell line of which 50% of the cells contained HIV DNA as noted by fluorescence of the PNA probe was found to contain $1x10^6$ copies of HIV DNA per $1x10^6$ cells. ACH-2 had a 43% PNA-positivity and $3.6x10^5$ HIV DNA copies per $1x10^6$ cells. 8E5 had a 74% PNA-positivity and $8.4x10^5$ HIV DNA copies per $1x10^6$ cells. OM1O.1 also had a 74% PNA-positivity and $8.0x10^5$ HIV DNA copies per $1x10^6$ cells.

The infection protocol used to infect PBMC with the BaL virus was verified by increasing p24 concentration (0 pg/mL to 116.4 pg/mL) from day 1 post-infection to day 10 post-infection, Table 4.3.

Results from the detection of HIV DNA amongst the various PBMC-infected cell populations using the two techniques of flow-FISH, and fluorescence activated cell sorting (FACS) combined with the multiplex real-time PCR assay are shown in Table 4.4. Three PBMC cell populations were sorted using FACS and consisted of non-monocytes (CD14-), activated monocytes (CD14+/16+), and non-activated monocytes (CD14+/16-). The use of flow-FISH enabled the CD14- cells to be further analyzed into activated non-monocytes (CD14-/16+) and non-activated non-monocytes (CD14-/16-). Table 4.4 summarizes the HIV DNA results of the various cell fractions that were analyzed using both techniques. Generally both techniques gave comparable results demonstrating that the CD14+/16+ cell fraction contained the highest level of HIV DNA in all of sampled post-infection days.

Discussion

The main goal of this chapter was to demonstrate the feasibility and reliability of flow-FISH in the analysis HIV DNA in monocytes with the long-term goal to translate the technology to future studies.

The first experiments were completed in HIV-infected and HIV-negative cell lines to validate the PNA probe in detecting HIV DNA. Ideally, the HIV-infected cell lines were supposed to contain one HIV DNA copy per cell, binding of the PNA probe to HIV DNA in HIV-infected cell lines was not 100% but instead had a 43-74% positivity range, Figure 4.6A-D. While the reasons for discordant results are unknown, one hypothesis may be that the high specificity of the PNA probe may affect its binding due to variations in the targeted HIV binding sites as a one base pair mismatch highly effects its binding efficiency. As HIV is replicated in cells, a high frequency of error occurs and may lead to mutations in this particular region. Regardless, there was a clear distinction between PNA-positive and PNA-negative cells as depicted by the OM10.1 dot plot, Figure 4.6E. Furthermore, some non-specific binding occurred in the HIV-negative cell lines with PNA positivity ranging between 2.4-7.0%, Figure 4.7A-C. Similar to the results noted in HIV-infected cell lines, some fluorescence was detected in HIV-negative cell lines for unknown reasons; however, one possible explanation could be explained by the amount of cells used for analyzing the unstained and stained fractions. Since the unstained cells were needed to set the threshold for positivity, much less cells were needed than the stained fraction. The difference in cell amounts typically does not affect the majority of flow cytometry analyses but it may affect flow-FISH analyses, which involves exposure to harsh conditions that mainly consist of the 80°C heating

requirement of the PNA probe. Heat treatment results in an increase in cell size and may lead to increased autofluorescence [114]. Analysis of more cells may intensify autofluorescence shown through a broadened peak, Figure 4.7A-C. A broader peak would the lead to a shift the threshold.

The next experiments were designed to test the sensitivity of the PNA probe. An HIV-infected cell line (OM10.1) was titrated with an HIV-negative cell line (H9) and tested with the PNA probe. OM10.1 was chosen due to its higher PNA positivity in comparison to other HIV-infected cell lines. Five titrations were tested: 100% OM10.1 (0% H9); 75% OM10.1 (25% H9); 50% OM10.1 (50% H9); 25% OM10.1 (75% H9); and 0% OM10.1 (100% H9) with the following PNA positivity: 68%, 28%, 19%, 10%, and 5% respectively. As demonstrated by these results, the titration of OM10.1 with H9 led to a decrease in PNA fluorescent detection. Nonetheless, PNA probe detection differed from the expected percentages. For example, based on the 68% positivity of the 100% OM10.1 sample, the expected percentages were as follows: 51% for the 75% sample; 34% for the 50% sample; 17% for the 25% sample; and 0% for the 0% sample, Figure 4.8A-F. Thus, the 75%, 50% and 25% sample results were lower than expected but the 0% sample had 5% PNA positivity compared to the expected 0%. Based on the titration results, the hypothesis was that the sensitivity of the PNA probe decreased with lower HIV DNA levels. The 5% PNA positivity in the 0% sample be may be due to the autofluorescence of the cells as shown in the HIV-negative cell lines.

The stringent heating conditions required by the flow-FISH methodology could potentially influence the results thus optimizing the influence on cell surface labeling is essential. This was accomplished by comparing CD14 antibody binding in standard

conditions to that of flow-FISH. As was expected, use of heat caused the cells to increase in size, Figure 4.9A-B, resulting in decreased fluorescence as noted in the peak shift with lower intensity, Figure 4.10A-B. Additionally, the heated cells have increased autofluorescence that is also shown by the peak shift due to higher intensity fluorescence. Despite these intensity changes, CD14 detection was unchanged in both conditions with only a 0.5% difference. This experiment demonstrated that cell identification based on cell surface labeling in the flow-FISH assay is relatively reliable and accurate.

Upon confirmation that the PNA probe and the CD14 antibody were independently reliable, combining both in the assay to assess cells was then attempted. PBMC from HIV-positive individuals were analyzed with flow cytometry and fluorescent microscopy. By flow cytometry, CD14 cells [115] and HIV DNA (yellow) were uniquely identified, Figure 4.11. It was also possible to assess the amount of HIV DNA within the CD14 cells. Fluorescent microscopy enabled the visualization cells containing HIV DNA and within the monocytes from the PBMC sample. Furthermore, superimposing the two images allowed the visualization of the monocytes containing HIV DNA, Figure 4.12.

Subsequently, an attempt was made to simultaneously label two surface receptors with the PNA probe. Under the stringent conditions necessary for the PNA probe, limitations on fluorescent molecules had to be considered. The majority of organic fluorescent molecules are sensitive to extreme temperatures. As a result, the second surface receptor, CD16, labeled with a biotin-streptavidin binding system through the use of quantum dots (Qdots) that emit in the optimal fluorescence channels, Figure 4.13. Figure 4.14, detected CD14, CD16, and HIV DNA enabling identification of HIV DNA within various PBMC cell populations: activated non-monocytes (CD14-/16+), non-

activated non-monocytes (CD14-/16-), activated monocytes (CD14+/16+), and non-activated monocytes (CD14-/16-). The data showed that the majority of the PBMC were non-monocytes (CD14- cells) but that the monocytes (CD14+) contain more HIV DNA, Table 4.1. Moreover, the activated subsets harbored higher HIV DNA then their non-activated counterparts; consistent with the hypothesis that activated cells are more easily infected with HIV.

Although the flow-FISH technique appeared to be efficient at identifying different cell populations and the amount of HIV DNA that they contained, the assay remained to be validated. The flow-FISH assay and the multiplex real-time PCR assay to detect HIV DNA in cellular subsets will require validation using clinical specimens. Initially, cultured cells were used which included HIV-infected cell lines and established HIV-infected PBMC. Four HIV-infected cell lines were used to compare HIV DNA amounts: U1, ACH-2, 8E5, and OM10.1; with the majority of the cells showing comparable HIV DNA levels ranging from 7-16% difference with the exception of U1, which had a 50% difference, Table 4.2. Differences between the two techniques may be due to the different HIV regions targeted by the primers and probes. The PNA probe targets the *pol* gene while the primers in the multiplex PCR assay detects the *gag* gene. Another possible reason to account for the differences could be due to genetic susceptibility for nucleic acid mutations, which would affect the binding of the probe or primer. Mutations would have a greater impact on the PNA probe because of its decreased efficiencies with mismatches. This is most apparent with the U1 cell line, which portrays 50% PNA probe positivity and a disproportional copy number of $1x10^6$ HIV DNA copies per $1x10^6$ cells. A 50% PNA probe positivity would be equivalent to

$5x10^5$ HIV DNA copies per $1x10^6$ cells, which is 50% of the copy number calculated from the multiplex real-time PCR reaction.

Analysis of HIV DNA in HIV infected PBMC established in the laboratory using both techniques detected similar HIV DNA revealing the highest levels in activated monocytes (CD14+/16+) with the second highest levels in non-activated monocytes (CD14+/16-). Confirmed by both techniques, these results support findings that peripheral monocytes are more permissive to infection in comparison to non-monocytes that are primarily T-lymphocytes regardless of the fact that lymphocytes compose the majority of PBMC [74]. In vitro, the apparent decrease in apparent number of monocytes post-infection is most likely due to the phenomena of cellular clumping while in culture. During post-infection, the cells were maintained in culture in special plates to prevent monocytes from adhering and differentiate into macrophages. Monocytes have a natural tendency of adherence so since they are not able to adhere to the plate, they will presumably adhere to each other.

There may be advantages for using both techniques in analyzing HIV DNA. Flow-FISH allowed for more cell fractions to be analyzed and was less time consuming while the use of FACS and real-time PCR provided more detailed information regarding quantity of cells sorted and HIV DNA copy numbers. Each technique provides unique advantages associated thus a combination of both assay may be beneficial providing an adequate number of cells are available. Future directions to utilize the flow-FISH technique in a more efficient manner could focus on redesigning the PNA probe to target the same *gag* region used as the primers for the multiplex real-time PCR HIV copy

number assay. Or to alternatively redesign primers and probes for the HIV copy number assay to detect the *pol* region that the PNA probe binds to.

Overall, this chapter established the feasibility of the flow-FISH assay that was designed to detect HIV DNA within activated and non-activated monocytes and non-monocytes. It is comparable to a current method of detecting HIV DNA established in the laboratory and has been demonstrated to work in PBMC. Therefore, the applications of this technique in future HAND studies may help expand our current understanding of the disease.

Table 4.1 Flow-FISH Results

Cell Fraction	% of Total Popl'n	% PNA-Positive
CD14-/16+	13.7%	48.6%
CD14-/16-	70.1%	40.6%
CD14+/16+	3.4%	73.4%
CD14+/16-	12.8%	59.9%

Table 4.2. Cell Line Comparison

HIV Cell Line	PNA Probe Positivity	HiV DNA per 1x 10^6 Cells
U1	50%	$1x10^6$
ACH-2	43%	$3.6x10^5$
8E5	74%	$8.4x10^5$
OM10.1	74%	$8.0x10^5$

Table 4.3. p24 Results

Sample	p24 Conc (pg/mL)
Day 1 post-infection	0
Day 5 post-infection	31.3
Day 10 post-infection	116.4

Table 4.4

Table 4.4. Flow-FISH versus FACS/PCR

Sample	Cell Fraction	Flow-FISH		FACS/PCR	
		% of Total Popl'n	**% PNA-Positive**	**Amt of Cells Sorted**	**HIV DNA per Cell**
Day 1 pi	CD14-/16+	20%	21%	5000	0.97
	CD14-/16-	51%	35%		
	CD14+/16+	27%	89%	5000	3.80
	CD14+/16-	3%	62%	49	1.21
Day 5 pi	CD14-/16+	11.5%	24%	5000	0.98
	CD14-/16-	79.6%	28%		
	CD14+/16+	5.7%	81%	1461	3.82
	CD14+/16-	3.2%	52%	212	3.25
Day 10 pi	CD14-/16+	9.3%	10%	5000	0.26
	CD14-/16-	74.2%	14%		
	CD14+/16+	6.1%	65%	324	2.50
	CD14+/16-	10.5%	22%	44	1.85

Figure 4.1 – Drawings that display characteristics of a peptide nucleic acid (PNA). A) Backbone structures that compare DNA and PNA oligonucleotides. B) DNA strand displacement called the D-loop that results from the binding of PNA to DNA. Obtained from Wang, G. and X.S. Xu, *Peptide nucleic acid (PNA) binding-mediated gene regulation.* Cell Res, 2004. **14**(2): p. 111-6.

Figure 4.1

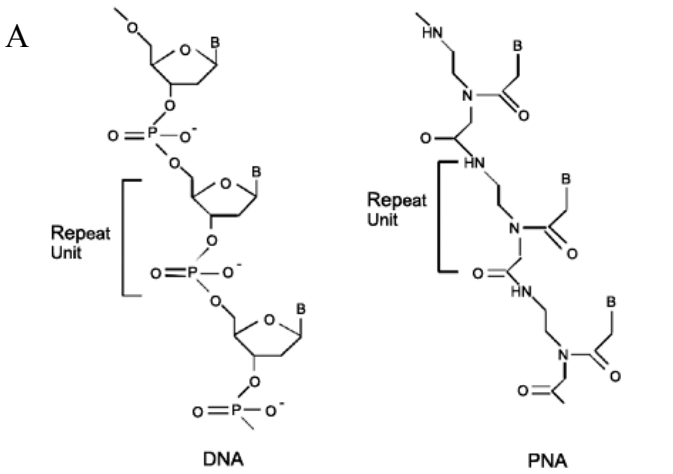

Wang, Xu. Cell Res 14(2):111-116.

Figure 4.2 – Absorption and emission profiles of Qdot nanocrystals (Invitrogen, Carlsbad, CA). Qdots are known for their braod absorption spectra and narrow emission profiles. Obtained from the Invitrogen Qdot brochure.

Figure 4.2

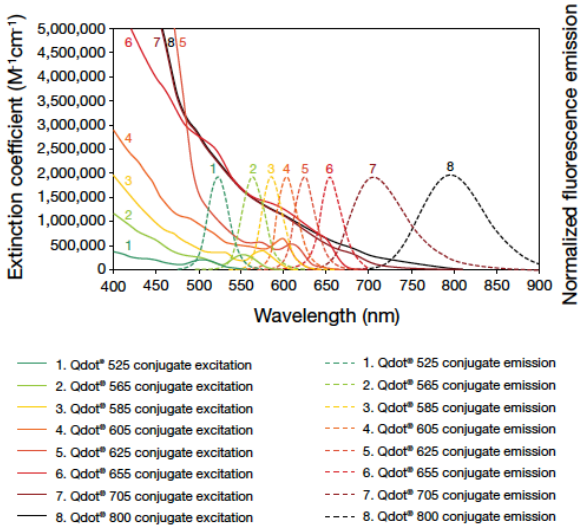

Invitrogen Corporation (Carlsbad, CA)

Figure 4.3 – The detection of HIV-1 with a peptide nucleic acid (PNA) probe in smeared lymphocytes from A) a HIV-negative donor and from B) a HIV-positive donor. The PNA-probe is conjugated to Fluorescein isothiocyanate (FITC). Images were obtain from studies done in Murakami, T., et al., *A novel method for detecting HIV-1 by non-radioactive in situ hybridization: application of a peptide nucleic acid probe and catalysed signal amplification.* J Pathol, 2001. **194**(1): p. 130-5.

Figure 4.3

A

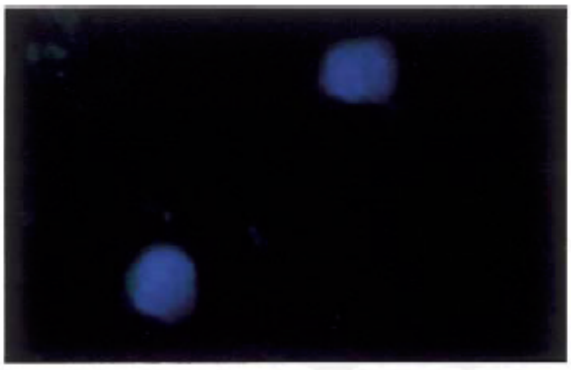

B

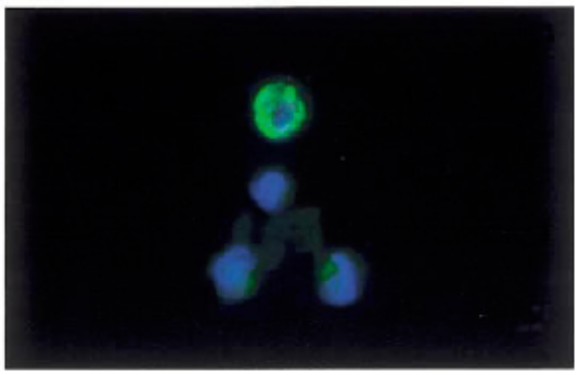

Murakami, T., et al., J Pathol, 2001. **194**(1): p. 130-5

Figure 4.4 – Illustration of flow-FISH technique that was designed to detect HIV DNA in CD14+/16+ cells. Anti-CD14-Alexa488 and anti-CD16-biotin antibodies are bound to the surface receptors of cells then Streptavidin-Qdot605 was added and bound to CD16-biotin. After the surface receptors are labeled, the peptide nucleic acid (PNA) that is conjugated to Cyanine 5 is added and binds to HIV DNA. Flow cytometry is used for fluorescence detection.

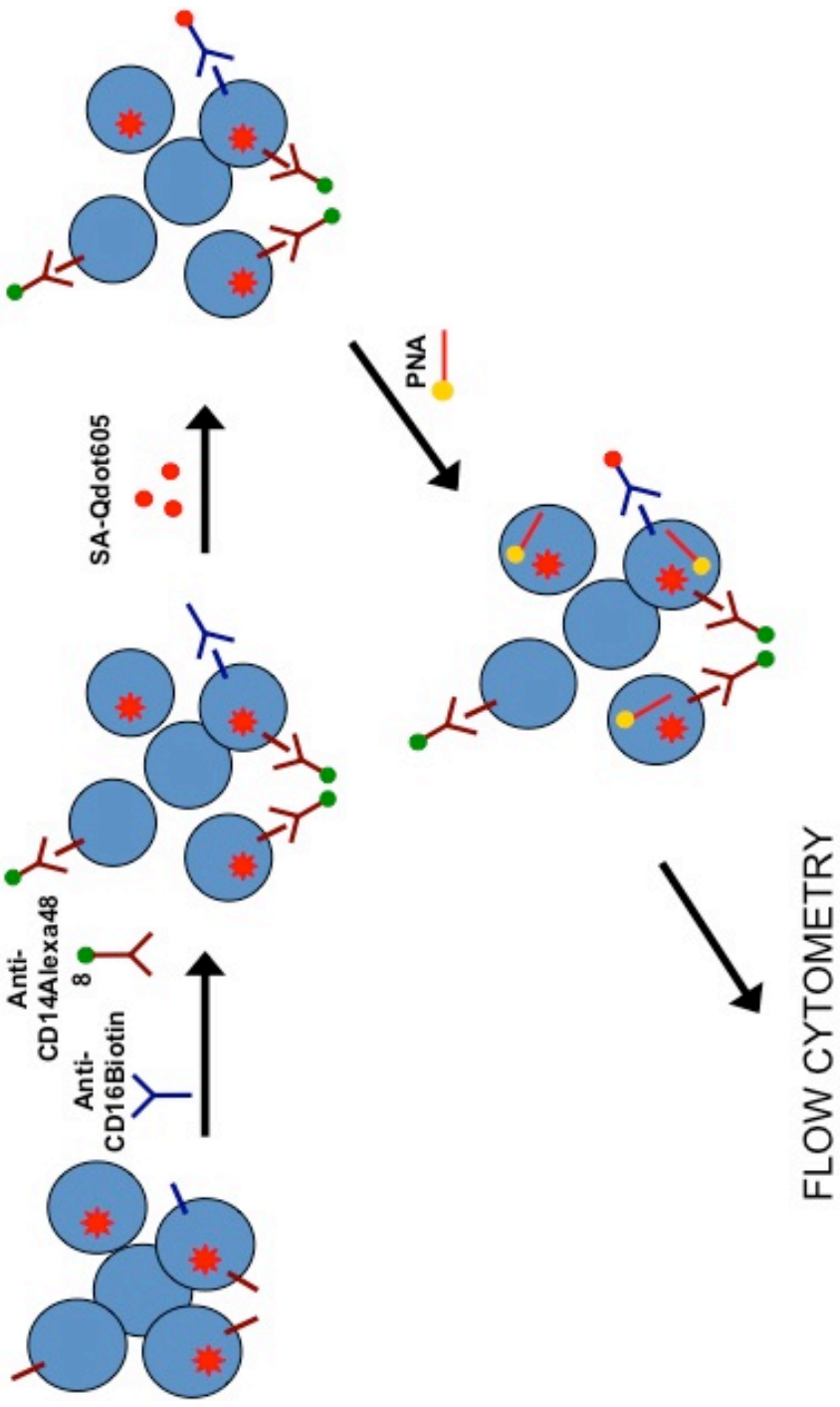
Anti-CD16Biotin
Anti-CD14Alexa488
SA-Qdot605
PNA
FLOW CYTOMETRY

Figure 4.4

Figure 4.5 – Experimental design used to compare fish-FLOW to the cell sorting/HIV DNA copy number assay. Briefly, peripheral blood mononuclear cells (PBMC) are infected with the HIV-1 BaL virus (R5 strain) and cultured over a period of 10 days. Cell and supernatant aliquots were taken on Days 1, 5, and 10 post-infection for p24 and HIV DNA analyses. This experiment was designed as a proof-of-concept test and was completed once.

Figure 4.5

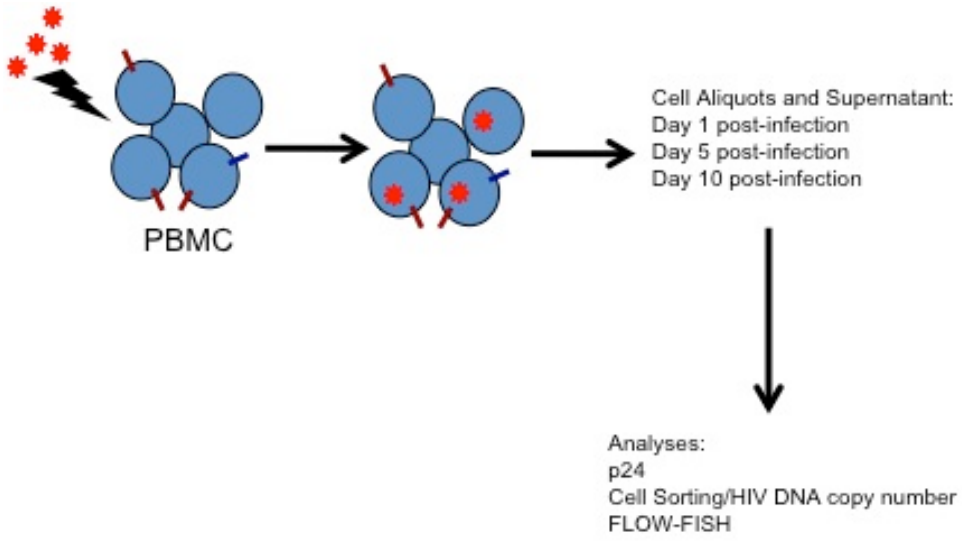
PBMC
Cell Aliquots and Supernatant:
Day 1 post-infection
Day 5 post-infection
Day 10 post-infection
Analyses:
p24
Cell Sorting/HIV DNA copy number
FLOW-FISH

Figure 4.6 – Histogram plots from the peptide nucleic acid (PNA) probe specificity test using HIV-positive cell lines. A) U1 monocytic; B) ACH-2 T-lymphocytic; C) 8E5 T-lymphocytic; and D) OM10.1 promyelocytic cell lines. E) Dot plot showing the OM10.1 cells that are labeled with the PNA probe, red: unstained cells and blue: PNA-positive cells. There was a 5-10% variation between multiple test runs in singlet on ACH-2, OM10.1, and 8E5. U1 was only tested once.

Figure 4.6

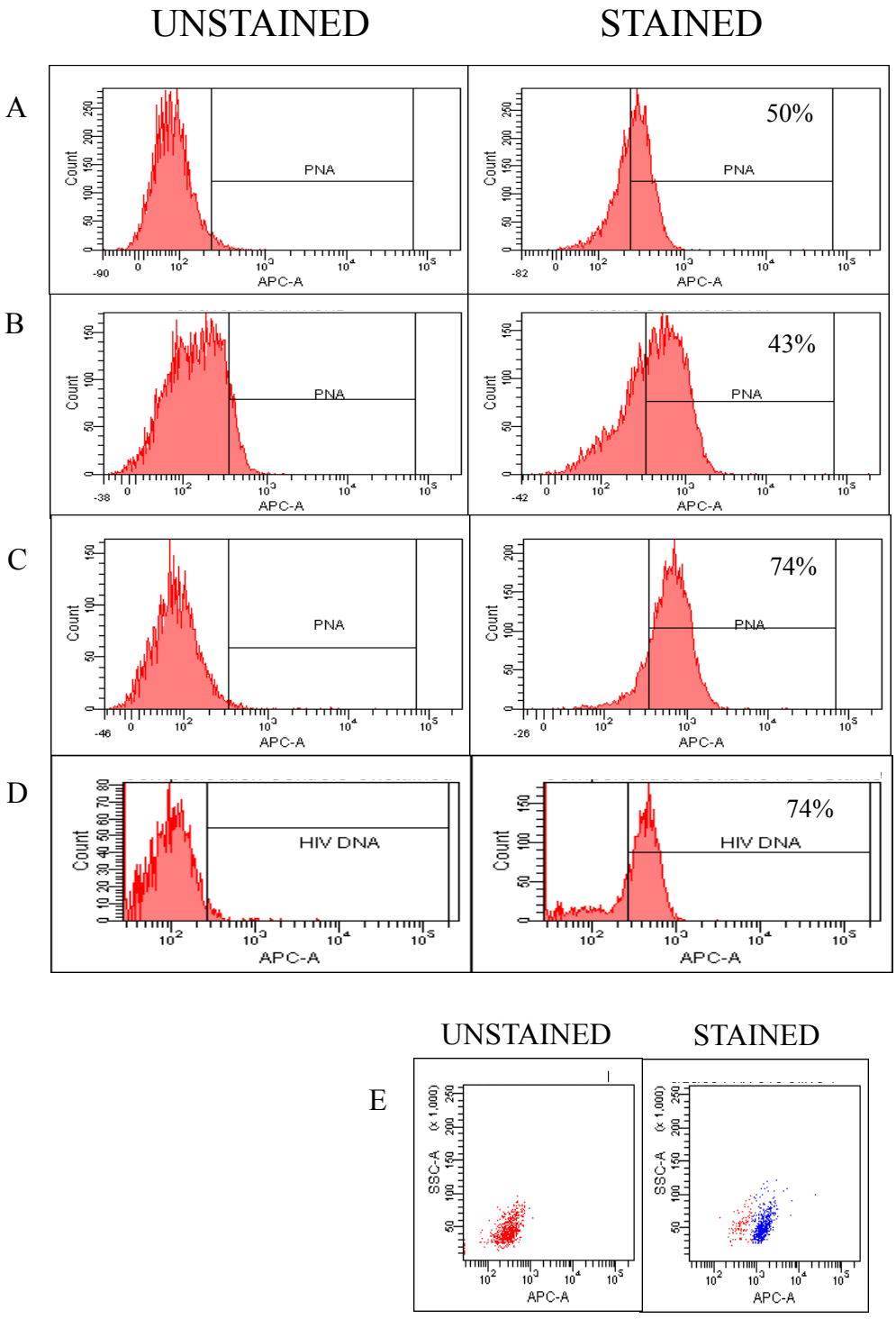
UNSTAINED
STAINED
A
B
C
D
E
PNA
HIV DNA
50%
43%
74%
74%
Count
APC-A
SSC-A
(x 1,000)

Figure 4.7 – Histogram plots from the peptide nucleic acid (PNA) probe specificity test using HIV-negative cell lines. A) U937 monocytic; B) Ramos B-lymphocytic; and C) THP-1 monocytic cell lines. HIV-negative cell lines were run once.

Figure 4.7

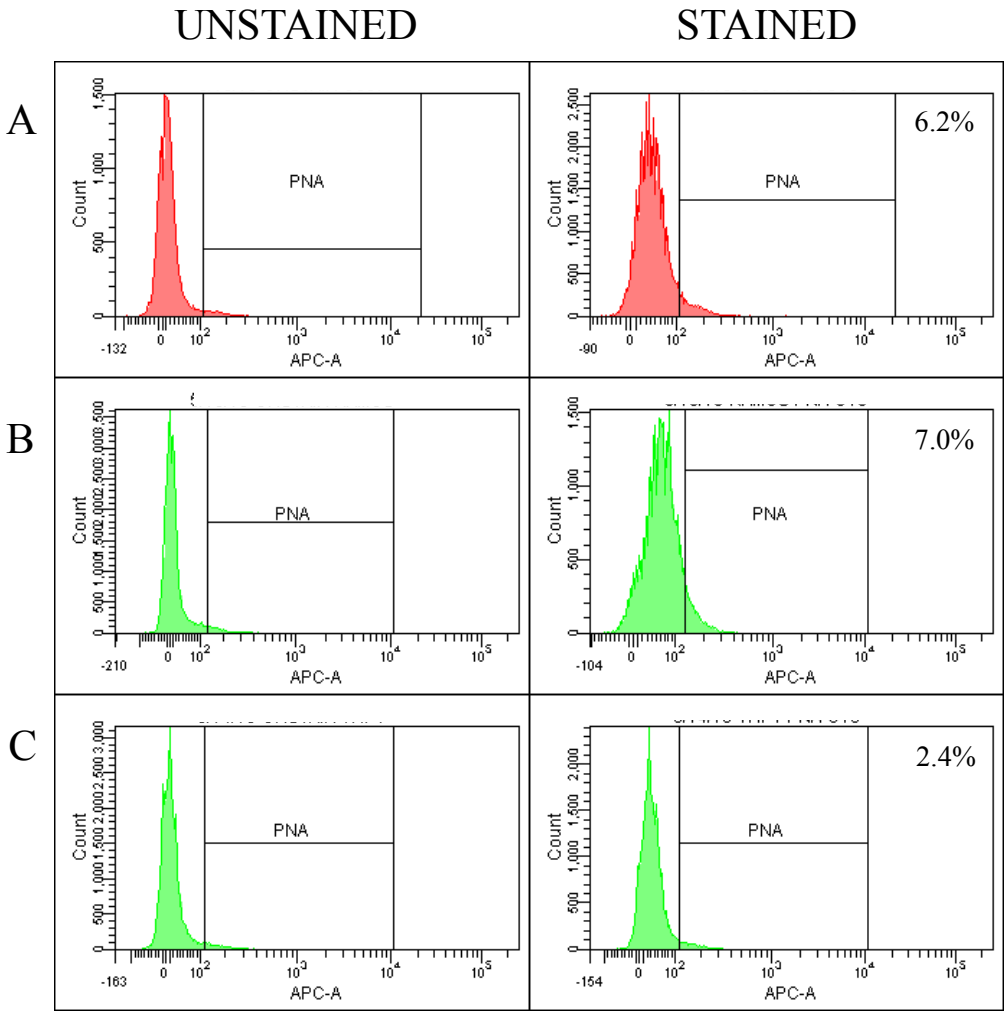

Figure 4.8 – Peptide nucleic acid (PNA) probe sensitivity test done through the titration of a HIV-positive cell line, OM10.1 with a HIV-negative cell line, H9. A) Unstained sample. The probe was used to detect HIV DNA in samples that contained B) 100% OM10.1; C) 75% OM10.1; D) 50% OM10.1; E) 25% OM10.1; and F) 0% OM10.1. Dilutions were tested once.

Figure 4.8

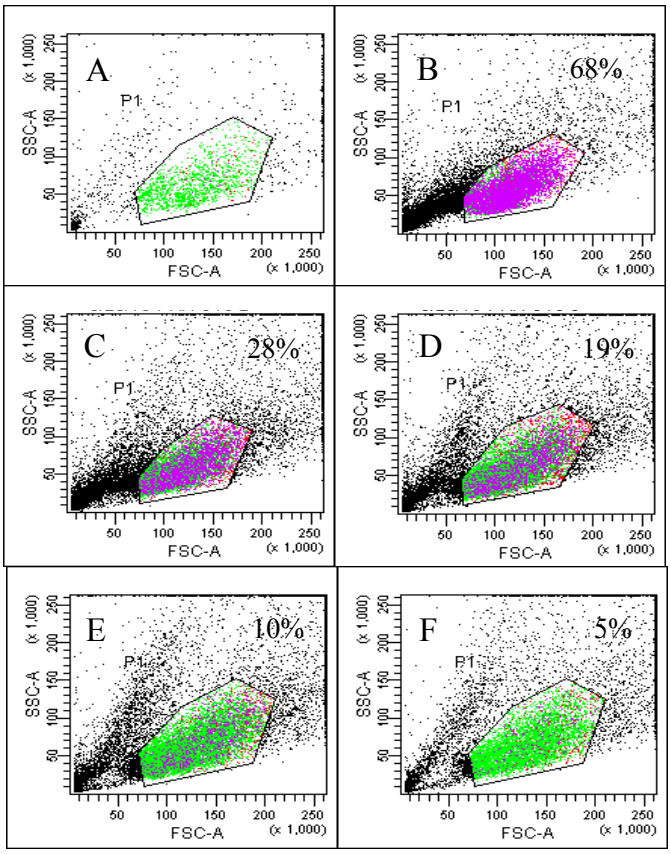
A
P1
B
68%
P1
C
28%
P1
D
19%
P1
E
10%
P1
F
5%
P1
SSC-A
(x 1,000)
FSC-A
(x 1,000)
50
100
150
200
250

Figure 4.9 – Forward scatter (FSC) and side scatter (SSC) dot plots of A) peripheral blood mononuclear cells (PBMC) that were stained with anti-CD14-Alexa 488 under normal conditions and B) PBMC that were stained with anti-CD14-Alexa 488 under the conditions of flow-FISH.

Figure 4.9

A

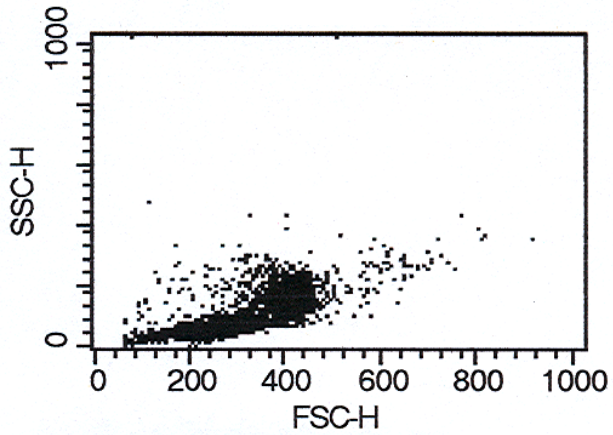
SSC-H
1000
0
0
200
400
600
800
1000
FSC-H

B

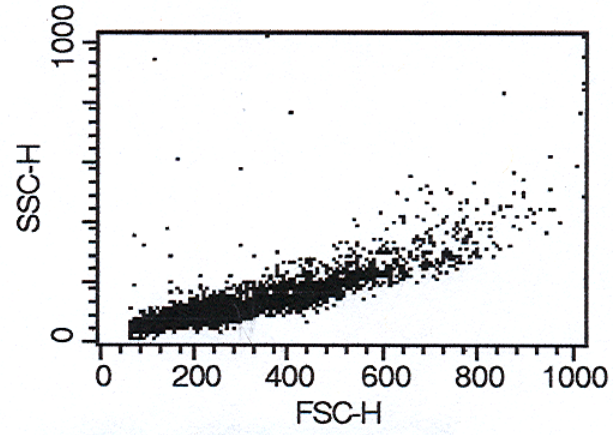
SSC-H
1000
0
0
200
400
600
800
1000
FSC-H

Figure 4.10 – Histogram plots of peripheral blood mononuclear cells (PBMC) that were that were A) stained with anti-CD14-Alexa 488 under normal conditions and B) PBMC that were stained with anti-CD14-Alexa 488 under the conditions of flow-FISH. The green line displays the unstained cell peaks.

Figure 4.10

A

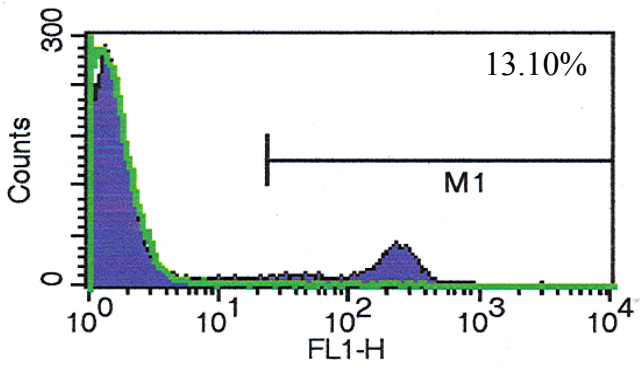

B

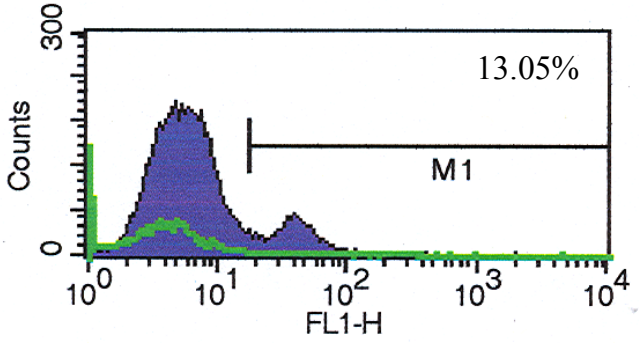

Figure 4.11 – Dot plots of HIV-infected peripheral blood mononuclear cells that are labeled with CD14-Alexa 488 and peptide nucleic acid (PNA)-Cyanine 5 to identify CD14+ cells (purple), HIV DNA (yellow), and CD14+ cells that contain HIV DNA. Unstained cells are red.

Figure 4.11

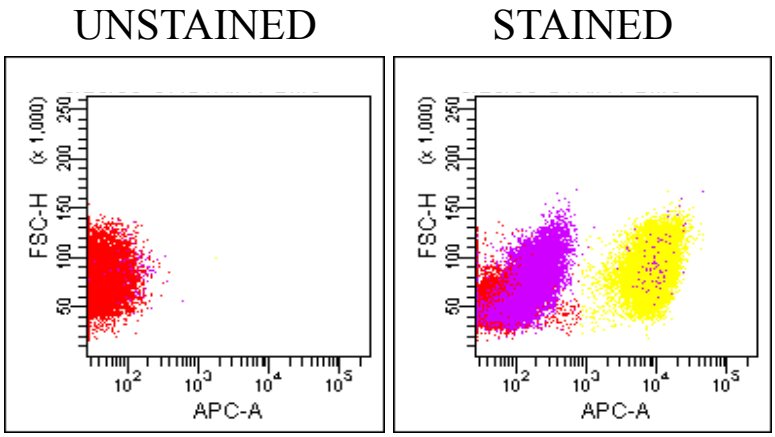

Figure 4.12 – Fluorescence microscopy images of peripheral blood mononuclear cells that are labeled with CD14-Alexa488 and peptide nucleic acid (PNA)-Cyanine 5. A) Brightfield image; B) Image showing cells containing HIV DNA; C) Image showing CD14+ cells; and D) overlay of images B and C showing CD14+ cells containing HIV DNA.

Figure 4.12

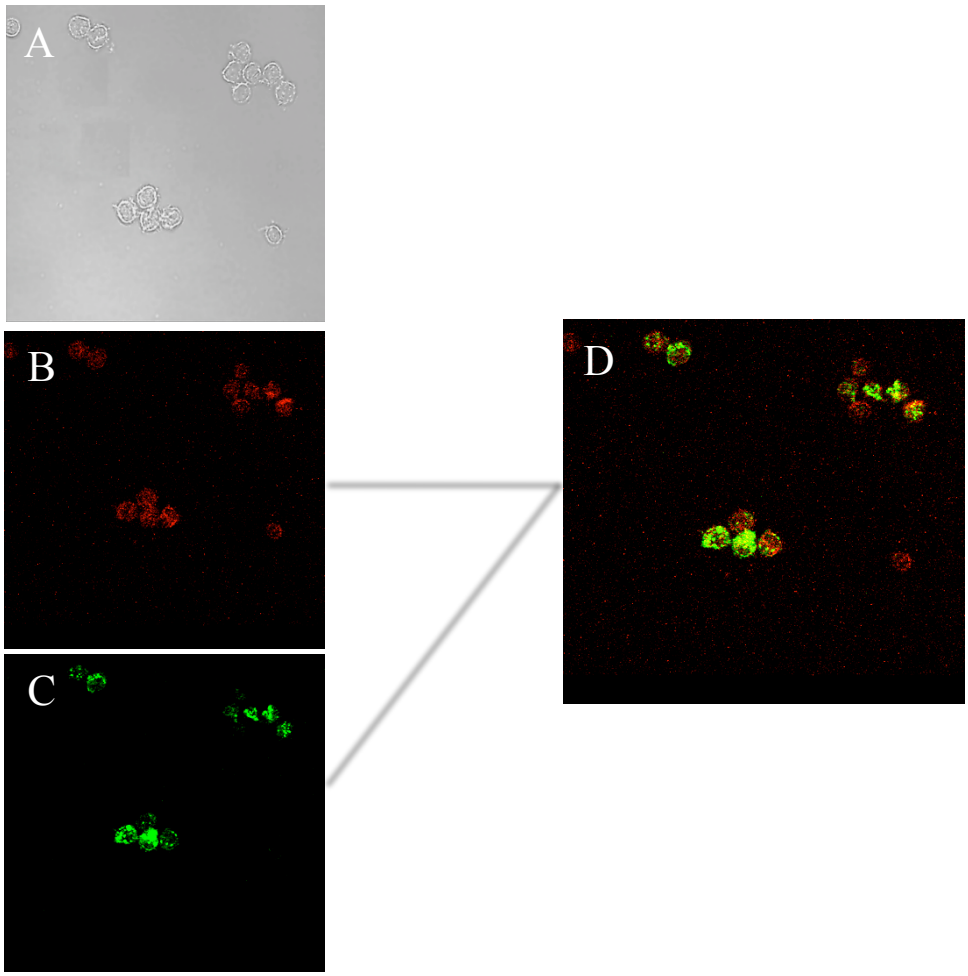

Figure 4.13 – Histogram plots showing the fluorescence of Streptavidin-Quantum dots (Qdot) 605 that are bound to biotin beads in the various emission channels. A) Gating on beads; B) Fluorescein isothiocyanate (FITC) channel; C) phycoerythring (PE) channel; D) PE-Texas Red channel; E) Phycoerythrin-Cyanine 7 (PE-Cy7 channel); F) Peridinin chlorphyll-Cy5.5 (PerCP-Cy5.5); G) APC (Allophycocyanin); and H) APC-Cy7.

Figure 4.13

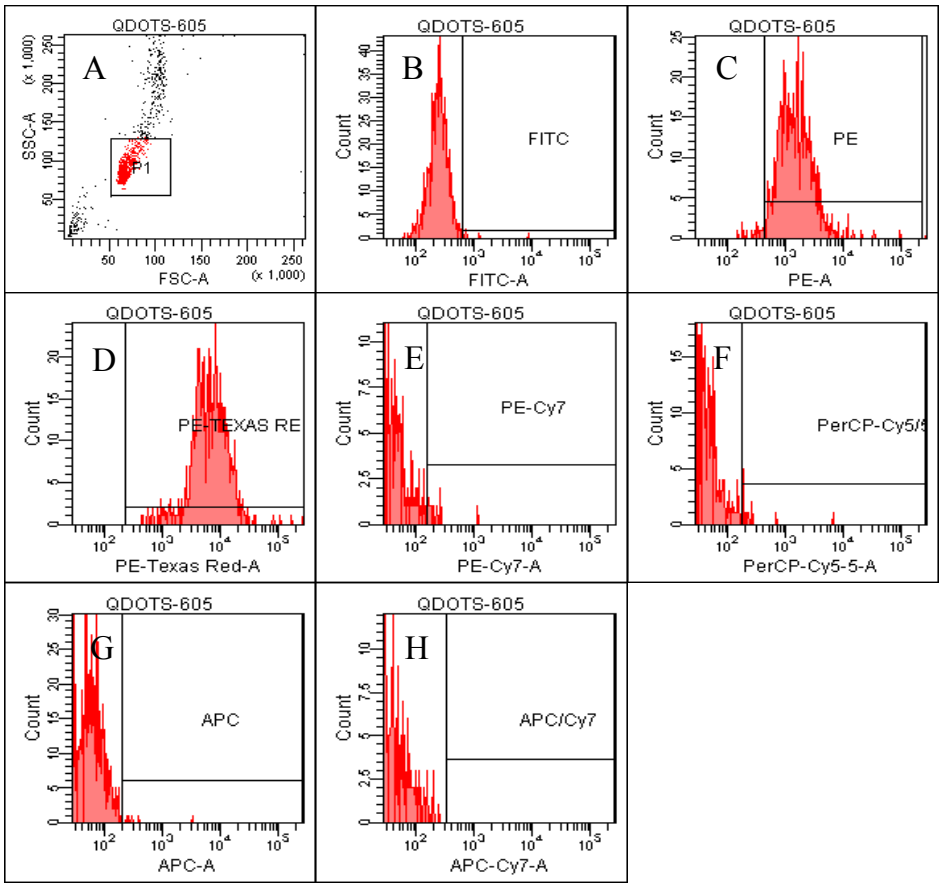
QDOTS-605
A
SSC-A
(x 1,000)
P1
FSC-A
(x 1,000)
B
FITC
Count
FITC-A
C
PE
PE-A
D
PE-TEXAS RE
PE-Texas Red-A
E
PE-Cy7
PE-Cy7-A
F
PerCP-Cy5-5-A
G
APC
APC-A
H
APC/Cy7
APC-Cy7-A

Figure 4.14 – The use of flow-FISH to analyze HIV DNA within various populations in peripheral blood mononuclear cells. A) Dot plot showing the various populations that were analyzed: CD14-/CD16- (bottom left); CD14-/CD16+ (top left); CD14+/16- (bottom right); and CD14+/16+ (top right). Histogram plots showing peaks for B) CD14; C) CD16; and D) PNA/HIV DNA.

Figure 4.14

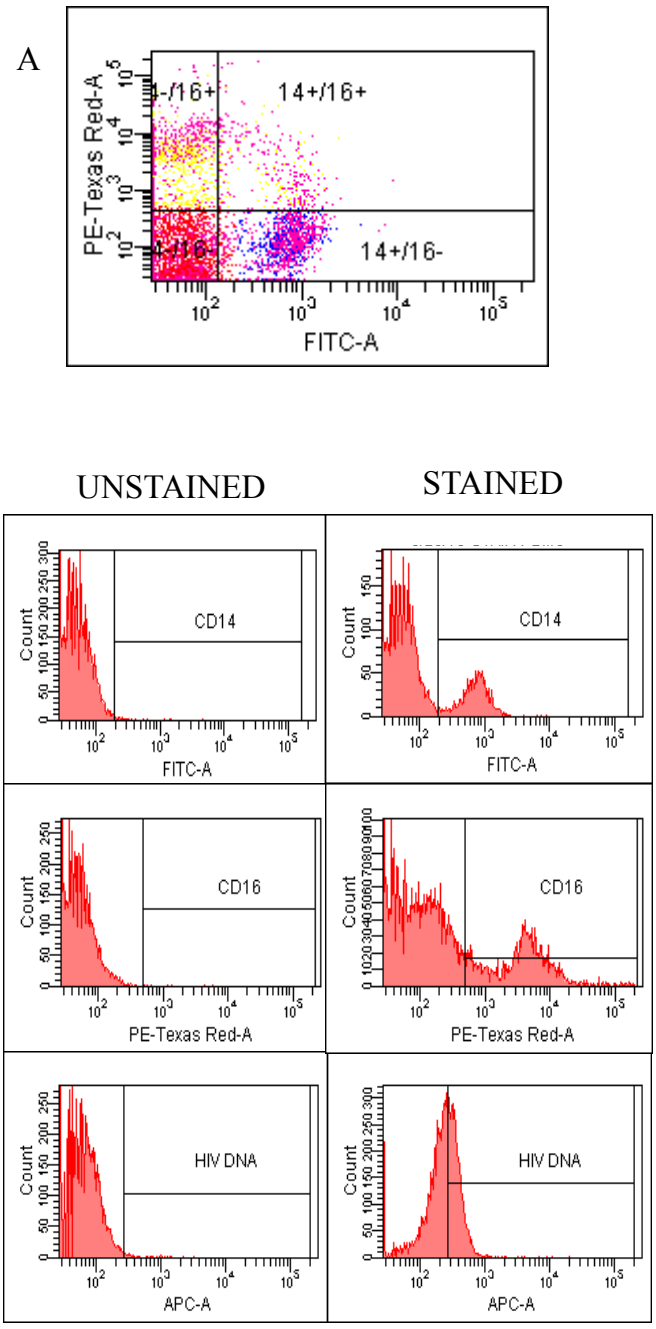
A
14+/16+
14+/16-
PE-Texas Red-A
FITC-A
UNSTAINED
STAINED
B
CD14
Count
FITC-A
C
CD16
PE-Texas Red-A
D
HIV DNA
APC-A

CHAPTER 5

HIV Integration and its Potential Role in HAND

Abstract

Background: Insertional mutagenesis occurs when HIV inserts itself near or within particular genes whose over or under expression may facilitate the development of HIV-related diseases. Though no HIV integration sites are known to promote HIV-associated neurocognitive disorders (HAND), it plausible that HIV may disrupt the expression of inflammatory or apoptotic genes that may contribute to HAND development. This is the first report that identifies HIV integration sites within various cerebrospinal fluid (CSF) cell subsets in HIV-positive individuals diagnosed with and without HAND. **Materials and Methods:** A DNA walking method was used to identify HIV integration sites in HIV-positive cell lines (OM10.1, ACH-2, and 8E5) along with CSF samples from individuals diagnosed with HAND (n=3) and normal cognition, NC (n=3). The CSF samples were sorted into CD14-, CD14+/16+, and CD14+/16- cell fractions; of which the DNA was extracted and underwent whole genome amplification. Identification of HIV integration sites was completed once for all samples. **Results and Conclusions:** The HIV integration assay was validated in an HIV-positive cell line through agreement with a previous publication that identifies HIV integration in 8E5 to be in chromosome 13. Common integration sites found within the various subsets and diagnosis include but were not limited to genes involved in apoptosis, macrophage behavior, and transcription regulation. These integration sites may play a role in the pathogenesis; therefore, more studies need to be done to validate these sites and to indentify more possible sites.

Overview

Subsequent to the internalization of viral RNA and reverse transcription of viral RNA into DNA, the integration of HIV-1 into the host cell genome is required for the production of viral progeny because it allows for the expression of viral genes and proteins [70, 116, 117]. This essential step of proviral formation is dependent on the catalytic activity of integrase [117]. Both the synthesis of viral DNA and the structure of the provirus have been intensely studied, however, the specifics of integration sites remain ambiguous. Despite this ambiguity, numerous studies have been undertaken to determine whether the previous theory of random integration still holds.

Studies have reported that transcriptionally active genomic regions such as DNase I hypersensitive sites [118] and CpG islands [68] are favored integration sites due to easy chromatin accessibility [116]. In addition, it has been shown that HIV-1 is preferentially integrated near repetitive elements such as L1Hs and Alu [69, 70], which are the two most common DNA repeated elements in the human genome. Furthermore, it was found that the provirus integrated proximal to genes that encoded proteins associated with the regulation of signal transduction networks, transcription and translation, as well as with other cellular processes [67].

Although the exact effects of preferential integration sites are currently unknown, many believe that it could potentially play a role in disease pathogenesis. This belief led to the formulation of a theory called insertional mutagenesis, which occurs when HIV-1 inserts itself into an essential coding region that causing the gene for which it codes for to be disrupted [71]. These insertion sites of the provirus may mediate the dysregulation of

specific gene expression events; thereby providing a possible mechanism that can contribute to the pathogenesis associated with HIV-associated neurocognitive disorders (HAND). Currently, the Trojan Horse mehanism is widely accepted as the model for HAND development. In this mechanism CD14+ monocytes, particularly the activated subset (CD14+/16+), are believed to transport the virus into the CNS. Once in the CNS, these cells then produce an overabundance of cytokines and other neurotoxins that eventually lead to neuronal apoptosis. In addition, HIV integration studies completed by Mack et al commonly identified HIV-1 integration sites within transcriptionally active host cell genomic regions and many sites that were proximal to genes associated with regulation of transcription, translation, signal transduction and other cellular processes. [67]. In HIV-associated dementia cases, they identified 15 chromosomal integration sites, Table 5.2. Furthermore, they found the high HIV DNA in tissue, Figure 5.2A, and HIV-1 p24 antigen to be predominantly localized to macrophages in the diseased CNS, Figure 5.2B. Therefore, it may be of importance then to determine if insertional mutagenesis plays a role in the cells of the monocytic lineage through the detection of integration sites within these cells.

The unknown flanking host DNA sequences adjacent to the integrated virus have been determined by genomic cloning, inverse PCR, biotinylated DNA labeling followed by PCR and other PCR-based methods, however, many disadvantages are associated with these methods (10). For example, genomic cloning is time consuming due to the requirement of establishing genomic DNA libraries and PCR based methods that consist of critical ligation, tailing or biotinylating steps (10). These disadvantages, however, can be overcome through the use of Seegene's DNA Walking *SpeedUp*™ Premix Kit

(Seegene Inc, Seoul, Korea), which utilizes Seegene's ACP™ (Annealing Control Primer) Technology.

Seegene's DNA Walking *SpeedUp*™ Premix Kit consists of a PCR Master Mix and unique DNA Walking ACP (DW-ACP) primers that are designed to capture unknown sites. Before this method can be used, target specific primers (TSP) must be designed to bind to various HIV-1 regions. This method involves three consecutive PCR reactions. In the first PCR reaction, four separate reactions are carried out, each of which uses one of the four ACP primers (DW-ACP) and a TSP that primes the known sequence (HIV-1). This results in the amplification of the target region from the template. The second and third reactions are nested PCR reactions that amplify the target from the first and second PCR products respectively, Figure 5.1A. The third PCR reaction is used for gel electrophoresis and the intense product bands are excised and the products are isolated, Figure 5.1B. The isolated products are then sent for direct sequencing to identify genes that are adjacent to or disrupted by HIV-1.

The scarcity of cells within the cerebrospinal fluid (CSF) make their analysis extremely challenging; therefore, the primary goal of this chapter is to demonstrate the feasibility of using the Seegene's DNA walking technique in the identification of HIV-1 integration sites within various cell fractions of the CSF, including non-monocytes (CD14-), activated monocytes (CD14+/16+), and non-activated monocytes (CD14+/16-) of HIV-infected individuals with HAND and normal cognition. It is hypothesized that individuals with HAND will have more identifiable integration sites, particularly in the monocytic cells, then those with normal cognition. These integration sites are possibly within genes that when disrupted would have an effect on the development and

maintenance of HAND. The results from this study will help to expand our knowledge of HAND pathogenesis through the involvement of insertional mutagenesis in the cells of monocytic lineage.

Materials and Methods

Patients and CSF DNA. DNA was extracted from the CSF cells obtained from 6 subjects that were enrolled in the Hispanic-Latino Longitudinal Cohort of HIV-seropositive women (HLLC), University of Puerto Rico Medical Sciences Campus (UPRMSC). These cells were sorted into three cell populations: CD14-, CD14+/16+, and CD14+/16- using fluorescent activated cell sorting (FACS). Once these cell fractions were obtained, the DNA was extracted using the QIAamp DNA Micro Kit (Qiagen, Valencia, CA) as per guidelines set by the manufacturer in the protocol handbook and eluted in 20 uL TE buffer. Half of the subjects were diagnosed with HAND and the other half were diagnosed as having normal cognition based on guidelines set in the American Academy of Neurology HIV dementia criteria (1991). The DNA from these cells was also in a multiplex HIV DNA assay to determine the amount of HIV DNA per cell.

DNA Repair and Whole Genome Amplification. Since the majority of the extracted DNA was used in the HIV DNA assay, the remaining DNA underwent whole genome amplification so that there was sufficient amount of DNA to detect HIV integration sites, Figure 5.3. A modified protocol using the REPLI-g formalin-fixed paraffin-embedded (FFPE) kit (Qiagen, Valencia, CA) was used in which began with a DNA repair step to allow repair of any DNA that could have been damaged in the cell sorting process. The DNA repair step includes a 60°C (60 minute) incubation of 10 uL of DNA with 1 uL of the proteinase K solution that was included in the kit to remove any contamination. The enzyme is then deactivated during a 10 minute 95°C incubation step. A random ligation step follows to piece together any fragments that may have resulted from the fixation

step, though the exposure to paraformaldehyde (PFA) was limited to minimize the damage. The ligation process included a 24°C (30 minute) incubation in 10 uL of FFPE mastermix, which included 8 uL FFPE buffer, 1 uL ligation enzyme, and 1 uL FFPE enzyme. An inactivation step followed with incubation at 95°C (10 minute) and repaired DNA was cooled to 4°C. Whole genome amplification (WGA) followed the repair process in which 30 uL of the REPLI-g mastermix is added to the repaired DNA. The REPLI-g mastermix included 29 uL of REPLI-g midi reaction buffer and 1 uL of REPLI-g Midi DNA polymerase. The WGA incubation occurs at 30°C (8 hours) and 95°C (10 minute) followed with the addition of 50 uL TE buffer.

An experiment was done to ensure that the use of WGA DNA gave reliable results that were equivalent to those that would be obtained from the same DNA that was not whole genome amplified. To test WGA DNA reliability, a PBMC DNA sample underwent WGA using the above protocol to be used in comparison to non-WGA PBMC DNA. Both the WGA and non-WGA PBMC DNA samples were used in the integration assay.

Determining Integration Primers. Several HIV-1 primers were designed using the complete HIV-1 genome (NCBI Reference Sequence NC_001802.1). The primers were used in a PCR reaction with the OM10.1, a promyelocytic cell line latently infected with HIV-1 to identify three reverse HIV-1 primers that would be optimal to use in the integration assay along with one HIV-1 reverse primer to be used for sequencing. The forward primers HIV-1 primers that were used with the reverse primers were 561, 269, and 81. The designed reverse primers were as follows: 1953, 1726, 1497, 1338, 1032,

988, 975, 879, 777, 699, 674, 464, and 187. The PCR reaction contained 1 uL of 10pmol/uL forward and reverse primers, 2.0x SensiMix NoRef buffer (Bioline, Taunton, MA), 100 ng 0M10.1 DNA and water in a final volume of 25 uL. The PCR cycling parameters were as followed: 95°C for 10 minutes, 40 cycles of 95°C for 10 seconds and 60°C for 30 seconds; and a final extension of 72°C for 7 minutes. The PCR products were visualized on a 1.5% ethidium bromide agarose gel using gel electrophoresis.

Identifying HIV-1 CSF Integration Sites. To identify HIV-1 integration sites, the DNA Walking SpeedUp Premix kit (Seegene Inc, Songpa-Gu, Seoul, Korea) protocol was adapted from the published Seegene user manual. Approximately 600 ng of repaired WGA CSF DNA was used as the template for the primary PCR reaction. Four separate reactions per sample were carried out in 2X SeeAmp™ ACP™ Master Mix II, each of which contained 4 μl of one of the four different 2.5 μM DW-ACP primers (1-4), 10 pM of target specific primer 1 (TSP1)-1338rev (Table 1), and water in a final volume of 50 μl. Primary PCR cycled as follows: 94°C for 5 min; 42°C for 1 min; 72°C for 3:50 min; 30 cycles of 94°C for 40 s, 55°C for 40 s, and 72°C for 3 min; and 72°C for 7 min. The primary PCR product was then purified using the QIAquick Spin Kit (Qiagen Inc, Valencia, CA) and eluted with 30 μl of TE. 3 μl of the purified primary PCR product was consequently used as the template for the second PCR reaction, which was also conducted in 2X SeeAmp™ ACP™ Master Mix II and contained 1 μl of 10 μM DW-ACPN along with 10 pM of TSP2-988rev in a total volume of 20 μl. Secondary PCR cycled as follows: 94°C for 3 min; 35 cycles of 94°C for 40s, 65°C for 40 s, and 72°C for 3 min; and 72°C for 7 min. The secondary PCR product was diluted 50 fold to

minimize laddering and then used as a template (1 ul) in the tertiary PCR reaction. This last PCR reaction also occurred in 2X SeeAmp^{TM} ACP^{TM} Master Mix II and contained 1 μl of 10μM Universal primer along with 10 pM of TSP3-699rev in a total volume of 30 ul. The tertiary PCR reaction cycled as follows: 94°C for 3 min; 40 cycles of 94°C for 40 s, 68°C for 40 s, and 72°C for 1:30 min; and 72°C for 7 min. The entire volume of the tertiary product (30 ul) was loaded and run on a 1.5% low melting ethidium bromide agarose gel. Visualized bands were then excised from the gel and purified using the QIAquick Gel Extraction Kit (Qiagen Inc, Valencia, CA) and eluted with 20 ul of TE. Three cell lines (OM10.1, 8E5 and ACH-2) were initially used for the optimization of the Seegene protocol. OM10.1 harbors a single integrated provirus and is clonally derived from infected HL-60 promyelocytes. 8E5 (ATCC 8993) is a T-lymphoblastoid cell line that contains a single copy of HIV per cell. Analogous to the other two cell lines, ACH-2, derived from infected A3.01 cells (a human CD4 T-cell line), also contains a single copy of HIV. Due to the time-consuming nature of the assay along with its associated costs, the identification of HIV-integration sites for all samples was completed once.

DNA Sequence Analysis. The purified tertiary PCR products were sent to Geneway, LLC (Hayward, CA) for DNA sequencing through an automated fluorescence technology. Reverse primer HIV209 was used as the sequencing primer. The resulting sequences were then analyzed for the presence of HIV-1 by aligning the sequences to HIV-1 (NCBI Reference Sequence NC_001802.1) using DNAdynamo (Blue Tractor Software). If more than one sequence was available for a sample, those corresponding sequences were first aligned with each other to obtain a consensus sequence prior to

alignment with HIV-1. Once the HIV-1 region in the sequence was identified, the adjacent genomic regions were analyzed by comparison to the human sequence database on the National Center for Biotechnology Information (NCBI) website (http://blast.ncbi.nlm.nih.gov/Blast.cgi) to generate a list of genes that have similar sequences to the flanking regions. UniProt (http://www.uniprot.org/) was used to determine the functions of the proteins that are encoded by the identifiable genes flanking HIV-1.

Results

Reliability of WGA DNA. Analysis of the resultant products that were obtained from the WGA and non-WGA PBMC DNA integration reactions revealed similar banding patterns. Though the non-WGA DNA contained additional bands that were not included in the WGA reactions, the main bands that would be chosen for excision were produced, Figure 5.4.

Optimal Integration Primers. The results from the first gel show that of all the primers tested, only the HIV-1 988 and 674 reverse primers combined with HIV-1 269 forward primer gave accurate results with the correct PCR product sizes, 719 and 405 base pairs respectively, Figure 5.5A. Since three primers are needed for the HIV integration assay, more reverse primers were tested in a second PCR reaction. The forward primers used for this reaction were 561 and 81. The HIV-1 reverse primers that produced accurate PCR product sizes were 1338, 1032, 975, 699, 464, and 187 that gave product sizes of 777, 951, 894, 618, 383, and 106 base pairs respectively, Figure 5.5B. Based on these results, HIV-1 1338 reverse primers was chosen as the primer for the first PCR reaction in the integration assay, HIV-1 988 reverse primer was chosen for the second PCR reaction, and HIV-1 699 was chosen for the third PCR reaction. These were chosen based on their optimal spacing between each other, which is needed for second and third nested PCR reactions.

Since HIV-1 699 reverse primer was used for the final reaction, a sequencing primer needed to be chosen that contained optimal spacing from location 699 in HIV-1;

therefore, three sequencing primers also designed from the HIV-1 genome (NCBI Reference Sequence NC_001802.1), were tested. The three designed HIV-1 reverse possible sequencing primers bound to the following HIV-1 locations: 464, 209, and 167. When tested with HIV-1 forward primer 81, it showed that all of the reverse primers had specific binding to HIV-1 apparent by its accurate PCR product sizes, Figure 5.6. Therefore, HIV-1 209 reverse primer was used to sequence the product obtained from the HIV integration assay.

Cell Line Integration Sites. The sequencing results from the integration assay were aligned with the HIV-1 sequence (NC_001802.1) to identify the presence of HIV-1 within the sequence. The excised PCR products from OM10.1 that were submitted for sequencing are shown in Figure 5.7. Analysis of the sequences revealed the following integration sites: OM10.1– Homo sapiens IL-9 Receptor, Pan troglodytes BRCA1 (BRCA1) gene; ACH-2 - Homo sapiens chromosome 16 clone RP11-1072A3; 8E5 - Homo sapiens sequence flanking HIV-1 integration site (chromosome 13).

HIV-1 Integration Site Identification. The HIV-1 integration sites were identified in CSF DNA from three different cell fractions, CD14-, CD14+/16+, and CD14+/16-, of subjects (n=6) that were enrolled in the Hispanic-Latino Longitudinal Cohort of HIV-seropositive women (HLLC). The subjects included those diagnosed with HAND (n=3) and normal cognition (n=3). Based on the resultant agarose gels from the normal cognition and HAND individuals, Figure 5.8, it is clearly visible that HAND gels contain more product bands than the normal cognition ones.

CSF Cell Fractions Sequencing Results. The product bands that are encased by a box are the ones able to be sequenced. The Annealing Control Primer (ACP) primer reactions that produced multiple bands aligned with one another with the smaller band having the shorter sequence, Figure 5.10A, corresponding to the bands found in lane 22, Figure 5.9. In addition, the different ACP reactions that was detecting integration sites within the same cell fraction also aligned with each other, Figure 5.10B, corresponding to bands found in lanes 22 and 23, Figure 5.9. A consensus sequence was created through the alignment of all the above bands, which was then aligned to HIV-1 to locate its location in the host genome, Figure 5.10C. Despite the alignments, closer inspection of sequencing alignment reveals that mismatching does exist, Figure 5.11.

Sequences flanking the identified HIV-1 virus at its 5' and 3' ends were compared to the databases in NCBI blast to determine if there was any similarity to known genes or transcripts, Figure 5.12. Gene similarities to the sequences flanking HIV are listed in Tables 5.3-6. Though it is clearly evident that HAND individuals contain more identifiable integration sites than the normal cognition individuals, common integration sites occur across the both diagnoses and are not found just within particular CSF cell subsets but also found across the various subsets, Table 5.7. Interestingly, three of the sites had roles in apoptosis (cytochrome c oxidase subunit II, mitochondrion, and unc-5/13-homolog C like); two of the sites were involved with macrophage behavior (vasohibin 1 and ADAM metallopeptidases); and one site regulated transcription (estrogen-related receptor beta).

Discussion

Designing and identifying target specific primers (TSPs) that bind to various regions of HIV-1 allowed for their use in Seegene's DNA walking technique that identified HIV-1 integration sites. This technique was validated through the identification of integration sites that were obtained from HIV-infected cell lines that were consistent with other publications. The consistent integration site of 8E5 to other publications verify the reliability of this assay [119, 120].

Due to the scarcity of CSF cells, their analysis is extremely difficult and it becomes even more complex when trying to analyze various cells fractions within the CSF. In cases such as these, it has become common practice to utilize whole genome amplification (WGA) to produce high yields of DNA from small or precious samples. This chapter demonstrated that HIV-1 integration sites were identifiable in WGA CSF cell fraction samples that included non-monocytes (CD14-), activated monocytes (CD14+/16+), and non-activated monocytes (CD14+/16-). Although there is some loss of product bands in the WGA DNA when comparing them to the integration reactions in non-WGA DNA, the intense product bands that would be chosen for excision are still retained. Though it is beneficial when analyzing CSF cells, WGA may produce sequencing variations during amplification. These sequencing variations may be the cause of mismatches observed during the alignment of the sample products, Figure 5.10. Nonetheless, multiple bands within the same reaction that identifies the same integration sites are optimal as a more accurate consensus sequence is obtained from their alignment. WGA was required for these samples since their DNA was also used in other downstream

applications; however, it may be beneficial to use non-WGA DNA for more precise result.

The various CSF cell fractions were sorted using fluorescence-activated cell sorting (FACS) and their level of HIV DNA was also determined, Table 5.7. In some cases as seen in PR1 CD14+/16+ and PR3 CD14+/16+, no cells were acquired. Although no cells were obtained, those sorting tubes still underwent the same procedures (extraction and WGA) as the other tubes for control purposes. While no HIV DNA was detectable in these cells, they contained observable product bands, Figure 5.8. However, sequencing of the product bands revealed that only the PR1 CD14+/16+ sample was able to be sequenced but the flanking sequences surrounding HIV-1 did not have known gene similarities. This may have been caused by contamination during cell sorting and careful parameters should be taken to prevent its reoccurrence. Although HIV DNA was undetectable in the multiplex PCR assay, Table 5.7, even the slightest contamination would be apparent in integration detection due to the three consecutive PCR reactions. Regardless, integration sites were only identified within the various CSF cell fractions that contained cells, some of the sites were common.

It is very possible that insertional mutagenesis may impact HAND development by the fact that HAND individuals had more identifiable integration sites than the HIV-infected normal cognition individuals. Table 5.8 is a compilation of common integration sites across the different diagnoses and various CSF cell fractions. Despite the small samples size that was analyzed, it was encouraging to find that possible integration sites may indeed exist. More importantly, it was surprising to find multiple common sites

involved in apoptosis and macrophage behavior. There was also one site involved in the regulation of transcription.

Based on the current accepted Trojan Horse theory where monocytes transport HIV into the CNS and are also responsible for increased inflammatory cytokine release in the CNS that ultimately result in neuronal apoptosis leading to neurocognitive disorders; it is entirely plausible that the disruption of genes that are involved in apoptosis, macrophage behavior, and transcription would likely have an effect on the development and maintenance of HAND. Interestingly, one of the 15 integration sites indentified in HIV-associated dementia cases also involved apoptosis, Table 5.2. This similarity suggests a possible preferential site in apoptosis-related genes.

Since the monocytes have been recognized as playing a prominent role in HAND development, it would be valuable to find a way to measure the level of impact that they would have on disease onset especially since the use antiretroviral therapy has decreased the amount of reliable biomarkers. Our lab currently measures the amount of HIV DNA contained within monocytic cells and determines the correlation it has with the severity of HAND. We have consistently found that individuals with HAND contained higher amounts of HIV DNA in comparison to HIV-infected individuals with normal cognition [50, 51, 76, 78]; therefore, it would be of high interest to indentify integration sites within monocytes to determine if insertional mutagenesis may assist with HAND development.

Due to the high monocytic involvement in HAND that is recognized through HIV DNA detection, it is interesting to find then that common identifiable integration sites are not isolated to just monocytic cells. It may be that HIV may have preferential integration

sites regardless of cell type, all of which could contribute to disease pathogenesis. Nonetheless, the effect of insertional mutagenesis would be enhanced in monocytes since they are longer-lived than lymphocytes. Although more samples would need to be analyzed to support these findings, the results are promising due to the common integration sites that were detected across samples. In addition, many of the non-common integration sites also encoded other mitochondrial proteins and transcriptional regulators, Tables 5.3-6. Analysis of a larger sample size would determine any significance to their gene disruption. It would also be substantial to analyze integration sites within these same cell fractions of the periphery and compare them to the CSF to determine similarities or divergence. These analyses will assist with our understanding of HAND through expanded knowledge of the viral behavior in the periphery and in the CNS.

Table 5.1. Primer Sequences

Primer	Sequence (5'-3')
DW-ACP1	ACP-AGGTC
DW-ACP2	ACP-TGGTC
DW-ACP3	ACP-CGGTC
DW-ACP4	ACP-CGGTC
DW-ACPN	ACPN-GGTC
Universal Primer	TCACAGAAGTATGCCAAGCGA
3'HIV1338	ATCTTGTGGGGTGGCTCCTT
3'HIV988	TATCCCATTCTGCAGCTTCC
3'HIV975	TAT CCC ATT CTG CAG CTT CC
3'HIV699	TGT CAG CTG CTG CTT GCT
5'HIV209	TCG CTT TCA GGT CCC TGT T

Table 5.2. The 15 Integration Sites Identified by Mack et al

Dementia		
AD-1	KIAA0690	hypothetical protein
AD-2	TOP1	DNA topoisomerse
AD-3	NT_031737.12[d]	putative gene
AD-5	NT_010808.2[d]	putative gene
AD-6	NT_035014.4[d]	putative gene
AD-7	SDHB	TCA succinate dehydrogenase
AD-8	CHD2	DNA helicase, alters transcription regulation
AD-9	FLJ12085	hypothetical protein domain homology to GTP-activator activity on Rab-like GTPase
AD-10	LZ16	contains ankyrin repeats, 3 carcinoma susceptibility protein
AD-11	NT_005367.83[d]	putative gene
AD-12	BECN1	interacts with BCL2, protects cell from viral-induced apoptosis
AD-13	NXF1	mediator of mRNA nuclear export interacts with retroviral proteins
AD-14	PM5	collagenase gene family
AD-15	NT_035359.10	

Table 5.3. Integration Sites Identified in the Normal Cognition (NC) Individuals

Patient	Diagnosis	Cell Fraction	HIV-1 Integration Sites (Chromosome/Function)
PR1	NC	CD14-	None Detected
		CD14+/16+	None Detected
		CD14+/16-	None Detected
PR2	NC	CD14-	Chrom 3: hypothetical protein Chrom 7: UDP-GalNAc:polypeptide N-acetylgalactosaminyltransferase Chrom 9: solute carrier family 24 Chrom 11: proline rich Gla (G-carboxyglutamic acid) 4 (transmembrane) Chrom 14: vasohibin 1 Chrom 14: estrogen-related receptor beta
		CD14+/16+	Chrom 1: matrilin 1, cartilage matrix protein Chrom 1/8/11/16: hypothetical protein Chrom 2: RAB6C, member RAS oncogene family Chrom 6: unc-5 homolog C-like Chrom 8: myc proto-oncogene protein Chrom 8: leucine rich repeat and fibronectin type III domain Chrom 10: MYST histone acetyltransferase (monocytic leukemia) 4 Chrom 10: adenosine deaminase, RNA-specific, B2 Chrom 11: chapsyn-110 isoform 1 Chrom 11: spermatogenesis associated 19 Chrom 12: acetoacetyl-CoA synthetase Chrom 12: transmembrane protein 132B
		CD14+/16-	None Detected
PR3	NC	CD14-	Chrom 5: hypothetical protein Chrom 5: PROP paired-like homeobox 1 Chrom 12: calcium channel Chrom 13: fibroblast growth factor 14 isoform 1B Chrom 15: unc-13 homolog C Chrom 15: ribosomal protein L24-like
		CD14+/16+	None Detected
		CD14+/16-	None Detected

Table 5.4. Integration Sites Identified in Patient PR4

Patient	Diagnosis	Cell Fraction	HIV-1 Integration Sites (Chromosome/Function)
PR4	MCMD	CD14-	None Detected
		CD14+/16+	None Detected
		CD14+/16-	Chrom 11: proline rich Gla (G-carboxyglutamic acid) 4 (transmembrane) Chrom 14: estrogen-related receptor beta Chrom 14: vasohibin 1

Table 5.5. Integration Sites Identified in Patient PR5

Patient	Diagnosis	Cell Fraction	HIV-1 Integration Sites (Chromosome/Function)
PR5	HAD	CD14-	Chrom 2: Homo sapiens WD repeat domain 12 (WDR12), mRNA Chrom 10: Homo sapiens interferon-induced protein with tetratricopeptide repeats 5 (IFIT5), mRNA Chrom 2/4/6/9: hypothetical protein Chrom 2: HIV-1 Rev binding protein isoform ½ Chrom 2: cytochrome P450, family 26, subfamily b, polypeptide 1 Chrom 2: calcium binding protein 39 Chrom 2: solute carrier family 39 (zinc transporter), member 10 Chrom 2: neurexophilin 2 Chrom 2: low density lipoprotein-related protein 1B precursor Chrom 2: glycosyltransferase-like domain containing 1 isoform a/b Chrom 2: tensin Chrom 4: recombining binding protein suppressor of hairless isoform 3 Chrom 4: stromal interaction molecule 2 Chrom 4: protocadherin 7 isoform c precursor Chrom 4: cyclin I/G2 Chrom 4: aminoadipate aminotransferase Chrom 4: polypeptide N-acetylgalactosaminyltransferase 17 Chrom 4: serine/threonine protein phosphatase with EF-hand motifs 2 Chrom 4: similar to cytochrome c oxidase subunit II Chrom 5: arrestin domain containing 3 Chrom 5: ADAM metallopeptidase with thrombospondin type I motif Chrom 5: prolactin receptor Chrom 5: catenin (cadherin-associated protein), delta 2 Chrom 5: dynein, axonemal, heavy chain 5 Chrom 6: mannosidase, alpha, class 1A Chrom 6: FGFR1 oncogene partner isoform b Chrom 6: chemokine (C-C motif) receptor 6 Chrom 7: olfactory receptor, family 2, subfamily F Chrom 8: glutamate-rich 1 Chrom 9: spermatid perinuclear RNA binding protein Chrom 9: astrotactin 2 isoform a/c Chrom 11: interleukin 10 receptor Chrom 13: A-kinase anchor protein 11 Chrom 13: MYC binding protein Chrom 13: beta 1,3-galactosyltransferase-like Chrom 13: relaxin/insulin-like family peptide receptor 2 Chrom 13: component of golgi transport complex 3 Chrom 13: sprouty 2 Chrom 13: slit and trk like 1 protein Chrom 16: protein kinase Myt1 isoform 2 Chrom 16: claudin 9 Chrom 16: ataxin 2-binding protein 1 isoform 4
		CD14+/16+	Chrom 1: potassium channel, subfamily T, member 2 Chrom 2/4/7/8/17: hypothetical protein Chrom 2: activin A receptor Chrom 3: leucyl-tRNA synthetase 2, mitochondrial precursor Chrom 4: calmegin Chrom 4: LPS-responsive vesicle trafficking Chrom 4: translocation associated membrane protein 1-like 1 Chrom 4: GRB2-associated binding protein 1 isoform b/a Chrom 4: DNA-damage-inducible transcript 4-like Chrom 4: nuclear receptor subfamily 3, group C, member 2 Chrom 5: F-box protein 38 isoform a Chrom 5: serotonin 5-HT4 receptor isoform a Chrom 5: fer (fps/fes related) tyrosine kinase Chrom 7: transformer-2 alpha Chrom 7: GLI-Kruppel family member GLI3 Chrom 7: coiled-coil domain containing 126 Chrom 7: met proto-oncogene isoform a precursor Chrom 7: caveolin 1 Chrom 8: claudin 23 Chrom 8: pragmin Chrom 8: collagen, type XXII, alpha 1 Chrom 10: neuregulin 3 Chrom 11: Ras association (RalGDS/AF-6) domain family Chrom 14: RAD51-like 1 isoform 3
		CD14+/16-	Chrom 6: glutamate-cysteine ligase, catalytic subunit Chrom 9: cylicin 2 Chrom 9: glutamate receptor, ionotropic, N-methyl-D-aspartate 3A Chrom 11: potassium voltage-gated channel Chrom 15: arrestin domain containing 4 Chrom 15: spermatogenesis associated 8 Chrom 16: chromodomain protein, Y-like 2

Table 5.6. Integration Sites Identified in Patient PR6

Patient	Diagnosis	Cell Fraction	HIV-1 Integration Sites (Chromosome/Function)
PR6	HAD	CD14-	cytochrome c oxidase subunit II, mRNA (transcript) Mitochondrion Chrom 1/2/5/8/22: hypothetical protein Chrom 3: calcium-activated potassium channel beta 2 subunit Chrom 7: MAD1-like 1 protein Chrom 10: ADAM metallopeptidase domain 12 isoform 1 preproprotein Chrom 12: neurotensin/neuromedin N preproprotein preproprotein Chrom 14: A-kinase anchor protein 6 Chrom 17: heat shock transcription factor family member 5 Chrom 21: neural cell adhesion molecule 2 precursor Chrom 21: mitochondrial ribosomal protein L39 isoform a
		CD14+/16+	cytochrome c oxidase subunit II, mRNA (transcript) Mitochondrion Chrom 1/2/5/6/7/8/10/15/17: hypothetical protein Chrom 1: cAMP-dependent protein kinase catalytic subunit beta isoform Chrom 2: DEAD (Asp-Glu-Ala-Asp) box polypeptide 18 Chrom 3: ephrin receptor EphA3 isoform b precursor Chrom 4: F-box only protein 8 Chrom 4: dopamine receptor D5 Chrom 7: zinc finger protein 727 Chrom 8: CUB and Sushi multiple domains 3 isoform 2 Chrom 10: protocadherin 15 isoform CD3-2 precursor Chrom 11: ADP-ribosyltransferase 5 precursor Chrom 14: A-kinase anchor protein 6 Chrom 15: cancer susceptibility candidate 5 isoform 2 Chrom 16: olfactory receptor, family 2, subfamily C, member 1 Chrom 21: chloride intracellular channel 6
		CD14+/16-	None Detected

Table 5.7. Common Integration Sites

Integration Site(s)	Patient/Cell Fraction	Function
vasohibin 1	PR2 (CD14-) PR4 (CD14+/16-)	Angiogenesis inhibitor; inhibits migration, proliferation and network formation by endothelial cells as well as angiogenesis; inhibits tumor growth and tumor angiogenesis; inhibits artery neointimal formation and macrophage infiltration.
estrogen-related receptor beta	PR2 (CD14-) PR4 (CD14+/16-)	Nuclear receptor; transcription regulation
cytochrome c oxidase subunit II	PR5 (CD14-) PR6 (CD14-) PR6 (CD14+/16+)	Component of the respiratory chain; catalyzes the reduction of oxygen to water; associates with cyclin G1; upregulates p53 and induces apoptosis
mitochondrion	PR6 (CD14-) PR6 (CD14+/16+)	Releases of cytochrome c; caspase activation leading to apoptosis; free radical formation
unc-5-homolog C like unc-13-homolog C like	PR2 (CD14+/16+) PR3 (CD14-)	Netrin-1 receptors required for axon guidance; dependence receptor able to induce apoptosis in absence of ligands
A-kinase anchor protein 11 A-kinase anchor protein 6	PR5 (CD14-) PR6 (CD14+/16+)	Binds to type II regulatory subunits of protein kinase; anchors/targets them to the nuclear membrane or sarcoplasmic reticulum
ADAM metallopeptidase (thrombospondin type I motif) ADAM metallopeptidase (domain 12 isoform 1)	PR5 (CD14-) PR6 (CD14-)	Skeletal muscle regeneration; macrophage-derived giant cells (MGC) and osteoclast formation from mononuclear precursors
Olfactory receptor, family 2, subfamily F, member 1/2 Olfactory receptor, family 2, subfamily C, member 1	PR5 (CD14-) PR6 (CD14+/16+)	Odorant G-protein coupled receptor
F-box protein 38 isoform a F-box only protein 8	PR5 (CD14+/16+) PR6 (CD14+/16+)	Recognizes and binds phosphorylated proteins and promotes their ubiquitination and degradation; promotes the activation of ARF through replacement of GDP with GTP

Table 5.8. CSF HIV DNA Results

Patient	CSF Cell Fraction	CSF Cell Count	HIV DNA per Cell	Diagnosis
PR1	CD14-	33	0.4	[2]NC
	CD14+/16+	0	[1]UND	
	CD14+/16-	18	[1]UND	
PR2	CD14-	595	0.2	[2]NC
	CD14+/16+	4	1.8	
	CD14+/16-	1	16.9	
PR3	CD14-	825	0.9	[2]NC
	CD14+/16+	0	[1]UND	
	CD14+/16-	7	0.7	
PR4	CD14-	1648	0.2	[3]MCMD
	CD14+/16+	93	1.1	
	CD14+/16-	68	5.0	
PR5	CD14-	488	0.3	[4]HAD
	CD14+/16+	212	0.6	
	CD14+/16-	55	2.5	
PR6	CD14-	1050	6.6	[4]HAD
	CD14+/16+	65	9.7	
	CD14+/16-	236	11.9	

PR: Puerto Rico; [1]Undetermined; [2]Normal Cognition; [3]Minor Cognitive Motor Disorder; [4]HIV-Associated Dementia;

Figure 5.1 – Overview of Seegene's DNA Walking *SpeedUp*™ technique. A) Flow chart illustrating the procedure. B) Corresponding agarose gels of the three PCR reactions involved in the technique. Obtained from the DNA Walking SpeedUp Kit user manual (Seegene, Seoul, Korea).

Figure 5.1

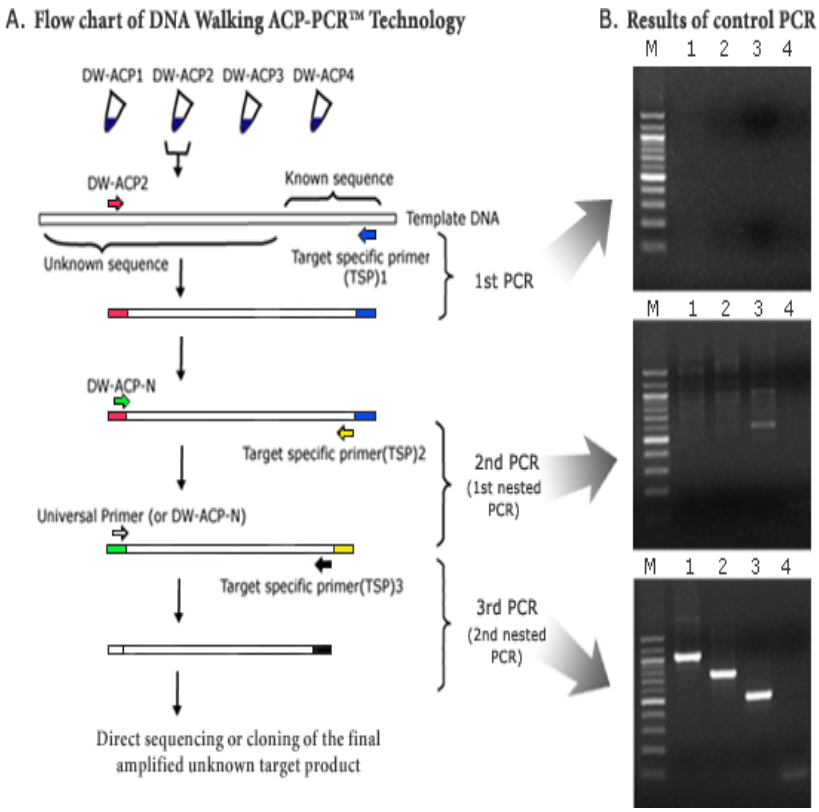

Seegene Inc (Seegene, Seoul, Korea)

Figure 5.2 – CNS tissue staining revealing A) HIV DNA and B) p24 staining localized to macrophages. Obtained from studies done by Mack, K.D., et al., *HIV Insertions Within and Proximal to Host Cell Genes Are a Common Finding in Tissues Containing High Levels of HIV DNA and Macrophage-Associated p24 Antigen Expression.* JAIDS, 2003. **33**(3): p. 308-320.

Figure 5.2

A

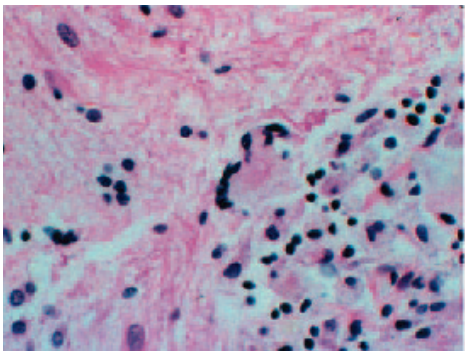

B

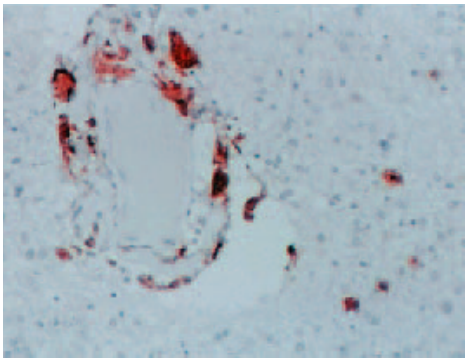

Mack, K.D., et al.,. *JAIDS, 2003.* ***33(3): p. 308-320.***

Figure 5.3 – Illustration of formalin-fixed paraffin embedded (FFPE) REPLI-g technique for whole genome amplification (WGA). Obtained from the REPLI-g FFPE Handbook (Qiagen, Valencia, CA)

Figure 5.3

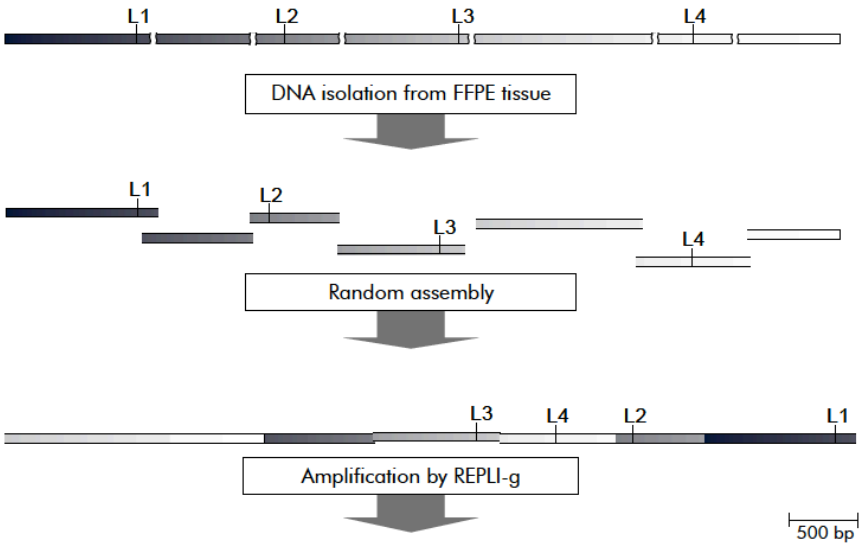

Qiagen (Valencia, CA)

Figure 5.4 – 1.5% agarose gel of PCR products resulting from the DNA walking technique to identify HIV integration sites in WGA and non-WGA PBMC samples. M: 100 base pair ladder; 1: ACP-1 non-WGA PBMC DNA; 2: ACP-2 non-WGA PBMC DNA; 3: ACP-3 non-WGA PBMC DNA; 4: ACP-4 non-WGA PBMC DNA; 5: ACP-1 WGA PBMC DNA; 6: ACP-2 WGA PBMC DNA; 7: ACP-3 WGA PBMC DNA; and 8: ACP-4 WGA PBMC DNA.

Figure 5.4

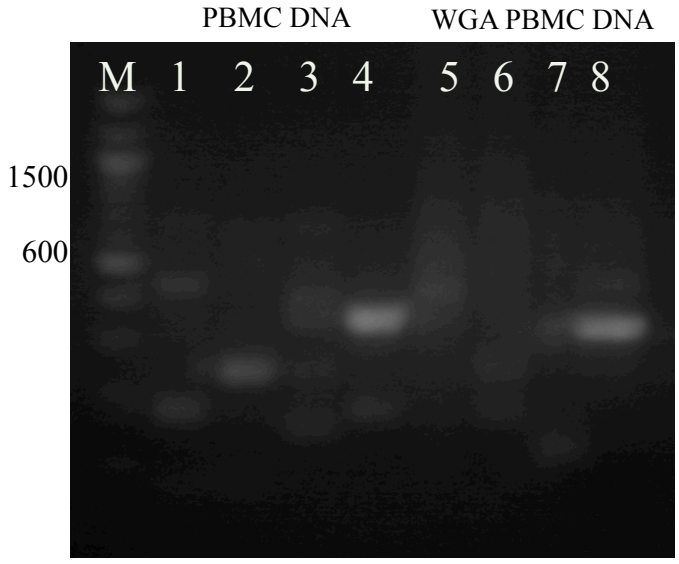

Figure 5.5 – Two 1.5% agarose gels depicting PCR products of HIV reverse primers that were designed for use as nested primers in the HIV integration assay. Expected product sizes are in parentheses. A) M: 100 base pair ladder; 1: 269-1497 (1228 base pairs); 2: 269-1338 (1069 base pairs); 3: 269-988 (719 base pairs); 4: 269-674 (405 base pairs). B) M: 100 base pair ladder; 1: 561-1726 product (1165 base pairs); 2: 561-1338 product (777 base pairs); 3: 561-879 product (318 base pairs); 4: 561-777 product (216 base pairs); 5: 81-1953 product (1872 base pairs); 6: 81-1032 product (951 base pairs); 7: 81-975 product (894 base pairs); 8: 81-699 product (618 base pairs); 9: 81-464 product (383 base pairs); 10: 81-187 product (106 base pairs).

Figure 5.5

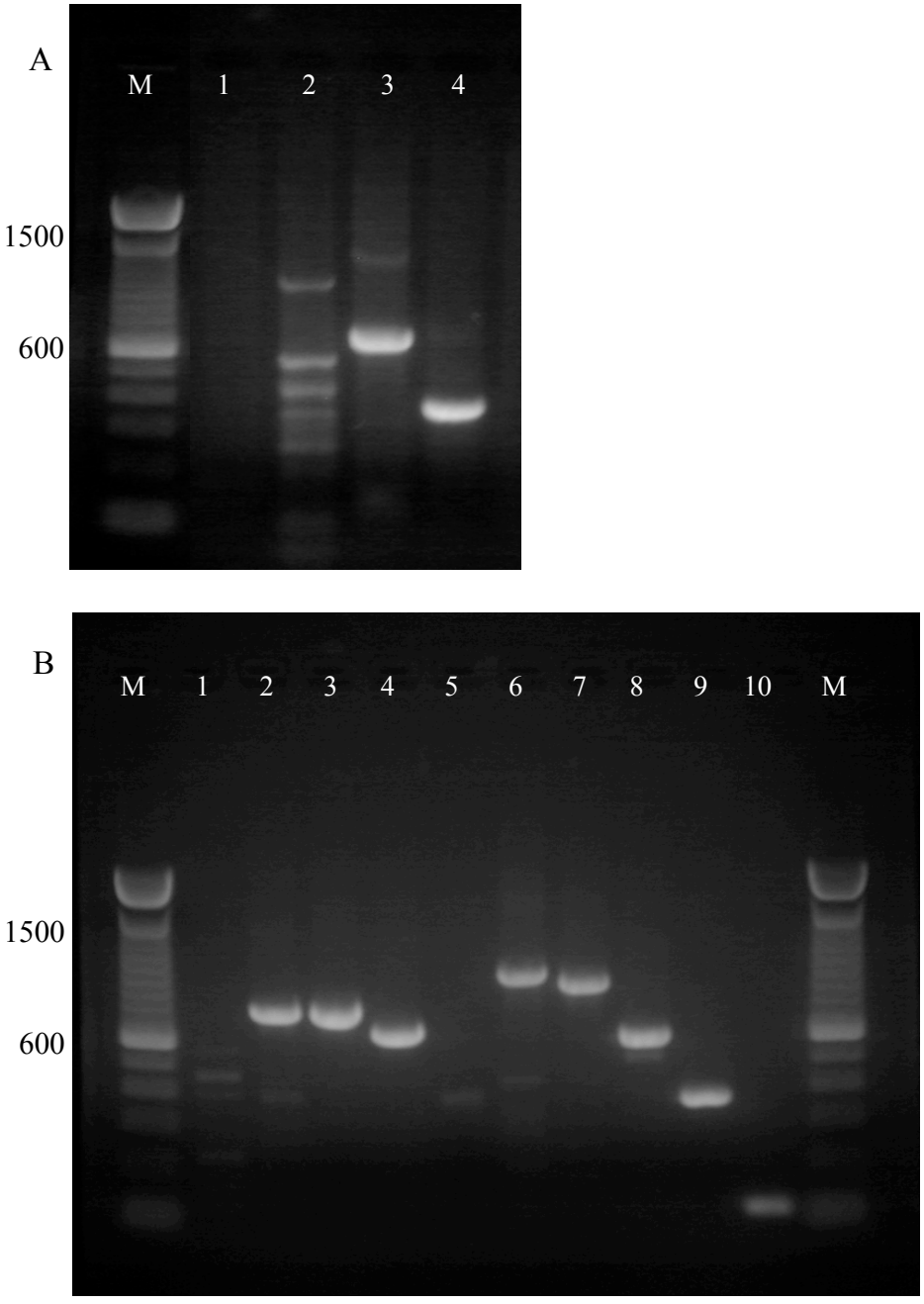

Figure 5.6 – 1.5% agarose gel depicting PCR products of designed HIV reverse sequencing primers. Expected product sizes are in parentheses. M: 100 base pair ladder; 1: 81-464 (383 base pairs); 2: 81-209 (128 base pairs); 3: 81-167 (86 base pairs); B: blank.

Figure 5.6

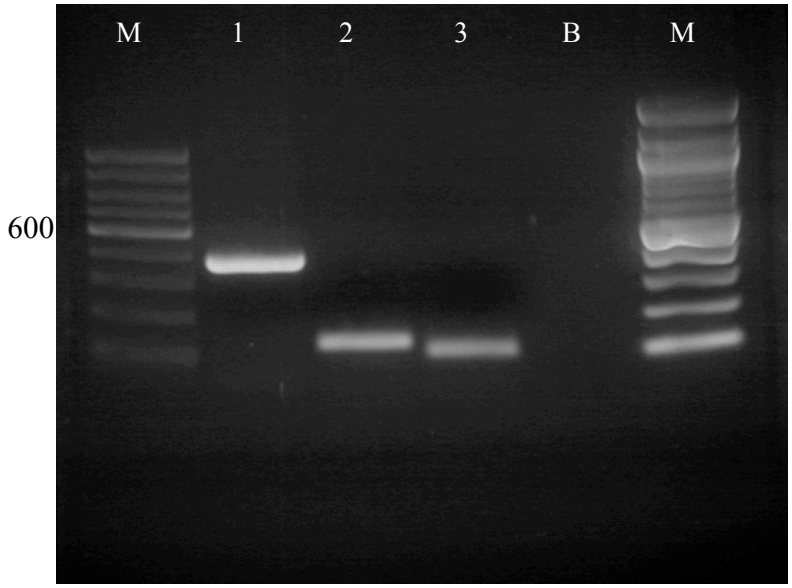

Figure 5.7 – 1.5% agarose gel revealing PCR products to determine HIV integration sites. M: 100 base pair ladder; 1: ACP-1 product; 2: ACP-2 product; 3: ACP-3 product; and 4: ACP-4 product.

Figure 5.7

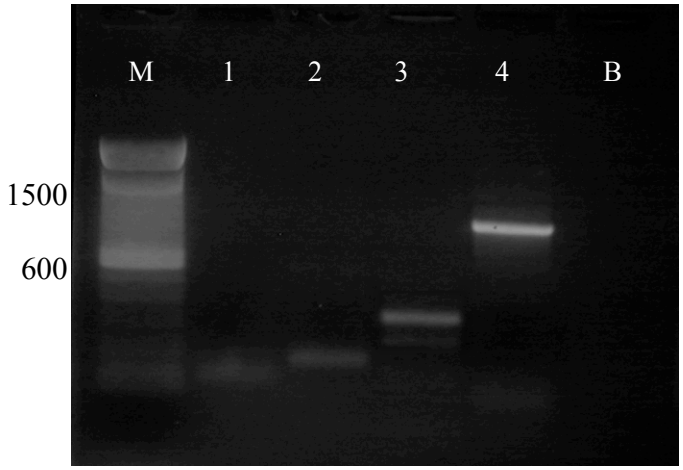

Figure 5.8 – 1.5% agarose gels of PCR products that detect HIV integration sites within various CSF cell fractions of NC individuals. M: 100 base pair ladder; 1-4: ACP products of PR1 CD14-; 5-8: ACP products of PR1 CD14+/16+; 9-12: ACP products of PR1 CD14+/16-; 13-16 ACP products of PR2 CD14-; 17-20: ACP products of PR2 CD14+/16+; 21-24: ACP products of PR2 CD14+/16-; 25-28: ACP products of PR3 CD14-; 29-32: ACP products of PR3 CD14+/16+; and 33-36: ACP products of PR3 CD14+/16-.

Figure 5.8

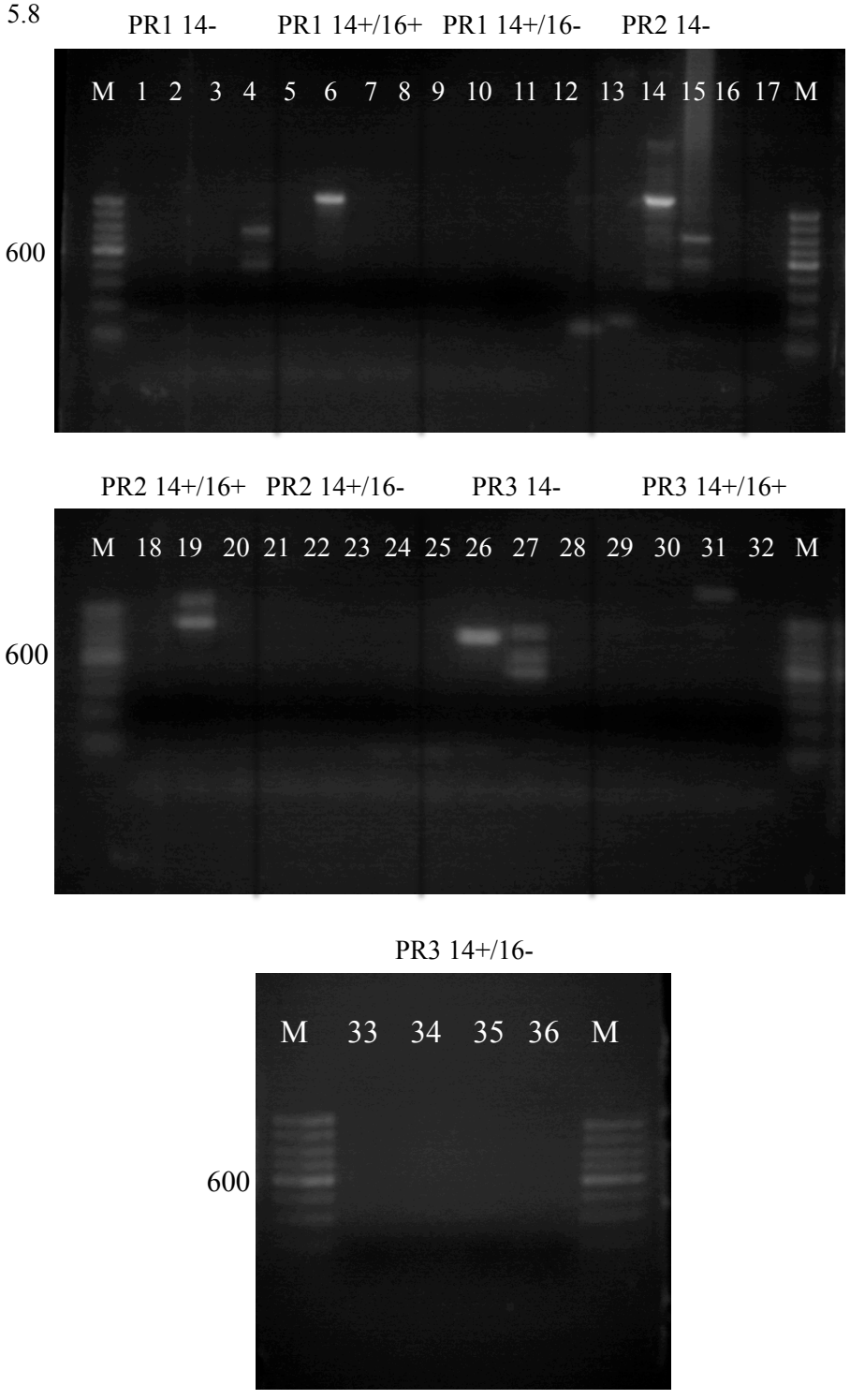
PR1 14-
PR1 14+/16+
PR1 14+/16-
PR2 14-
M 1 2 3 4 5 6 7 8 9 10 11 12 13 14 15 16 17 M
600
PR2 14+/16+
PR2 14+/16-
PR3 14-
PR3 14+/16+
M 18 19 20 21 22 23 24 25 26 27 28 29 30 31 32 M
600
PR3 14+/16-
M 33 34 35 36 M
600

Figure 5.9 – 1.5% agarose gels of PCR products that detect HIV integration sites within various CSF cell fractions of HAND individuals. M: 100 base pair ladder; 1-4: ACP products of PR4 CD14-; 5-8: ACP products of PR4 CD14+/16+; 9-12: ACP products of PR4 CD14+/16-; 13-16 ACP products of PR5 CD14-; 17-20: ACP products of PR5 CD14+/16+; 21-24: ACP products of PR5 CD14+/16-; 25-28: ACP products of PR6 CD14-; 29-32: ACP products of PR6 CD14+/16+; and 33-36: ACP products of PR6 CD14+/16-.

Figure 5.9

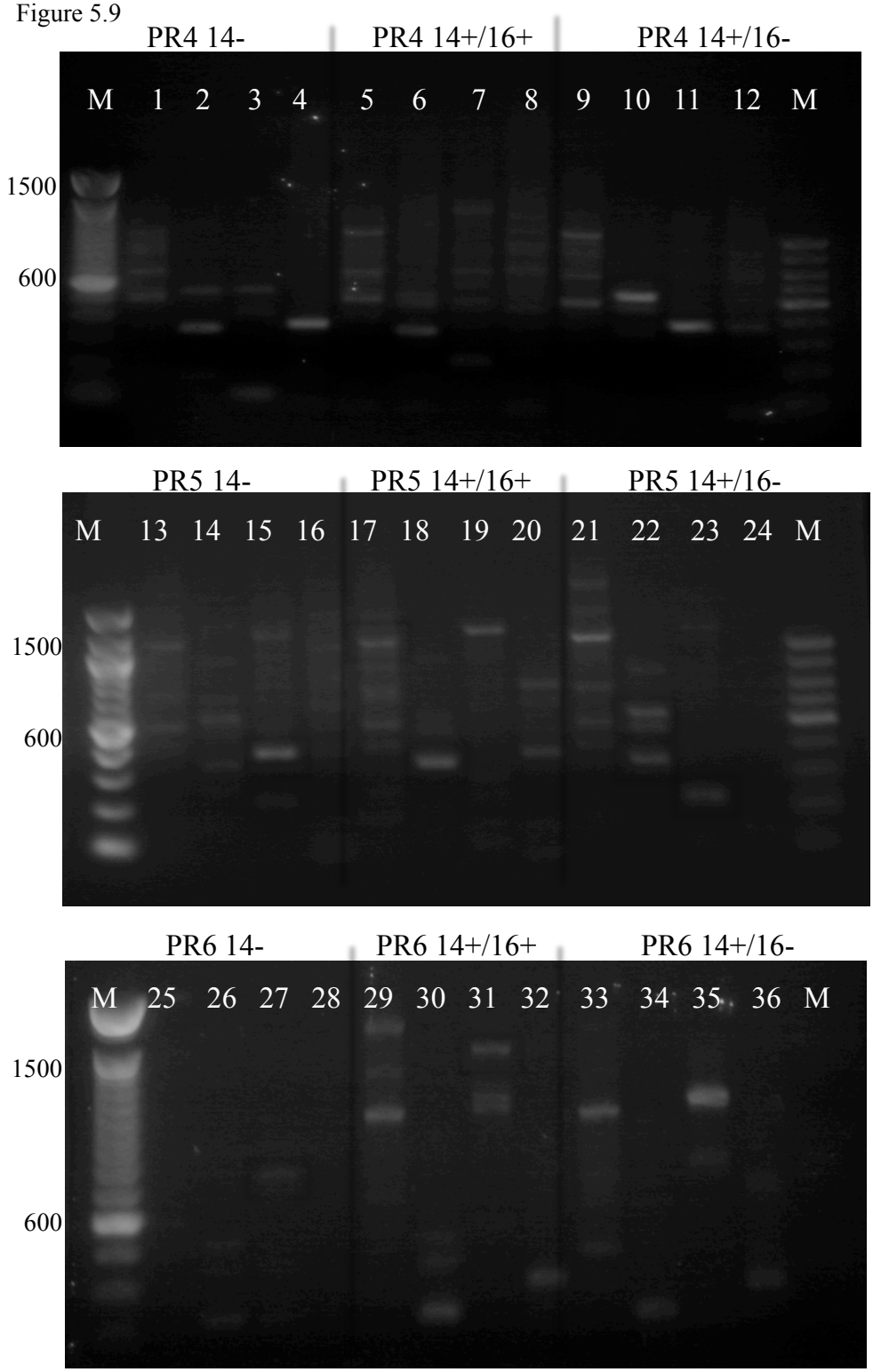
PR4 14-
PR4 14+/16+
PR4 14+/16-
M 1 2 3 4 5 6 7 8 9 10 11 12 M
1500
600
PR5 14-
PR5 14+/16+
PR5 14+/16-
M 13 14 15 16 17 18 19 20 21 22 23 24 M
1500
600
PR6 14-
PR6 14+/16+
PR6 14+/16-
M 25 26 27 28 29 30 31 32 33 34 35 36 M
1500
600

Figure 5.10 – Graphical overview of sequencing alignment. A) Alignment of PCR product bands resulting from bands in lane 22 of the gel in Figure 5.9. B) Alignment of PCR product bands resulting from bands in lanes 22 and 23 of the gel in Figure 5.9. C) Alignment of PCR product bands from bands in lanes 22 and 23 in the gel in Figure 5.9 and HIV-1.

Figure 5.10

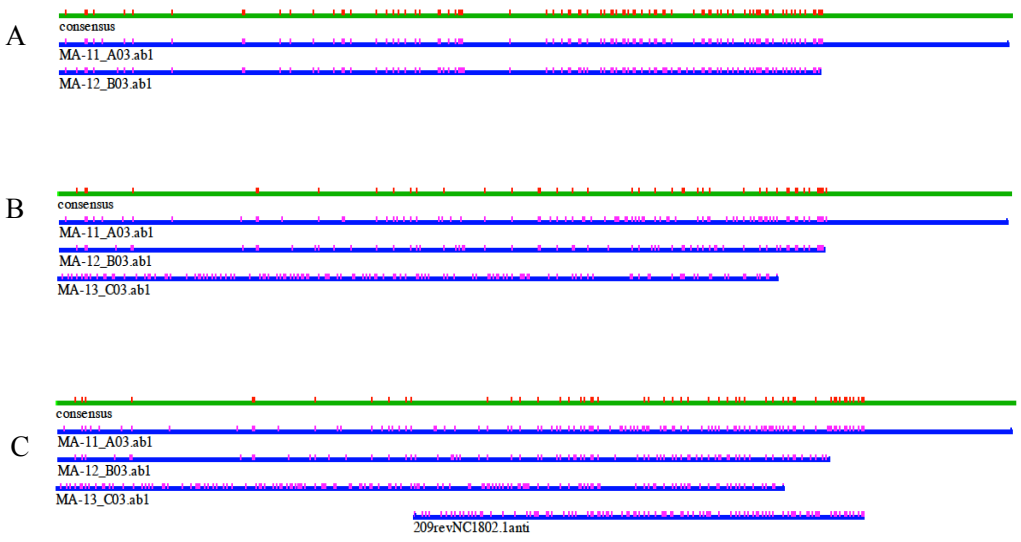
A
consensus
MA-11_A03.ab1
MA-12_B03.ab1
B
consensus
MA-11_A03.ab1
MA-12_B03.ab1
MA-13_C03.ab1
C
consensus
MA-11_A03.ab1
MA-12_B03.ab1
MA-13_C03.ab1
209revNC1802.1anti

Figure 5.11 – Consensus sequence resulting from the alignment of PCR product bands detecting the integration sites within the same CSF cell fraction. Corresponds to PCR bands from lane 22 of the gel in Figure 5.9.

Figure 5.11

CCNGANAANCAAANNAAACTTCCCTCNNCTAAAAAAATTT
TTGTTTNNCTTTAAAAAGNNNTTCNNGNGCCCTCTCCCCNT
GNTCNCTCTGNANNGNCNGNNANCGGTAAATCNNGTTNTT
CTGNATGGAAAANACCNTGNGGNGGAGNCCGCCCNTCGAT
CTCTCGTGGTTTNAACGCCNCNNCCTTATATACACCT_TGNT
TATGGGGCGCCATACCTGGGANNTATCCGTC_GTTCTTTGN
ACGACGCAAANTATTNATCTCNTCANTCNCCGGGTACNGA_
CGATCACATTCTGTGGNTGAAGTCGNNGGAAGAAGGANTC
CTGNCGGCGGNTGANNNCATAAAAANTTNGTGNNNGGCGT
CTGTTTTGAATGTTTTTGCCCGCCACAAAAC

Figure 5.12 – Consensus sequence corresponding to the PR5 CD14+/16- sample (lanes 22-23, Figure 5.9) revealing the location of HIV-1 (red). Sequences flanking HIV-1 were analyzed for sequence similarities to known genes.

Figure 5.12

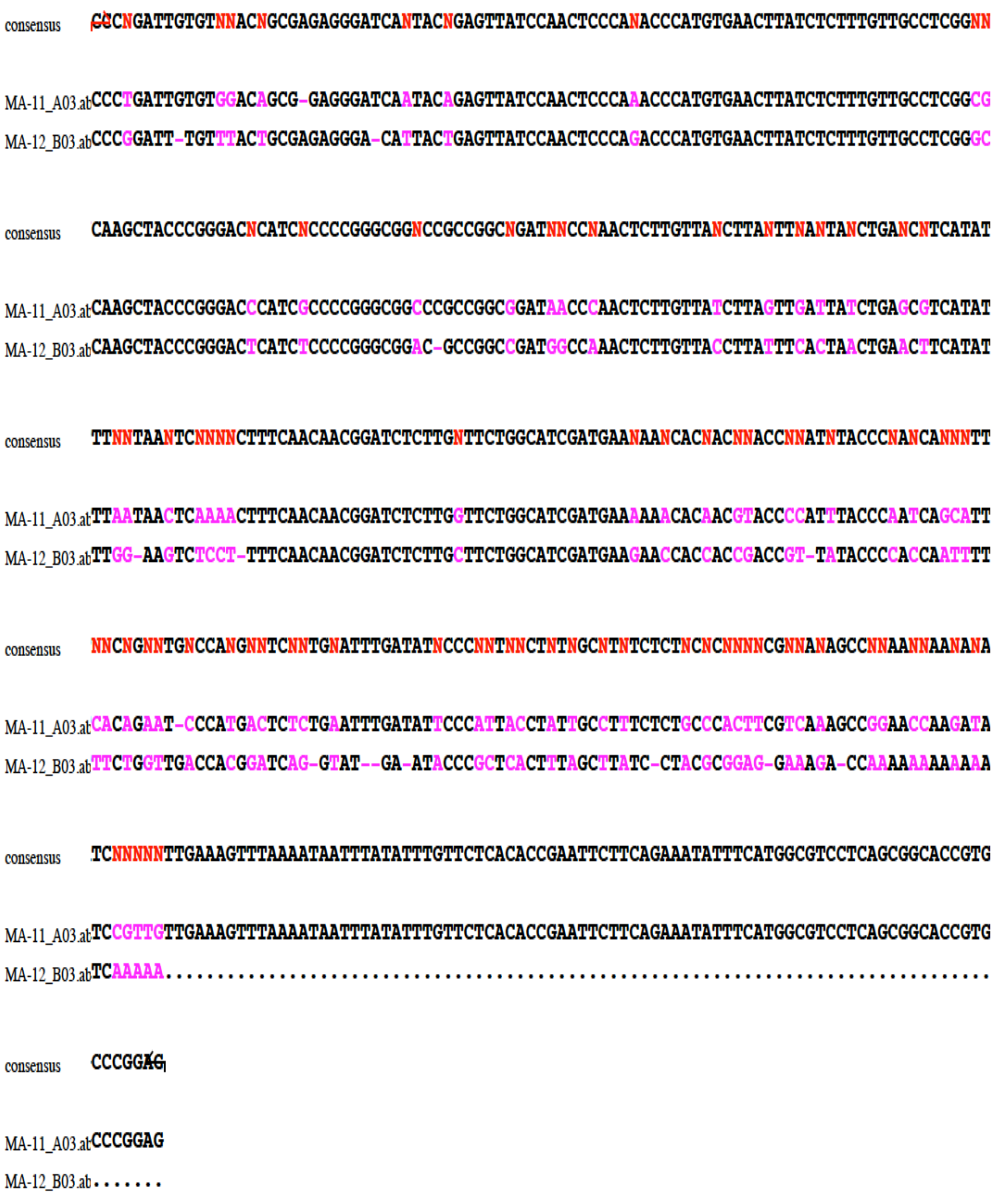
consensus CCCNGATTGTGTNNACNGCGAGAGGGATCANTACNGAGTTATCCAACTCCCANACCCATGTGAACTTATCTCTTTGTTGCCTCGGNN
MA-11_A03.ab CCCTGATTGTGTGGACAGCG-GAGGGATCAATACAGAGTTATCCAACTCCCAACCCATGTGAACTTATCTCTTTGTTGCCTCGGCG
MA-12_B03.ab CCCGGATT-TGTTTACTGCGAGAGGGA-CATTACTGAGTTATCCAACTCCCAGACCCATGTGAACTTATCTCTTTGTTGCCTCGGGC
consensus CAAGCTACCCGGGACNCATCNCCCCGGGCGGNCCGCCGGCNGATNNCCNAACTCTTGTTANCTTANTTNANTANCTGANCNTCATAT
MA-11_A03.ab CAAGCTACCCGGGACCCATCGCCCCGGGCGGCCCGCCGGCGGATAACCCAACTCTTGTTATCTTAGTTGATTATCTGAGCGTCATAT
MA-12_B03.ab CAAGCTACCCGGGACTCATCTCCCCGGGCGGAC-GCCGGCCGATGGCCAAACTCTTGTTACCTTATTTCACTAACTGAACTTCATAT
consensus TTNNTAANTCNNNNCTTTCAACAACGGATCTCTTGNTTCTGGCATCGATGAANAANCACNACNNACCNNATNTACCCNANCANNNTT
MA-11_A03.ab TTAATAACTCAAAACTTTCAACAACGGATCTCTTGGTTCTGGCATCGATGAAAAAACACAACGTACCCCATTTACCCAATCAGCATT
MA-12_B03.ab TTGG-AAGTCTCCT-TTTCAACAACGGATCTCTTGCTTCTGGCATCGATGAAGAACCACCACCGACCGT-TATACCCCACCAATTTT
consensus NNCNGNNTGNCCANGNNTCNNTGNATTTGATATNCCCNNTNNCTNTNGCNTNTCTCTNCNCNNNNCGNNANAGCCNNAANNAANANA
MA-11_A03.ab CACAGAAT-CCCATGACTCTCTGAATTTGATATTCCCATTACCTATTGCCTTTCTCTGCCCACTTCGTCAAAGCCGGAACCAAGATA
MA-12_B03.ab TTCTGGTTGACCACGGATCAG-GTAT--GA-ATACCCGCTCACTTTAGCTTATC-CTACGCGGAG-GAAAGA-CCAAAAAAAAAAA
consensus TCNNNNNTTGAAAGTTTAAAATAATTTATATTTGTTCTCACACCGAATTCTTCAGAAATATTTCATGGCGTCCTCAGCGGCACCGTG
MA-11_A03.ab TCCGTTGTTGAAAGTTTAAAATAATTTATATTTGTTCTCACACCGAATTCTTCAGAAATATTTCATGGCGTCCTCAGCGGCACCGTG
MA-12_B03.ab TCAAAAA.....
consensus CCCGGAG
MA-11_A03.ab CCCGGAG
MA-12_B03.ab .....

Chapter 6

Discussion

Highly active antiretroviral therapy (HAART) has effectively impacted the long-term prognosis of patients infected with the human immunodeficiency virus, type 1 (HIV-1) through its effect on viral replication. The clinical success is apparent as patients live longer with resulting low or undetectable plasma HIV-RNA levels and subsequent improvements in CD4 T-cell counts. Clinically, this potentially translates into decreased opportunistic infections and other AIDS-related illnesses, which historically resulted in increased morbidity and mortality. One particular AIDS-related illness is HIV-associated neurocognitive disorder (HAND) and the characteristics of HAND have changed since the beginning of the HIV epidemic with the overall prevalence and morbidity continuing to be a challenges in the era of HAART. Unlike its effects on HIV-RNA replication and levels, HAART has little impact on HIV DNA, which may provide clues on mechanisms why eradication of the virus remains elusive.

The persistence of HIV-DNA has led others to focus on its impact in the contribution towards HIV disease progression and HIV-associated diseases [52-55, 121]. Rouzioux et al found a correlation between the level of HIV-DNA and AIDS progression that was independent of HIV RNA levels and CD4 T-cell counts [56]. The persistence of HIV DNA could be an indication of the presence of viral reservoirs. Many of these reservoirs are believed to lie in memory T-cells [57-59] but the involvement of monocytes is increasing being recognized as an important player in disease pathogenesis. Thus the monocytes' relationship to HAD neuropathogenesis has generated a great deal

of interest through the "Trojan Horse" analogy where HIV-infected monocytes traffic into the CNS [5, 10, 11, 37, 38, 50, 122, 123]. Further investigations led to the identification of a unique subset of activated monocytes, $CD14^{+}/CD16^{+}$ that were more permissive to infection and harbored the viral DNA in vivo [11, 74, 122]. These findings were corroborated from data from the Hawaii Center for AIDS that linked individuals with HAD to higher amounts of circulating HIV DNA compared to HIV-infected individuals with normal cognition [50, 51]. We also found that $CD14^{+}/CD16^{+}$ monocytes contributed to the majority of the total PBMC HIV DNA when compared to levels in non-monocytes, CD14- [50, 51]. Overall, these data suggested a connection between HIV-DNA and HAD; with the possibility that HIV-DNA could be biomarker for assessing severity of HAND. Although our previous studies provided some insight into the role of HIV DNA in HIV-1 neuropathogenesis, further advances in understanding how the viral DNA is involved in the mechanisms could benefit from improvements in the molecular tools used to measure HIV DNA.

The main purpose of this dissertation then was to assay for HIV DNA in various cellular locations that included the periphery, cerebrospinal fluid (CSF), and central nervous tissue (CNS). The goal was to demonstrate the feasibility of analyzing the cell populations in these various regions through the use of novel techniques that were tailored for the analysis of these cells of interest.

The first objective focused on CD14+/16+ monocytes hypothesizing that HIV DNA copies would be the highest in subjects with HAND with similar HIV DNA levels found in CSF. Consistent with findings from previous studies [74], analysis of the following PBMC populations: non-monocytes (CD14-), activated monocytes

(CD14+/16+), and non-activated monocytes (CD14+/16-) found the highest HIV DNA levels in the CD14+/16+ cell population in the HAND subjects. Interestingly, the subjects with normal cognition had the highest HIV DNA levels in their CD14+/16- cell population. This finding supports the Trojan horse theory where monocytes transport the virus from the periphery across barriers to enter other compartments such as the CNS and CSF. Although the highest levels were found in the monocyte populations, the fact these cells were of activated subset in HAND subjects was consistent with CD14+/16+ cells being important in of the pathogenesis of HAND.

The hypothesis that similar HIV DNA levels would be found in CSF cellular subsets was not corroborated in the study. Instead, HIV DNA levels were lowest in CD14- cells and highest in CD14+/16- irrespective of diagnosis. One difference that was observed amongst the different diagnoses was the percentages of the cell fractions in relation to the total cells. From the Hispanic-Latino Longitudinal Cohort of HIV-seropositive women (HLLC), HAND individuals were found to have higher percentages of CD14+/16+ cells compared to normal cognition (NC) individuals; while HAND individuals from the Hawaii Aging with HIV Cohort (HAHC) were found to have higher percentages of CD14- cells compared to NC individuals. The reasons for this difference are unclear but one possible theory is that the HIV DNA copies per cell in the different PBMC subsets could reflect ongoing neuropathogenesis that affects an individual's subsequent HAND status. For example, the high CD14+/16+ percentages of the HAHC NC subjects could be explained by the neurocognitive impairment status noted in subsequent annual study visits. Similarly, the explanations for the percentages of the different CSF cellular fractions and the significantly high HIV DNA levels in the

CD14+/16- cells are also unclear. However, one hypothesis lies in the possibility that a monocyte viral reservoir exists in the CSF. It would then be possible that upon migration of the CD14+/16+ cells into the CSF through the choroid plexus, a high level of activation would no longer be necessary and therefore the cells mitigate back to their non-activated phenotype. This would result in the establishment of CSF viral reservoirs and providing an environment where the virus can evolve through compartmentalization.

The second objective was to show that the highest HIV DNA copies would be found in CD14+/16+ monocytes isolated from the basal ganglia while lower HIV DNA copy numbers would be in the frontal cortex. A modified laser-capture microdissection (LCM) protocol was used to identify and extract CD14+/16+ cells in CNS tissue of subjects with HIV-encephalitis (HIVE) and non-HIVE. HIV DNA was measured in CD14+/16+ cells and compared to other CNS cells (CD14-) in basal ganglia and frontal cortex. In the basal ganglia, higher HIV DNA levels were found in CD14- cells in both HIVE and non-HIVE brain sections. In the frontal cortex, slightly higher HIV DNA levels were found in CD14+/16+ cells in HIVE brains and higher levels were found in CD14- cells in the non-HIVE brains. From paired specimens in the basal ganglia, higher HIV DNA levels were found in CD14+/16+ of HIVE brains, whereas higher HIV DNA levels were found CD14- cells in the non-HIVE brain. These findings suggest a relationship between CNS CD14+/16+ cells and CNS inflammation. Overall, HIV DNA levels were significantly higher in the basal ganglia than in the frontal cortex regardless of diagnosis, which supports the hypothesis. These findings are consistent with work by other reporting on the effect of HIV on the basal ganglia and neurocognitive impairment and subcortical demenita [62-64, 124]. In contrast, other groups have shown that the

frontal cortex may be involved in neurocognitive impairment under different settings [99, 100, 125]. The work reported here suggest that differences in HIV DNA copy numbers amongst the CNS cell populations of the HIVE versus non-HIVE brains were more noticeable in the frontal cortex; thus future strategies will focus on measuring the CD14+/16+ cells in this region in larger number of specimens.

The third objective set out to identify HIV-1 integration sites in activated monocytes to determine if preferential integration sites could be found in subjects with HAND. Using an optimized modified method, CSF cell fractions including CD14-, CD14+/16+ and CD14+/16- cells from HAND and NC individuals were analyzed for HIV integration sites within the host genome. HIV integration sites were sequenced and of interest were that some of the integration sites were common across cell fractions and neurocognitive status. What was unanticipated were some integration sites representing families of genes that were shared amongst the cell fractions including three of the sites involved in apoptosis, two associated with macrophage behavior, and one site involved in transcription regulation. These results suggest that insertional mutagenesis might be involved in neuropathogenesis and opens the door to future investigations in the development and maintenance of HAND. A next step in pursuing these ideas would be expand the sample size to verify these preliminary results and to analyze the same cell populations in different locations such as the periphery and CNS to identify integration sites that are unique to each region and common across all regions.

The final objective of these studies developed an HIV DNA assay using a peptide nucleic acid (PNA) probe in combination with flow cytometry to analyze PBMC and CSF cells. PNA probes are synthetic oligonucleotides with an uncharged backbone that

allows it to bind strongly to its targets and penetrate into cells more easily than DNA. These probes were used in a novel flow-FISH technique that was designed to detect HIV DNA within various cell populations including CD14-/16-, CD14-/16+, CD14+/16+, and CD14+/16- cells. Prior to its use, the specificity of the probe was tested using HIV-positive and HIV-negative cell lines. In the HIV-positive cell lines the PNA probe binding rates ranged from 43-74%. The lower than expected PNA positivity in some of these cell lines may be contributed to the high specificity of the probe. It has been shown that even a one base pair mismatch causes a dramatic decrease in binding efficiencies [103]. On the other hand, the binding rates in the HIV-negative cell lines ranged from 2.4-7%, which was most likely due to the autofluorescence of the cells that resulted from stringent conditions required for the PNA probe. The sensitivity of the PNA probe in detecting HIV DNA was also determined in a titration experiment that showed decreasing PNA probe binding with increased dilution of an HIV-positive cell line. However, the results showed diminishing sensitivity with increased cell line dilution, which could have been explained by the high sensitivity of the probe. A comparison of the novel flow-FISH technique to the cell sorting and multiplex HIV DNA assay was then completed. The slight differences that were discovered between the two methods could be attributed to the unique regions in the HIV-1 genome that were targeted by the assays. The PNA probe detected a region in the *pol* gene whereas the multiplex real-time PCR assay detected a region in the *gag* gene. The *pol* gene has previously been shown to be susceptible to high mutation rates [84, 126, 127], which could adversely impact the efficiency of the PNA probe binding. Future strategies could target designing another PNA probe that would bind to the same region of HIV as the multiplex PCR assay. Overall, the present studies

showed that the flow-FISH technique could successfully detect HIV DNA in different cell populations and utilizing the tool in conjunction with other molecular methodologies may assist in providing insight on the neuropathogeneiss of HAND.

In summary, the research undertaken in this dissertation study developed new tools and technologies for utilization in experiments designed to characterize HIV DNA in monocyte subsets. These unique molecular tools were tailored to assess HIV DNA in a wide spectrum of specimen quantities. The expectation is that utilization of these techniques will be further expanded to contribute to the field in understanding the mechanisms by which HIV monopolizes monocytes as the cells transition from the periphery into the CNS and lead to HAND. Future areas and targets for study call for to the need to expand the preliminary work with larger samples sizes to validate the findings described in this dissertation.

The results from this study supplement current beliefs of monocyte behavior in the context of HAND. The circulating monocytes with high HIV DNA copies in activated monocytes (CD14+/16+) support the hypothesis that monocytes can traffic the virus across barriers that include the blood brain barrier and the choroid plexus allowing them to gain access into the CNS and CSF respectively. As observed in the LCM studies, the monocytes could then differentiate into perivascular macrophages and microglial cells once in the CNS. Since it was found that the activated subsets of these cells contain high levels of HIV DNA in HIVE brains, these cells may be responsible for viral persistence through the infection of other macrophages and microglial cells. The persistent production of HIV proteins could potentially lead to a continuous release of inflammatory cytokines and chemokines from these cells. The release of inflammatory molecules

together with HIV proteins ultimately results in the neuronal apoptosis. Based on the results of the LCM study, it can be hypothesized that greater activity was occurring in the basal ganglia but there was still measureable activity occurring in the frontal cortex. The CSF studies suggested that the CD14+/16+ cells return to their normal states (CD14+/16) when they enter the CSF. Returning to their normal state allowed them to establish viral reservoirs and provided an environment for the virus to evolve and evade treatment especially since antiretroviral concentrations are lower in the CSF. The integration study suggested a mechanism in which the virus could directly influence neuronal apoptosis. Through insertional mutagenesis, HIV could integrate near or within genes that are involved in apoptosis and disrupt their normal function. As a result, apoptosis could become dysregulated and could potentially lead to increased neuronal death.

In conclusion, the information gained from these exploratory studies provided additional insight in the involvement of activated monocytes in the development of HAND. In addition, the information provided data from molecular tools to monitor the levels of HIV DNA within these cells of interest. The information gained from this study and from future studies could expand upon our current understanding on the neuropathogeneis of HAND.

APPENDIX

Singleplex versus Multiplex Real-Time PCR in the Detection of HIV DNA

Singleplex real-time PCR reaction amplification plots of A) B-globin and B) Gag:

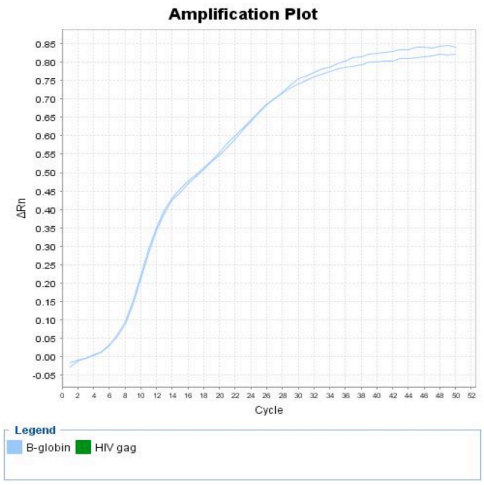

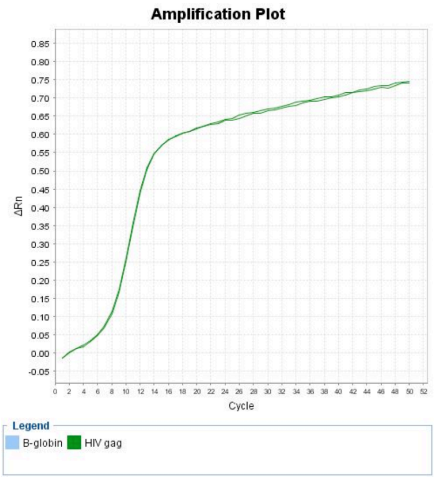

Multiplex real-time PCR reaction amplification plot:

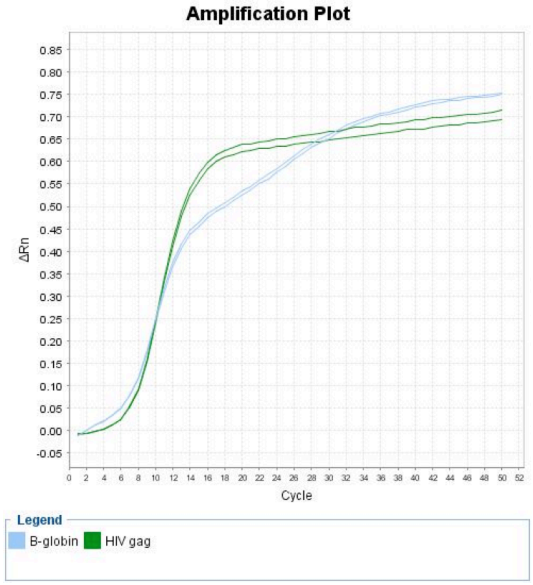

Threshold cycle comparison between multiplex and singleplex PCR reactions of plasmid dilutions, $1x10^{7}$-$1x10^{1}$, and HIV-positive cell lines: 8E5 and OM10.1:

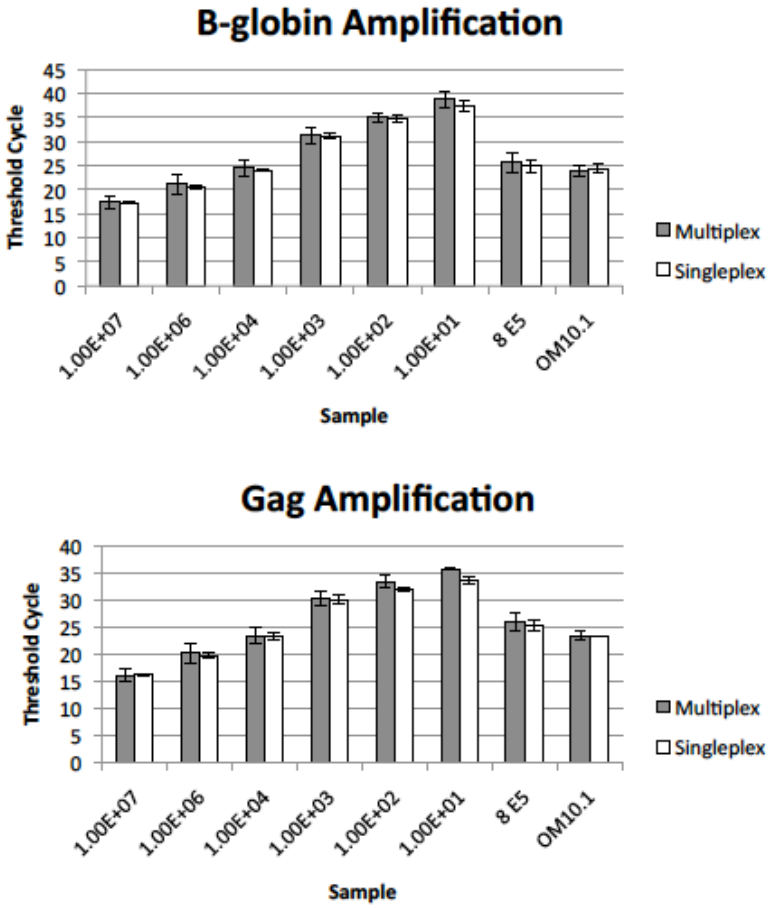

REFERENCES

1. Liner, K.J., 2nd, C.D. Hall, and K.R. Robertson, *Impact of human immunodeficiency virus (HIV) subtypes on HIV-associated neurological disease.* J Neurovirol, 2007. **13**(4): p. 291-304.
2. Clifford, D.B., *HIV-associated neurocognitive disease continues in the antiretroviral era.* Top HIV Med, 2008. **16**(2): p. 94-8.
3. Mishra, M., et al., *Clade-specific differences in neurotoxicity of human immunodeficiency virus-1 B and C Tat of human neurons: significance of dicysteine C30C31 motif.* Ann Neurol, 2008. **63**(3): p. 366-76.
4. Williams, R., et al., *Nonhuman primate models of NeuroAIDS.* J Neurovirol, 2008. **14**(4): p. 292-300.
5. González-Scarano, F. and J. Martín-García, *The neuropathogenesis of AIDS.* Nature Reviews Immunology, 2005. **5**: p. 69-81.
6. Bandaru, V.V., et al., *Associative and predictive biomarkers of dementia in HIV-1-infected patients.* Neurology, 2007. **68**(18): p. 1481-7.
7. McArthur, J.C., et al., *Human immunodeficiency virus-associated neurocognitive disorders: Mind the gap.* Ann Neurol, 2010. **67**(6): p. 699-714.
8. Kaul, M., G.A. Garden, and S.A. Lipton, *Pathways to neuronal injury and apoptosis in HIV-associated dementia.* Nature, 2001. **410**(6831): p. 988-94.
9. Thieblemont, N., et al., *CD14lowCD16high: a cytokine-producing monocyte subset which expands during human immunodeficiency virus infection.* Eur J Immunol, 1995. **25**(12): p. 3418-24.
10. Kim, W.K., et al., *Monocyte/macrophage traffic in HIV and SIV encephalitis.* J Leukoc Biol, 2003. **74**(5): p. 650-6.
11. Pulliam, L., et al., *Unique monocyte subset in patients with AIDS dementia.* Lancet, 1997. **349**(9053): p. 692-5.
12. Neuenburg, J.K., et al., *Enrichment of activated monocytes in cerebrospinal fluid during antiretroviral therapy.* AIDS, 2005. **19**(13): p. 1351-9.
13. Fischer-Smith, T., et al., *Macrophage/microglial accumulation and proliferating cell nuclear antigen expression in the central nervous system in human immunodeficiency virus encephalopathy.* Am J Pathol, 2004. **164**(6): p. 2089-99.
14. Fischer-Smith, T., et al., *CNS invasion by CD14+/CD16+ peripheral blood-derived monocytes in HIV dementia: perivascular accumulation and reservoir of HIV infection.* J Neurovirol, 2001. **7**(6): p. 528-41.
15. Kusdra, L., et al., *Elevation of CD69+ monocyte/macrophages in patients with Alzheimer's disease.* Immunobiology, 2000. **202**(1): p. 26-33.
16. Szaflarska, A., et al., *Antitumor response of CD14+/CD16+ monocyte subpopulation.* Exp Hematol, 2004. **32**(8): p. 748-55.
17. Ellery, J., R.J. McDermott, and P.J. Ellery, *Computers as a formal continuing education tool: moving beyond intention.* Am J Health Behav, 2007. **31**(3): p. 312-22.
18. Sadeghi, H.M., et al., *Phenotypic and functional characteristics of circulating monocytes of elderly persons.* Exp Gerontol, 1999. **34**(8): p. 959-70.

19. Ziegler-Heitbrock, H.W., et al., *The novel subset of CD14+/CD16+ blood monocytes exhibits features of tissue macrophages.* Eur J Immunol, 1993. **23**(9): p. 2053-8.
20. Ziegler-Heitbrock, H.W., B. Passlick, and D. Flieger, *The monoclonal antimonocyte antibody My4 stains B lymphocytes and two distinct monocyte subsets in human peripheral blood.* Hybridoma, 1988. **7**(6): p. 521-7.
21. Ziegler-Heitbrock, L., *The CD14+ CD16+ blood monocytes: their role in infection and inflammation.* J Leukoc Biol, 2007. **81**(3): p. 584-92.
22. Sonza, S., et al., *Monocytes harbour replication-competent, non-latent HIV-1 in patients on highly active antiretroviral therapy.* Aids, 2001. **15**(1): p. 17-22.
23. Gartner, S. and Y. Liu, *Insights into the role of immune activation in HIV neuropathogenesis.* J Neurovirol, 2002. **8**(2): p. 69-75.
24. Gorry, P.R., et al., *Macrophage tropism of human immunodeficiency virus type 1 isolates from brain and lymphoid tissues predicts neurotropism independent of coreceptor specificity.* J Virol, 2001. **75**(21): p. 10073-89.
25. Williams, K.C. and W.F. Hickey, *Central nervous system damage, monocytes and macrophages, and neurological disorders in AIDS.* Annu Rev Neurosci, 2002. **25**: p. 537-62.
26. Clay, C.C., et al., *Neuroinvasion of fluorescein-positive monocytes in acute simian immunodeficiency virus infection.* J Virol, 2007. **81**(21): p. 12040-8.
27. Liu, Y., et al., *Analysis of human immunodeficiency virus type 1 gp160 sequences from a patient with HIV dementia: evidence for monocyte trafficking into brain.* J Neurovirol, 2000. **6 Suppl 1**: p. S70-81.
28. Kumar, A.M., et al., *Human immunodeficiency virus type 1 RNA Levels in different regions of human brain: quantification using real-time reverse transcriptase-polymerase chain reaction.* J Neurovirol, 2007. **13**(3): p. 210-24.
29. Jones, G. and C. Power, *Regulation of neural cell survival by HIV-1 infection.* Neurobiol Dis, 2006. **21**(1): p. 1-17.
30. Hesselgesser, J., et al., *CD4-independent association between HIV-1 gp120 and CXCR4: functional chemokine receptors are expressed in human neurons.* Curr Biol, 1997. **7**(2): p. 112-21.
31. Hesselgesser, J., et al., *Neuronal apoptosis induced by HIV-1 gp120 and the chemokine SDF-1 alpha is mediated by the chemokine receptor CXCR4.* Curr Biol, 1998. **8**(10): p. 595-8.
32. Zheng, J., et al., *Intracellular CXCR4 signaling, neuronal apoptosis and neuropathogenic mechanisms of HIV-1-associated dementia.* J Neuroimmunol, 1999. **98**(2): p. 185-200.
33. Zhao, Y., et al., *Memantine for AIDS dementia complex: open-label report of ACTG 301.* HIV Clin Trials, 2010. **11**(1): p. 59-67.
34. Belge, K.U., et al., *The proinflammatory CD14+CD16+DR++ monocytes are a major source of TNF.* J Immunol, 2002. **168**(7): p. 3536-42.
35. Weber, C., et al., *Differential chemokine receptor expression and function in human monocyte subpopulations.* J Leukoc Biol, 2000. **67**(5): p. 699-704.
36. Verani, A., G. Gras, and G. Pancino, *Macrophages and HIV-1: dangerous liaisons.* Mol Immunol, 2005. **42**(2): p. 195-212.

37. Anderson, E., et al., *HIV-1-associated dementia: a metabolic encephalopathy perpetrated by virus-infected and immune-competent mononuclear phagocytes.* J Acquir Immune Defic Syndr, 2002. **31 Suppl 2**: p. S43-54.
38. Ozdener, H., *Molecular mechanisms of HIV-1 associated neurodegeneration.* J Biosci, 2005. **30**(3): p. 391-405.
39. Kramer-Hammerle, S., et al., *Cells of the central nervous system as targets and reservoirs of the human immunodeficiency virus.* Virus Res, 2005. **111**(2): p. 194-213.
40. Suarez, S., et al., *Outcome of patients with HIV-1-related cognitive impairment on highly active antiretroviral therapy.* AIDS, 2001. **15**(2): p. 195-200.
41. Sacktor, N., *The epidemiology of human immunodeficiency virus-associated neurological disease in the era of highly active antiretroviral therapy.* J Neurovirol, 2002. **8 Suppl 2**: p. 115-21.
42. Pierson, T., J. McArthur, and R.F. Siliciano, *Reservoirs for HIV-1: mechanisms for viral persistence in the presence of antiviral immune responses and antiretroviral therapy.* Annu Rev Immunol, 2000. **18**: p. 665-708.
43. Varatharajan, L. and S.A. Thomas, *The transport of anti-HIV drugs across blood-CNS interfaces: summary of current knowledge and recommendations for further research.* Antiviral Res, 2009. **82**(2): p. A99-109.
44. Price, R.W. and S. Spudich, *Antiretroviral therapy and central nervous system HIV type 1 infection.* J Infect Dis, 2008. **197 Suppl 3**: p. S294-306.
45. Letendre, S., et al., *Validation of the CNS Penetration-Effectiveness rank for quantifying antiretroviral penetration into the central nervous system.* Arch Neurol, 2008. **65**(1): p. 65-70.
46. Chang, L., et al., *Antiretroviral treatment alters relationship between MCP-1 and neurometabolites in HIV patients.* Antivir Ther, 2004. **9**(3): p. 431-40.
47. Zink, M.C., et al., *High viral load in the cerebrospinal fluid and brain correlates with severity of simian immunodeficiency virus encephalitis.* J Virol, 1999. **73**(12): p. 10480-8.
48. Zink, M.C. and J.E. Clements, *A novel simian immunodeficiency virus model that provides insight into mechanisms of human immunodeficiency virus central nervous system disease.* J Neurovirol, 2002. **8 Suppl 2**: p. 42-8.
49. Clements, J.E., et al., *The central nervous system is a viral reservoir in simian immunodeficiency virus--infected macaques on combined antiretroviral therapy: a model for human immunodeficiency virus patients on highly active antiretroviral therapy.* J Neurovirol, 2005. **11**(2): p. 180-9.
50. Shiramizu, B., et al., *Circulating proviral HIV DNA and HIV-associated dementia.* Aids, 2005. **19**(1): p. 45-52.
51. Shiramizu, B., et al., *HIV DNA and dementia in treatment-naive HIV-1-infected individuals in Bangkok, Thailand.* Int J Med Sci, 2007. **4**(1): p. 13-8.
52. Crowe, S.M. and S. Sonza, *HIV-1 can be recovered from a variety of cells including peripheral blood monocytes of patients receiving highly active antiretroviral therapy: a further obstacle to eradication.* J Leukoc Biol, 2000. **68**(3): p. 345-50.

53. Bruisten, S.M., et al., *Cellular proviral HIV type 1 DNA load persists after long-term RT-inhibitor therapy in HIV type 1 infected persons.* AIDS Res Hum Retroviruses, 1998. **14**(12): p. 1053-8.
54. Bush, C.E., et al., *Quantitation of unintegrated HIV-1 DNA in asymptomatic patients in the presence or absence of antiretroviral therapy.* AIDS Res Hum Retroviruses, 1993. **9**(2): p. 183-7.
55. Calcaterra, S., et al., *Comparative analysis of total and integrated HIV-1 DNA in peripheral CD4 lymphocytes and monocytes after long treatment with HAART.* J Infect, 2001. **43**(4): p. 239-45.
56. Rouzioux, C., et al., *Early Levels of HIV-1 DNA in Peripheral Blood Mononuclear Cells Are Predictive of Disease Progression Independently of HIV-1 RNA Levels and CD4+ T Cell Counts.* J Infect Dis, 2005. **192**(1): p. 46-55.
57. Hermankova, M., et al., *Analysis of human immunodeficiency virus type 1 gene expression in latently infected resting CD4+ T lymphocytes in vivo.* J Virol, 2003. **77**(13): p. 7383-92.
58. Finzi, D., et al., *Latent infection of CD4+ T cells provides a mechanism for lifelong persistence of HIV-1, even in patients on effective combination therapy.* Nat Med, 1999. **5**(5): p. 512-7.
59. Chun, T.W., et al., *Presence of an inducible HIV-1 latent reservoir during highly active antiretroviral therapy.* Proc Natl Acad Sci U S A, 1997. **94**(24): p. 13193-7.
60. Ho, D.D., T.R. Rota, and M.S. Hirsch, *Infection of monocyte/macrophages by human T lymphotropic virus type III.* J Clin Invest, 1986. **77**(5): p. 1712-5.
61. Nicholson, J.K., et al., *In vitro infection of human monocytes with human T lymphotropic virus type III/lymphadenopathy-associated virus (HTLV-III/LAV).* J Immunol, 1986. **137**(1): p. 323-9.
62. Berger, J.R. and G. Arendt, *HIV dementia: the role of the basal ganglia and dopaminergic systems.* J Psychopharmacol, 2000. **14**(3): p. 214-21.
63. Wang, G.J., et al., *Decreased brain dopaminergic transporters in HIV-associated dementia patients.* Brain, 2004. **127**(Pt 11): p. 2452-8.
64. Ances, B.M., et al., *Caudate blood flow and volume are reduced in HIV+ neurocognitively impaired patients.* Neurology, 2006. **66**(6): p. 862-6.
65. Paul, D.B., et al., *Short-term stability of HIV provirus levels in the peripheral blood of HIV-infected individuals.* J Med Virol, 1995. **47**(3): p. 292-7.
66. Graybiel, A.M., *The basal ganglia: learning new tricks and loving it.* Curr Opin Neurobiol, 2005. **15**(6): p. 638-44.
67. Mack, K.D., et al., *HIV Insertions Within and Proximal to Host Cell Genes Are a Common Finding in Tissues Containing High Levels of HIV DNA and Macrophage-Associated p24 Antigen Expression.* JAIDS, 2003. **33**(3): p. 308-320.
68. Scherdin, U., K. Rhodes, and M. Breindl, *Transcriptionally active genome regions are preferred targets for retrovirus integration.* J Virol, 1990. **64**(2): p. 907-12.
69. Stevens, S.W. and J.D. Griffith, *Human immunodeficiency virus type 1 may preferentially integrate into chromatin occupied by L1Hs repetitive elements.* Proc Natl Acad Sci U S A, 1994. **91**(12): p. 5557-61.

70. Stevens, S.W. and J.D. Griffith, *Sequence analysis of the human DNA flanking sites of human immunodeficiency virus type 1 integration.* J Virol, 1996. **70**(9): p. 6459-62.
71. Killebrew, D. and B. Shiramizu, *Pathogenesis of HIV-associated non-Hodgkin lymphoma.* Curr HIV Res, 2004. **2**(3): p. 215-21.
72. Killebrew, D.A. and B. Shiramizu. *Identification of Preferential HIV-1 Integration Sites*. in *Twenty Years of HIV Research: From Discovery to Understanding (X2)*. 2003. Banff, Alberta, Canada.
73. Antinori, A., et al., *Updated research nosology for HIV-associated neurocognitive disorders.* Neurology, 2007. **69**(18): p. 1789-99.
74. Ellery, P.J., et al., *The CD16+ monocyte subset is more permissive to infection and preferentially harbors HIV-1 in vivo.* J Immunol, 2007. **178**(10): p. 6581-9.
75. Jaworowski, A., et al., *CD16+ monocyte subset preferentially harbors HIV-1 and is expanded in pregnant Malawian women with Plasmodium falciparum malaria and HIV-1 infection.* J Infect Dis, 2007. **196**(1): p. 38-42.
76. Shiramizu, B., et al., *Amount of HIV DNA in peripheral blood mononuclear cells is proportional to the severity of HIV-1-associated neurocognitive disorders.* J Neuropsychiatry Clin Neurosci, 2009. **21**(1): p. 68-74.
77. Shiramizu, B., et al. *Presence of CD14/16-Positive Monocytes/Macrophages in Older HIV Seropositive Individuals with Dementia*. in *5th International Symposium of Neurovirology*. 2003. Baltimore, MD.
78. Shiramizu, B., et al., *HIV proviral DNA associated with decreased neuropsychological function.* J Neuropsychiatry Clin Neurosci, 2007. **19**(2): p. 157-63.
79. Alexaki, A. and B. Wigdahl, *HIV-1 infection of bone marrow hematopoietic progenitor cells and their role in trafficking and viral dissemination.* PLoS Pathog, 2008. **4**(12): p. e1000215.
80. Kivisakk, P., et al., *Human cerebrospinal fluid central memory CD4+ T cells: evidence for trafficking through choroid plexus and meninges via P-selectin.* Proc Natl Acad Sci U S A, 2003. **100**(14): p. 8389-94.
81. Mitchell, K., et al., *Monocyte chemoattractant protein-1 in the choroid plexus: a potential link between vascular pro-inflammatory mediators and the CNS during peripheral tissue inflammation.* Neuroscience, 2009. **158**(2): p. 885-95.
82. Schnell, G., et al., *Compartmentalized human immunodeficiency virus type 1 originates from long-lived cells in some subjects with HIV-1-associated dementia.* PLoS Pathog, 2009. **5**(4): p. e1000395.
83. Pillai, S.K., et al., *Genetic attributes of cerebrospinal fluid-derived HIV-1 env.* Brain, 2006. **129**(Pt 7): p. 1872-83.
84. Caragounis, E.C., et al., *Comparison of HIV-1 pol and env sequences of blood, CSF, brain and spleen isolates collected ante-mortem and post-mortem.* Acta Neurol Scand, 2008. **117**(2): p. 108-16.
85. Burkala, E.J., et al., *Compartmentalization of HIV-1 in the central nervous system: role of the choroid plexus.* AIDS, 2005. **19**(7): p. 675-84.
86. Harrington, P.R., et al., *Cross-sectional characterization of HIV-1 env compartmentalization in cerebrospinal fluid over the full disease course.* AIDS, 2009. **23**(8): p. 907-15.

87. Valcour, V., et al., *Higher frequency of dementia in older HIV+ individuals. The Hawaii Aging with HIV Cohort.* Neurology, 2004. **63**: p. 822-827.
88. Wojna, V. and A. Nath, *Challenges to the diagnosis and management of HIV dementia.* AIDS Read, 2006. **16**(11): p. 615-6, 621-4, 626, 629-32.
89. Wojna, V., et al., *Prevalence of human immunodeficiency virus-associated cognitive impairment in a group of Hispanic women at risk for neurological impairment.* J Neurovirol, 2006. **12**(5): p. 356-64.
90. Sacktor, N., et al., *Neuropsychological test profile differences between young and old human immunodeficiency virus-positive individuals.* J Neurovirol, 2007. **13**(3): p. 203-9.
91. Janssen, R.S., D.R. Cornblath, and L.G. Epstein, *Nomenclature and research case definitions for neurological manifestations of human immunodeficiency virus type 1 (HIV-1) infection.* Neurology, 1991. **41**: p. 778-785.
92. Shiramizu, B., et al., *Assessment of HIV-1 DNA copies per cell by real-time polymerase chain reaction.* Frontiers in Bioscience, 2004. **9**: p. 255-261.
93. Shiramizu, B., et al., *Correlation of Circulating Proviral HIV DNA and with HIV-Associated Dementia.* AIDS, 2004. **Accepted**.
94. Valcour, V.G., et al., *HIV DNA and cognition in a Thai longitudinal HAART initiation cohort: the SEARCH 001 Cohort Study.* Neurology, 2009. **72**(11): p. 992-8.
95. Ransohoff, R.M., P. Kivisakk, and G. Kidd, *Three or more routes for leukocyte migration into the central nervous system.* Nat Rev Immunol, 2003. **3**(7): p. 569-81.
96. Coleman, C.M. and L. Wu, *HIV interactions with monocytes and dendritic cells: viral latency and reservoirs.* Retrovirology, 2009. **6**: p. 51.
97. Alexaki, A., Y. Liu, and B. Wigdahl, *Cellular reservoirs of HIV-1 and their role in viral persistence.* Curr HIV Res, 2008. **6**(5): p. 388-400.
98. Fischer-Smith, T., et al., *Monocyte/macrophage trafficking in acquired immunodeficiency syndrome encephalitis: lessons from human and nonhuman primate studies.* J Neurovirol, 2008. **14**(4): p. 318-26.
99. Sailasuta, N., K. Shriner, and B. Ross, *Evidence of reduced glutamate in the frontal lobe of HIV-seropositive patients.* NMR Biomed, 2009. **22**(3): p. 326-31.
100. English, C.D., et al., *Elevated frontal lobe cytosolic choline levels in minimal or mild AIDS dementia complex patients: a proton magnetic resonance spectroscopy study.* Biol Psychiatry, 1997. **41**(4): p. 500-2.
101. Agrawal, L., et al., *Dopaminergic neurotoxicity of HIV-1 gp120: reactive oxygen species as signaling intermediates.* Brain Res, 2010. **1306**: p. 116-30.
102. Sluka, P., et al., *Application of laser-capture microdissection to analysis of gene expression in the testis.* Prog Histochem Cytochem, 2008. **42**(4): p. 173-201.
103. Wang, G. and X.S. Xu, *Peptide nucleic acid (PNA) binding-mediated gene regulation.* Cell Res, 2004. **14**(2): p. 111-6.
104. Nielsen, P.E., *Sequence-selective DNA recognition by synthetic ligands.* Bioconjug Chem, 1991. **2**(1): p. 1-12.
105. Nielsen, P.E., et al., *Sequence-selective recognition of DNA by strand displacement with a thymine-substituted polyamide.* Science, 1991. **254**(5037): p. 1497-500.

106. Klepfish, A., et al., *Successful treatment of aggressive HIV-associated non-Hodgkin's lymphoma with combination chemotherapy, biotherapy with rituximab and HAART: presentation of a therapeutic option.* Leuk Lymphoma, 2003. **44**(2): p. 349-51.
107. Schmid, I., et al., *Simultaneous flow cytometric analysis of two cell surface markers, telomere length, and DNA content.* Cytometry, 2002. **49**(3): p. 96-105.
108. Kapoor, V., et al., *Quantum dots thermal stability improves simultaneous phenotype-specific telomere length measurement by FISH-flow cytometry.* J Immunol Methods, 2009. **344**(1): p. 6-14.
109. Potter, A.J. and M.H. Wener, *Flow cytometric analysis of fluorescence in situ hybridization with dye dilution and DNA staining (flow-FISH-DDD) to determine telomere length dynamics in proliferating cells.* Cytometry A, 2005. **68**(1): p. 53-8.
110. Schmid, I., et al., *Simultaneous flow cytometric measurement of viability and lymphocyte subset proliferation.* J Immunol Methods, 2001. **247**(1-2): p. 175-86.
111. Baerlocher, G.M., et al., *Flow cytometry and FISH to measure the average length of telomeres (flow FISH).* Nat Protoc, 2006. **1**(5): p. 2365-76.
112. Molenaar, C., et al., *Visualizing telomere dynamics in living mammalian cells using PNA probes.* EMBO J, 2003. **22**(24): p. 6631-41.
113. Murakami, T., et al., *A novel method for detecting HIV-1 by non-radioactive in situ hybridization: application of a peptide nucleic acid probe and catalysed signal amplification.* J Pathol, 2001. **194**(1): p. 130-5.
114. Hennings, L., et al., *Dead or alive? Autofluorescence distinguishes heat-fixed from viable cells.* Int J Hyperthermia, 2009. **25**(5): p. 355-63.
115. *Clinical confirmation of the American Academy of Neurology algorithm for HIV-1-associated cognitive/motor disorder. The Dana Consortium on Therapy for HIV Dementia and Related Cognitive Disorders.* Neurology, 1996. **47**(5): p. 1247-53.
116. Brooun, A., D.D. Richman, and R.S. Kornbluth, *HIV-1 preintegration complexes preferentially integrate into longer target DNA molecules in solution as detected by a sensitive, polymerase chain reaction-based integration assay.* J Biol Chem, 2001. **276**(50): p. 46946-52.
117. Vandegraaff, N., et al., *Kinetics of human immunodeficiency virus type 1 (HIV) DNA integration in acutely infected cells as determined using a novel assay for detection of integrated HIV DNA.* J Virol, 2001. **75**(22): p. 11253-60.
118. Miller, M.D., Y.C. Bor, and F. Bushman, *Target DNA capture by HIV-1 integration complexes.* Curr Biol, 1995. **5**(9): p. 1047-56.
119. Deichmann, M., M. Bentz, and R. Haas, *Ultra-sensitive FISH is a useful tool for studying chronic HIV-1 infection.* J Virol Methods, 1997. **65**(1): p. 19-25.
120. Rodriguez-Alfageme, C., et al., *B cells malignantly transformed by human immunodeficiency virus are polyclonal.* Virology, 1998. **252**(1): p. 34-8.
121. Clarke, J.R., et al., *HIV-1 proviral DNA copy number in peripheral blood leucocytes and bronchoalveolar lavage cells of AIDS patients.* Clin Exp Immunol, 1994. **96**(2): p. 182-6.
122. Kusdra, L., D. McGuire, and L. Pulliam, *Changes in monocyte/macrophage neurotoxicity in the era of HAART: implications for HIV-associated dementia.* Aids, 2002. **16**(1): p. 31-8.

123. McElrath, M.J., R.M. Steinman, and Z.A. Cohn, *Latent HIV-1 infection in enriched populations of blood monocytes and T cells from seropositive patients.* J Clin Invest, 1991. **87**(1): p. 27-30.
124. Castelo, J.M., et al., *Putamen hypertrophy in nondemented patients with human immunodeficiency virus infection and cognitive compromise.* Arch Neurol, 2007. **64**(9): p. 1275-80.
125. Tracey, I., et al., *Brain choline-containing compounds are elevated in HIV-positive patients before the onset of AIDS dementia complex: A proton magnetic resonance spectroscopic study.* Neurology, 1996. **46**(3): p. 783-8.
126. Smit, T.K., et al., *Independent evolution of human immunodeficiency virus (HIV) drug resistance mutations in diverse areas of the brain in HIV-infected patients, with and without dementia, on antiretroviral treatment.* J Virol, 2004. **78**(18): p. 10133-48.
127. Katzenstein, T.L., et al., *Phylogeny and resistance profiles of HIV-1 POL sequences from rectal biopsies and blood.* J Med Virol, 2010. **82**(7): p. 1103-9.